

## INTERSTELLAR POLYCYCLIC AROMATIC HYDROCARBONS: THE INFRARED EMISSION BANDS, THE EXCITATION/EMISSION MECHANISM, AND THE ASTROPHYSICAL IMPLICATIONS

L. J. ALLAMANDOLA,<sup>1</sup> A. G. G. M. TIELENS,<sup>1,2</sup> AND J. R. BARKER<sup>3</sup>

Received 1988 September 27; accepted 1989 May 5

### CONTENTS

I. Introduction	734	46-E10	ii) Deuterium Enrichment	754	46-G2
II. Spectroscopy	735	46-E11	b) Chemical Attack by O and H Atoms	755	46-G3
a) The Interstellar Emission Spectrum	735	46-E11	c) Molecular Structure	756	46-G4
b) Comparison with the Spectra of PAH-related Materials	737	46-E13	d) PAH Production and Carbon Particle Formation	757	46-G5
c) Interstellar Feature Assignments	738	46-E14	i) Growth in Circumstellar Shells	757	46-G5
i) The 3200-2700 cm <sup>-1</sup> (3.13-3.7 μm) Region	739	46-F1	ii) PAHs, PAH Clusters, and Amorphous Carbon Particles	760	46-G8
ii) The 2000-1000 cm <sup>-1</sup> (5-10 μm) Region	740	46-F2	V. Astrophysical Applications	762	46-G10
iii) The 1000-500 cm <sup>-1</sup> (10-20 μm) Region Feature	742	46-F4	a) Size Estimates	762	46-G10
iv) The 500-10 cm <sup>-1</sup> (20-1000 μm) Region	743	46-F5	i) PAH Molecules	762	46-G10
v) The Vibrational Quasi-Continuum	744	46-F6	ii) PAH Clusters	763	46-G11
III. Infrared Emission from Vibrationally Excited Molecules	745	46-F7	b) The Abundance of Interstellar PAHs	763	46-G11
a) Calculated Infrared Fluorescence Intensities	745	46-F7	i) The UV Absorption Properties of PAHs	764	46-G12
i) Infrared Fluorescence Intensities	745	46-F7	ii) The Fraction of C in Small Interstellar PAHs	764	46-G12
ii) Rate of Deactivation by Infrared Fluorescence	748	46-F10	iii) The Fraction of C in Large PAHs	764	46-G12
iii) Infrared Fluorescence Dependence on Molecular Size and Vibrational Energy Content	749	46-F11	c) PAHs and the UV Extinction Curve	765	46-G13
b) Regions of Applicability of the Thermal Approximation	750	46-F12	d) Dehydrogenation of Interstellar PAHs	765	46-G13
IV. Chemistry	753	46-G1	e) Deuterium Enrichments of Interstellar PAHs	766	46-G14
a) Photon-Induced Reactions of Aromatics	753	46-G1	f) Negative PAH Ions	767	47-A1
i) CH Bond Rupture	753	46-G1	g) Gas Heating	769	47-A3
			h) Anionic, Cationic, and Neutral PAHs: Influence on Interstellar Extinction	770	47-A4
			VI. CONCLUSIONS	772	47-A6

### ABSTRACT

This article presents a comprehensive treatment of the polycyclic aromatic hydrocarbon (PAH) hypothesis. The interstellar, infrared spectral features which have been attributed to emission from highly vibrationally excited PAHs are discussed in detail. These include major (most intense) bands at 3040, 1615, "1310," 1150, and 885 cm<sup>-1</sup> (3.29, 6.2, "7.7," 8.7, and 11.3 μm), minor bands and broad features in the 3200-2700<sup>-1</sup> (3.1-3.7 μm), 1660-1100 cm<sup>-1</sup> (6.0-9 μm) and 910-770 cm<sup>-1</sup> (11-13 μm) regions, as well as the vibrational quasi-continuum spanning the entire mid-IR and the electronic transitions which contribute to the high-frequency IR continuum. All the major and minor bands, as well as the quasi-continuum, can be attributed to vibrational transitions in molecular-sized PAHs. The latter two broad features probably arise from very large PAHs, PAH clusters, and amorphous carbon particles. A precise match of the interstellar spectra with laboratory spectra is not yet possible because laboratory spectra are not available of PAHs in the forms probably present in the interstellar medium (completely isolated, ionized, some completely dehydrogenated, and containing between about 20 and 40 carbon atoms). The method with which one can calculate the IR fluorescence spectrum from a vibrationally excited *molecule* is also described in detail. Fluorescence band intensities, relaxation rates, and dependence on molecule size and energy content are treated explicitly. Analysis of the interstellar spectra indicates that the PAHs which dominate the infrared spectra contain between about 20 and 40 carbon atoms. The results obtained with this method are compared with the results obtained using a thermal approximation. It is shown that for high levels of vibrational excitation and emission from low-frequency modes, the two methods give similar results. However, at low levels of vibrational excitation and for the high-frequency modes (for example, the 3040 cm<sup>-1</sup>, 3.3 μm band), the thermal approach overestimates the emission intensities. For calculations of molecular reactions (such as H-loss, deuterium enrichment, and carbon skeleton rearrangement) a thermal approximation

<sup>1</sup>Space Science Division, NASA-Ames Research Center.

<sup>2</sup>Astronomy Department, University of California, Berkeley.

<sup>3</sup>Department of Atmospheric, Oceanic, and Space Sciences, University of Michigan.

is invalid. The relationship between PAH molecules and amorphous carbon particles is presented and their production in circumstellar shells is described. The most likely interstellar PAH molecular structures are discussed and the possibility of destructive reactions with interstellar oxygen and hydrogen atoms is considered in detail and found to be unimportant. Interstellar PAH size and abundance estimates are made. On the order of a few percent of the available interstellar carbon is tied up in the small (20–40 carbon atom) PAHs which are responsible for the sharp features, and a similar amount is tied up in the larger (200–500 carbon atom) PAHs or PAH clusters and amorphous carbon particles which are responsible for the broad components underlying the 1600–1100 and 900–770  $\text{cm}^{-1}$  (6–9 and 11–13  $\mu\text{m}$ ) regions. It is shown that the spectroscopic structure these PAHs and PAH-related materials produce in the UV portion of the interstellar extinction curve lie just below current detection limits but fall in the range detectable by the *Hubble Space Telescope*. Finally, the influence of PAH charge on the ultraviolet, visible, and infrared regions is described.

*Subject headings:* interstellar: grains — molecular processes

## I. INTRODUCTION

The family of interstellar infrared emission bands at 3040, 1615, “1310”, 1150, and 885  $\text{cm}^{-1}$  (3.29, 6.2, “7.7”, 8.7, and 11.3  $\mu\text{m}$ ) forms the core of an important problem in interstellar astrophysics. Since their discovery in 1973 by Gillett, Forrest, and Merrill, the bands have been found to be associated with a large number of stellar objects, planetary nebulae, reflection nebulae, H II, regions and extragalactic sources. These observations showed that the bands were due to a surprisingly widespread, extremely stable, interstellar constituent (see Willner [1984] and Allamandola [1984], respectively, for reviews of the observations and theories up to 1983). As the number and variety of objects found to emit these features increased, it became clear that identifying the carrier and elucidating the excitation-emission mechanism were the central issues.

Based on the comparable intensity of the 3040  $\text{cm}^{-1}$  (3.3  $\mu\text{m}$ ) band to the lower frequency bands and the close association with ultraviolet radiation, it was proposed that the emission was most likely due to IR molecular fluorescence pumped by ultraviolet photons (Allamandola and Norman 1978; Allamandola, Greenberg, and Norman 1979). Although the carrier proposed was incorrect (molecules frozen on 10 K dust grains), this excitation-emission mechanism is now generally accepted because of very important observations and analysis of reflection nebulae made by Sellgren (1984) which showed that the ultraviolet and visible photon fluxes in these objects were unable to sufficiently excite larger species to emit in the 3000  $\text{cm}^{-1}$  (3  $\mu\text{m}$ ) region.

Progress toward the hypothesis currently gaining acceptance, that aromatic hydrocarbons are responsible for the bands, began with the suggestion by Duley and Williams (1981) that the features arise from vibrations of chemical functional groups attached to the aromatic moieties present in small ( $\sim 100$  Å) amorphous carbon particles. Leger and Puget (1984, hereafter LP) and Allamandola, Tielens, and Barker (1985, hereafter ATBa) later proposed that vibrations in individual, molecule-sized (<10 Å) polycyclic aromatic hydrocarbons (PAHs) and PAH-like species were responsible for the bands. These planar organic molecules, made up of fused six-membered rings, are extremely stable. Leger, d’Hendecourt, and Boccarda (1987) contains a compendium of articles related to many aspects of the PAH hypothesis.

Apart from the overall resemblance of the interstellar IR band spectrum to the vibrational spectrum expected from PAH-like species (§ II), the results of recent related observa-

tions and experiments tend to favor an origin in aromatic hydrocarbons as well. Cohen *et al.* (1986, 1989) have shown that the fraction of total IR luminosity radiated by the “1300”  $\text{cm}^{-1}$  (“7.7”  $\mu\text{m}$ ) feature in planetary nebulae is strongly correlated with the amount of carbon available. Because the carriers must be produced in these nebulae under harsh conditions, they must be extremely stable and carbon-rich, two characteristics completely consistent with aromatic hydrocarbons. Cohen *et al.* also showed that, while there is variation among the relative IR band intensities for different objects, the bands are correlated in the sense that when one is present the others are as well, implying that a single family of chemical species is responsible. Circumstantial experimental evidence also exists which implies the presence of such stable hydrocarbons in the interstellar medium (ISM). Recently, Wdowiak, Flickinger, and Cronin (1988) have shown that there is a remarkable resemblance of the IR spectrum of the insoluble organic material from the Orgueil meteorite to the interstellar emission bands in the 2000–800  $\text{cm}^{-1}$  (5–12.5  $\mu\text{m}$ ) region. They suggest that at least some of this material is interstellar in origin. A similar case has been made for some of the aromatic carbon in interplanetary dust particles (Allamandola, Sandford, and Wopenka 1987).

The infrared emission spectrum is comprised of intense well-defined bands, weaker minor bands, and underlying broad features. Within the framework of the PAH model, spectroscopic analysis suggests that there are at least two classes of materials which can contribute to the spectra. Free, molecule-sized PAHs can account for all the bands in the spectra while amorphous carbon particles (which are primarily made up of an irregular “lattice” of interconnected PAHs) can contribute to the broad, underlying features which are especially prominent in high-excitation objects (Allamandola, Tielens, and Barker 1987, hereafter ATBb; Goebel 1987).

This picture of molecules rather than particles producing the discrete bands, especially those at the higher frequencies, is strengthened by considering the energetics of the emitting species. If an isolated molecule is highly excited by the absorption of an ultraviolet or visible photon it can undergo a limited number of processes of which the most important are ionization, dissociation, fluorescence, phosphorescence, internal conversion, and intersystem crossing (e.g., Calvert and Pitts 1966). Many of these processes leave the molecule vibrationally excited. In a collision-free environment the only relaxation channel is infrared fluorescence (IRF): the stepwise elimination of this energy by emitting infrared photons at frequencies corresponding to the fundamental vibrations of

the molecule. The relaxation time scale for IRF is typically on the order of a tenth of a second. It is this process which we believe is responsible for the well-defined bands and many of the minor components. In contrast, Duley and Williams (1988*a, b*) propose that the spectra arise from PAH moieties which comprise partially hydrogenated amorphous carbon particles in which each PAH structural unit is "loosely" connected to the lattice via a few bonds. The PAH units must indeed be loosely bound as, in general, nonradiative relaxation in solids is usually dominant because in the condensed phase the vibrational energy can be transferred efficiently into the low-lying vibrational modes ( $10\text{--}200\text{ cm}^{-1}$  phonons) of the lattice. Large molecules (such as PAHs) tend to have many low-lying fundamental modes in the  $50\text{--}400\text{ cm}^{-1}$  range that provide an effective channel through which the vibrational energy initially deposited in the molecule can be transferred into the phonon modes of the bulk material. In this case, nonradiative relaxation generally takes place in picoseconds ( $10^{-12}\text{ s}$ ), and IRF is not possible. Thus, while one may imagine that vibrationally excited PAH structural units in a larger particle are sufficiently decoupled from the lattice to permit IRF relaxation, this process must be demonstrated in the laboratory before it can be accepted.<sup>4</sup> IRF from the free PAH azulene, excited by ultraviolet photons, has been measured by Cherkneff and Barker (1989).

This article will discuss the vibrational assignments of the various interstellar infrared emission features, the infrared characteristics of PAHs, and the ultraviolet-visible pumped IR fluorescence mechanism. Some additional characteristics of PAHs which are of particular relevance to astrophysics are also reviewed. Because there exists a vast spectroscopic literature relevant to the PAH model in which the spectra presented on a linear wavenumber scale, infrared frequencies are expressed in wavenumbers ( $\text{cm}^{-1}$ ) with the corresponding wavelength in microns indicated in parentheses.

## II. SPECTROSCOPY

### *a) The Interstellar Emission Spectrum*

Examples of nearly complete, mid-IR interstellar emission spectra are shown in Figures 1*a, b*, 2, and 3. In addition to the major bands at  $3040$ ,  $1615$ , "1310,"  $1150$ , and  $885\text{ cm}^{-1}$  ( $3.29$ ,  $6.2$ , "7.7,"  $8.7$ , and  $11.3\text{ }\mu\text{m}$ ), these figures show that there are several weak bands and underlying broad features. Furthermore, there are striking variations in the underlying continua and small changes in the "1310"  $\text{cm}^{-1}$  band from one object to another. Any attempt to explain the IR emission phenomenon should address all of these aspects of the problem. All of the band peak frequencies, full widths at half-height (FWHM) and assignments are listed in Table 1. The salient

spectroscopic details are briefly summarized in the following four paragraphs. The spectra will be discussed in the frequency ranges:  $3200\text{--}2700\text{ cm}^{-1}$  ( $3.13\text{--}3.7\text{ }\mu\text{m}$ );  $2000\text{--}1000\text{ cm}^{-1}$  ( $5\text{--}10\text{ }\mu\text{m}$ );  $1000\text{--}500\text{ cm}^{-1}$  ( $10\text{--}20\text{ }\mu\text{m}$ ); and  $500\text{--}10\text{ cm}^{-1}$  ( $20\text{--}1000\text{ }\mu\text{m}$ ).

*The 4000–2700 cm<sup>-1</sup> (2.5–3.7 μm) regions.*— In addition to the major band at  $3040\text{ cm}^{-1}$  ( $3.29\text{ }\mu\text{m}$ ), many objects have several other weak components in this region as well. These include a broad emission plateau ( $3115\text{ to }2740\text{ cm}^{-1}$ ;  $3.21\text{ to }3.65\text{ }\mu\text{m}$ ) with superposed narrow emission bands at  $2940$ ,  $2890$ ,  $2850$ , and  $2810\text{ cm}^{-1}$  ( $3.4$ ,  $3.46$ ,  $3.51$ , and  $3.56\text{ }\mu\text{m}$ ) (Geballe *et al.* 1985; de Muizon *et al.* 1986). The relative strengths of these bands vary considerably from source to source as well as with distance from the illuminating object (Geballe *et al.* 1989). Reflection nebulae also show a lower intensity, near-IR continuum (Sellgren, Werner, and Dinerstein 1983) which may extend from the mid-IR (Sellgren *et al.* 1985) to the far red (Witt, Schild, and Kraiman 1984).

*The 2000–1000 cm<sup>-1</sup> (5–10 μm) regions.*— The most prominent bands in this region are the well-known  $1615$  and "1300"  $\text{cm}^{-1}$  ( $6.2$  and "7.7"  $\mu\text{m}$ ) features. The "1300"  $\text{cm}^{-1}$  ("7.7"  $\mu\text{m}$ ) band actually varies somewhat in peak position and profile; compare, for example, the feature in the spectrum of HD 44179 (Fig. 2) with that in Orion (Fig. 1*b*). There are also three weaker features at  $1905$ ,  $1785$ , and  $1450\text{ cm}^{-1}$  ( $5.25$ ,  $5.6$ , and  $6.9\text{ }\mu\text{m}$ ) (Bregman *et al.* 1983; Allamandola *et al.* 1989). The two major bands are often superposed on a much broader, roughly triangular shaped component which stretches from about  $1810\text{ to }1050\text{ cm}^{-1}$  ( $5.5\text{ to }9.5\text{ }\mu\text{m}$ ) and peaks near  $1165\text{ cm}^{-1}$  ( $8.5\text{ }\mu\text{m}$ ). This broad feature does not seem to be correlated with the  $1615$  and "1300"  $\text{cm}^{-1}$  ( $6.2$  and "7.7"  $\mu\text{m}$ ) bands or with the broad  $3115\text{--}2740\text{ cm}^{-1}$  ( $3.2\text{--}3.65\text{ }\mu\text{m}$ ) component (Bregman *et al.* 1989; Geballe *et al.* 1989).

*The 1000–500 cm<sup>-1</sup> (10–20 μm) region.*— The prominent  $890\text{ cm}^{-1}$  ( $11.2\text{ }\mu\text{m}$ ) feature which dominates this region has also been shown to be superposed on a broader component which extends from  $950\text{ to }740\text{ cm}^{-1}$  ( $10.5\text{ to }13.5\text{ }\mu\text{m}$ ), with evidence for an additional band at about  $790\text{ cm}^{-1}$  ( $12.7\text{ }\mu\text{m}$ ) (Cohen, Tielens, and Allamandola 1985). Quite recently, the substructure on this plateau apparent in some previously published spectra at  $840$  and  $790\text{ cm}^{-1}$  ( $11.9$  and  $12.7\text{ }\mu\text{m}$ ) (Aitken *et al.* 1979*a, b*; Aitken and Roche 1982) has been confirmed, and variations in relative band strengths as a function of position in the Orion Nebula have been reported (Witteborn *et al.* 1989; Roche, Aitken, and Smith 1989; Bregman *et al.* 1989).

*The 500–10 cm<sup>-1</sup> (20–1000 μm) region.*— Observations in this region which are related to the mid-IR bands are limited because of the dominance of emission from cold dust and interference with telluric water bands. Nonetheless some objects which emit the mid-IR features also exhibit behavior in this region which may be relevant. For example, the spectrum of NGC 7027 by McCarthy, Forrest, and Houck (1978) shows a broad feature from about  $625\text{ cm}^{-1}$  ( $16\text{ }\mu\text{m}$ ) to  $330\text{ cm}^{-1}$  ( $30\text{ }\mu\text{m}$ ) which slowly drops in intensity out to roughly  $250\text{ cm}^{-1}$  ( $40\text{ }\mu\text{m}$ ). Other spectra showing similar behavior can be found in the *IRAS* catalog. The  $12$  and  $25\text{ }\mu\text{m}$  nonequilibrium *IRAS* band emission from reflection nebulae (Castelaz, Sellgren, and Werner 1987), as well as their

<sup>4</sup>Because of the lack of low-lying fundamental vibrational modes in simple molecules, when they are trapped in low-temperature inert gas solids, they can remain vibrationally excited for time scales comparable to the infrared emission times and consequently emit IR photons at their fundamental frequencies (Legay 1977; Abouaf-Marquin, Dubost, and Legay 1970; Bondybey 1984). It was for this reason that Allamandola and Norman (1978) suggested that detectable levels of IR emission might be produced by the UV-visible pumped IR fluorescence from simple molecules frozen in mantles.

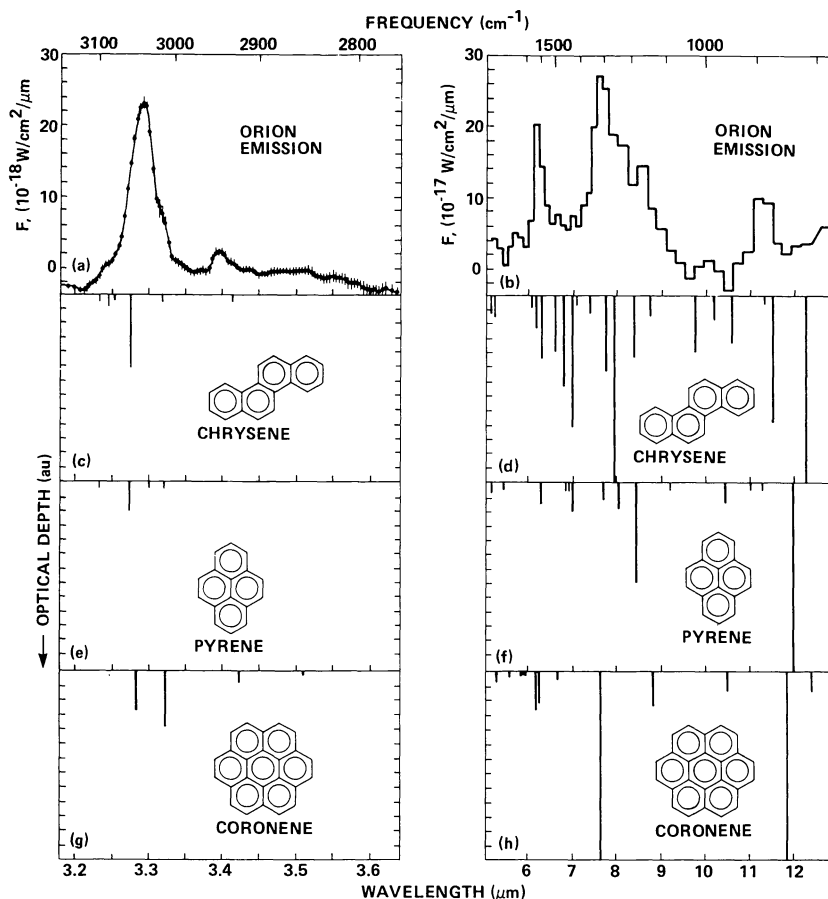


FIG. 1.—The 3–13  $\mu\text{m}$  emission spectrum from the Orion Bar compared with the absorption spectra of the PAHs chrysene, pyrene, and coronene suspended in KBr pellets. (Orion, Bregman *et al.* 1989; chrysene, Cyvin *et al.* 1982a; pyrene, Cyvin *et al.* 1979; coronene, Bakke *et al.* 1979; Cyvin *et al.* 1982b). A schematic representation for the absorption spectrum is used because the KBr pellet technique alters the spectrum, compared to that of a free species.

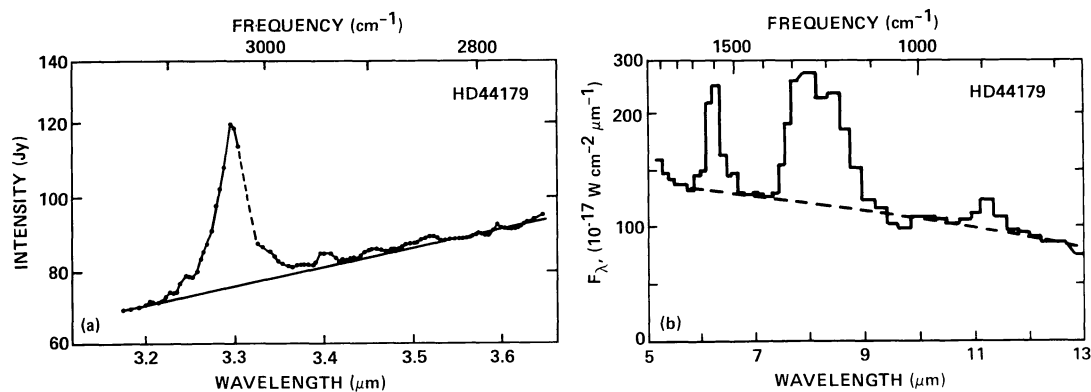


FIG. 2.—The infrared emission spectrum from the reflection nebula HD 44179, the Red Rectangle. Note that the “7.7  $\mu\text{m}$ ” feature here is quite different from the “7.7  $\mu\text{m}$ ” feature in the spectrum of the Orion Bar (Fig. 1) and NGC 7027 (Fig. 3). (a) from Geballe *et al.* 1985; (b) from Cohen *et al.* 1986.

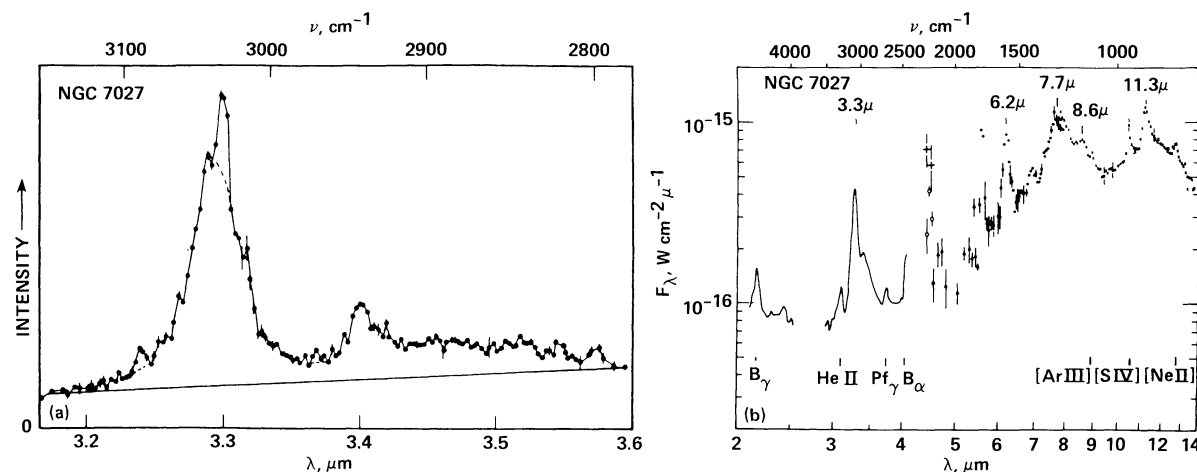


FIG. 3.—The infrared emission spectrum from the high-excitation planetary nebula NGC 7027. Note that the “7.7  $\mu\text{m}$ ” feature in this object differs markedly from the “7.7  $\mu\text{m}$ ” feature in the spectrum of the Red Rectangle shown in Fig. 2. (a) from Geballe 1984; (b) from Russell, Soifer, and Willner 1977.

intensity variations as a function of distance from the illuminating star (Luan *et al.* 1988), are probably all manifestations of emission from PAH-related materials. The high galactic latitude IR “cirrus” detected by Low *et al.* (1984), although not yet associated with discrete mid-IR bands, and the behavior of the 12 and 25  $\mu\text{m}$  *IRAS* band intensities from the clouds in the vicinity of hot stars (Boulanger *et al.* 1988) may also be related.

#### b) Comparison with the Spectra of PAH-related Materials

In Figure 1, the IR emission spectrum from position 4 in the Orion Bar is compared with a schematic version of the absorption spectra of three PAHs, chrysene ( $\text{C}_{18}\text{H}_{12}$ ), pyrene ( $\text{C}_{16}\text{H}_{10}$ ), and coronene ( $\text{C}_{24}\text{H}_{12}$ ). A similar comparison between the calculated emission spectra of different PAHs and several interstellar emission spectra can be found in LP and Leger and d’Hendecourt, 1987. The emission spectrum expected from chrysene is presented in ATBa and the calculation described in detail here, in § III. Perusal of dozens of IR absorption spectra of different PAHs assembled in the Sadler index confirms that they bear only a general resemblance to the interstellar spectra. The absorption (and calculated emission) spectra of PAHs (singly or in mixtures) generally fail to match the interstellar spectra in details such as band positions, relative intensities, or profiles across the entire mid-IR. While the resemblance suggests that PAH-like species are responsible, the differences imply that the interstellar mixture comprises species that have not been studied in the laboratory, but rather a mixture which includes some PAHs which are larger than those normally studied, ionized, dehydrogenated, and perhaps electronically excited.

The infrared signatures of amorphous carbon soots and chars also bear a general resemblance to the interstellar spectra (Fig. 4). For example, broad features at roughly 1610, 1300, and 885  $\text{cm}^{-1}$  (6.2, 7.7, and 11.3  $\mu\text{m}$ ) are evident in the extinction curve of amorphous carbon particles (Koiike, Hasegawa, and Manabe 1980; Borghesi *et al.* 1983). Sakata

*et al.* (1984) have shown that the absorption spectrum of the residue deposited by a methane plasma (quenched carbonaceous composite, QCC) also contains some bands suggestive of the interstellar spectral features. In ATBa we showed that there is a remarkable match between the Raman spectrum of auto soot and the 2000–1250  $\text{cm}^{-1}$  (5–8  $\mu\text{m}$ ) spectrum from the Orion Bar and pointed out that the infrared and Raman spectra of such carbonized materials are similar. Indeed, the IR spectrum of graphite ground for long periods of time shows two strong features at 1587 and 1360  $\text{cm}^{-1}$  (6.3 and 7.4  $\mu\text{m}$ ) (Friedel and Carlson 1972). Recently Goebel (1987) and Bussoletti, Colangeli, and Borghesi (1987) have also discussed the similarity between the interstellar emission spectrum and the absorption spectrum of amorphous carbon. This resemblance is not surprising as these materials are made up of a random mixture of PAHs linked by small amounts of nonaromatic hydrocarbons (see, for example, Oberlin, Boulmier, and Villey 1980; Oberlin 1984; and Marchand 1987). The overall emissivity of small particles comprised of PAH structural units will resemble PAH spectra, with the individual bands made less distinct due to the solid-state effects which produce line shifting, broadening, and intensity changes (Allamandola 1984). The infrared spectroscopic properties of small amorphous carbon particles will be largely determined by the properties of the PAHs of which they are made. As the particles get larger, bands will overlap and produce broad features, possibly showing some substructure indicative of the individual PAH structural units. Eventually bulk properties dominate and the broad features will appear as substructure on a strong continuum which follows a  $1/\lambda$  law (Tielens and Allamandola 1987a, b).

A very suggestive comparison of the interstellar spectra with a laboratory infrared absorption spectrum is afforded by that of the aromatic mixture reported by Mortera and Low (1983) and reproduced as the upper trace in Figure 4. The char was produced by heating organic samples under vacuum (Low and Mortera 1983). At the higher temperatures, the nonaromatic molecules decompose and rearrange into the thermodynamically more stable aromatic networks. While this

TABLE 1  
EMISSION COMPONENTS: PROPERTIES AND ASSIGNMENTS

$\nu$ ( $\text{cm}^{-1}$ )	$\lambda$ (microns)	FWHH ( $\text{cm}^{-1}$ )	Assignment
Major Bands			
3040 .....	3.29	30	Aromatic C-H stretch ( $\nu = 1 \rightarrow \nu = 0$ )
1615 .....	6.2	30	Aromatic C-C stretch
1315–1250 .....	7.6–8.0	70–200	Blending of several strong aromatic C-C stretching bands
1150 .....	8.7	...	Aromatic C-H in-plane bend
890.....	11.2	30	Aromatic C-H out-of-plane bend for nonadjacent, peripheral H atoms
Minor Features			
3085 .....	3.24	...	Overtone and/or combination involving fundamentals in the 1810–1050 $\text{cm}^{-1}$ (5.52–9.52 $\mu\text{m}$ ) range
2995 .....	3.34	...	Overtone and/or combination involving fundamentals in the 1810–1050 $\text{cm}^{-1}$ (5.52–9.52 $\mu\text{m}$ ) range
2940 .....	3.4	“20”	Aromatic C-H stretch ( $\nu = 2 \rightarrow \nu = 1$ )
2890 .....	3.46	...	Overtone/combination band involving fundamentals in the 1810–1050 $\text{cm}^{-1}$ (5.52–9.52 $\mu\text{m}$ ) range, aromatic C-H stretch (high $\nu$ ), aliphatic C-H stretch,?
2850 .....	3.51	...	Aromatic C-H stretch ( $\nu = 3 \rightarrow \nu = 2$ ), aliphatic C-H stretch, overtone/combination band involving fundamentals in the 1810–1050 $\text{cm}^{-1}$ (5.52–9.52 $\mu\text{m}$ ) range
2810 .....	3.56	...	Aromatic C-H stretch (high $\nu$ ), aldehydic C-H stretch, overtone/combination band involving fundamentals in the 1810–1050 $\text{cm}^{-1}$ (5.52–9.52 $\mu\text{m}$ ) range
1960–1890 .....	5.1–5.3	30	Combination of C-H out-of-plane and in-plane bend,?
1785–1755 .....	5.6–5.7	40	Overtone of 885 $\text{cm}^{-1}$ (11.3 $\mu\text{m}$ ) band; aromatic C-C stretch; Carbonyl C-O stretch,?
1470–1450 .....	6.8–6.9	30	Aromatic C-C stretch, aliphatic C-H deformation
840.....	11.9	...	C-H out-of-plane bend for doubly adjacent H atoms
790.....	12.7	...	C-H out-of-plane bend for triply adjacent H atoms
Broad Components			
2940 .....	3.5		Overlap of C-H stretching modes, shifted by anharmonic effects, with overtones and combinations of C-C stretch fundamentals in the 1670–1250 $\text{cm}^{-1}$ (6–8 $\mu\text{m}$ ) region, aliphatic C-H stretch?,?
3115–2740 <sup>a</sup> .....	3.21–3.65 <sup>b</sup>	“300”	
~1200.....	~8.5	“400”	Blending of many weak aromatic C-C stretching bands
1810–1050 <sup>a</sup> .....	5.52–9.52 <sup>b</sup>		Overlap of many aromatic C-H out-of-plane bending modes for nonadjacent as well as doubly and triply adjacent peripheral H-atoms
880.....	12	“160”	
950–740 <sup>a</sup> .....	10.5–13.5 <sup>b</sup>		
Red–Near-IR Continuum .....			Electronic transitions between low-lying levels in ionized and complexed PAHs and amorphous carbon particles
Mid-IR Continuum .....			Quasi-continuum formed by overlapping overtone and combination bands

NOTE.—value estimated from several published spectra. When the assignment is not clear, several possible explanations are listed. The first seems most likely.

<sup>a</sup>Rough limits of the feature.

method of producing the material is no more relevant to the interstellar problem than combustion or arc and microwave discharges, we believe that the good overall spectral agreement provides strong evidence that similar materials are involved. From the numerous spectra presented by Mortera and Low covering the 22°–600°C range, the two at 400 and 480°C have been selected to demonstrate the significant spectral differences between a mixture containing both aliphatic and aromatic hydrocarbons (400°C), and one primarily comprised of aromatic hydrocarbons (480°C) (Fig. 4).

### c) Interstellar Feature Assignments

Each of the features and assignments listed in Table 1 will now be considered in detail in the same frequency regions used to present the interstellar spectra. In each of the frequency regions the major bands will be discussed first, the minor bands next, and the broad features last. While the case is made that most of the spectral characteristics can be accounted for within the framework of the PAH model, several can also be rationalized by other carriers as well. More detailed identifications will have to await additional labora-

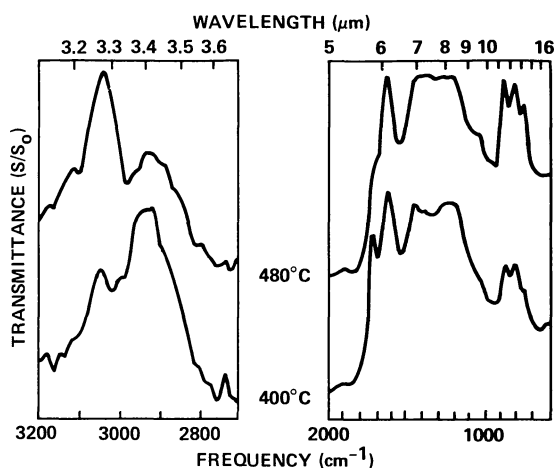


FIG. 4.—Infrared absorption spectra of chars at 400 and 480°C. Note the similarity between the 480°C char (a form of amorphous carbon) absorption spectrum, with the interstellar infrared emission spectrum and with the Raman spectrum of soot in ATBa. (Char spectra from Mortera and Low 1983).

tory data on PAHs in the forms expected in the interstellar medium, and higher spectral and spatial resolution observational data for more objects.

i) *The 3200–2700 cm<sup>-1</sup> (3.13–3.7 μm) Region*

1. *The 3040 cm<sup>-1</sup> (3.29 μm) major band.*—Figures 1, 2, and 3 show that this region is dominated by the 3050 cm<sup>-1</sup> (3.28 μm) emission band. This frequency is well known among IR spectroscopists as characteristic of the aromatic CH stretch (Herzberg 1968; Bellamy 1958). This frequency played a strong role in Duley and Williams first suggestion of an aromatic carrier of the interstellar spectra in 1981. The 30 cm<sup>-1</sup> FWHH is probably due more to nonradiative vibrational energy redistribution times within an individual molecule rather than the overlapping of bands from different PAHs along the line of sight (Allamandola, Tielens, and Barker 1985; Barker, Allamandola, and Tielens 1987). A homogeneous linewidth of 30 cm<sup>-1</sup> implies a redistribution time of about 0.2 picoseconds, a value consistent with the vibrational energy redistribution time in other large molecules (Amirav and Jortner, 1984; Amirav, Even, and Jortner 1981; Bondybey 1984). It has recently been found that the band is narrower than shown in Figure 2, by nearly a factor of 2, in the high flux vicinity of the star HD 44179 (Tokunaga *et al.* 1988).

2. *The minor bands in the 3200–2700 cm<sup>-1</sup> (3.13–3.7 μm) region.*—There are a number of weak bands in this region. Unresolved shoulders straddle the major band at about 3085 and 2995 cm<sup>-1</sup> (3.24 and 3.34 μm) (see Figs. 1a, 2a, and 3a). These fall in the range generally assigned to overtones and combination bands involving C-C stretching fundamentals in the 1810–1050 cm<sup>-1</sup> (5.52–9.52 μm) region and are responsible for most of the weak absorptions in Figures 1c, e, and g (Herzberg 1968; Bellamy 1958; Cyvin *et al.* 1979, 1982a, b). These features should always be present in emission when the

3040 cm<sup>-1</sup> (3.29 μm) major band is intense because any species with enough internal energy to populate the fundamental at 3050 cm<sup>-1</sup> contains enough energy to doubly populate the C-C stretching fundamentals. Fermi resonances between these different modes and the IR active C-H stretch will certainly contribute to the intensity enhancement as well. Many objects show a clear, weak band at about 2940 cm<sup>-1</sup> (3.4 μm) (Geballe *et al.* 1985), and weaker bands have recently been discovered at 2890, 2850, and 2810 cm<sup>-1</sup> (3.46, 3.51, and 3.56 μm) (de Muizon *et al.* 1986). We have attributed the 2940 cm<sup>-1</sup> and the 2850 cm<sup>-1</sup> bands to the ( $v=1$ ) ← ( $v=2$ ) and ( $v=2$ ) ← ( $v=3$ ) aromatic C-H stretch transition which have been shifted due to anharmonic effects (Barker, Allamandola, and Tielens 1987). Others have argued that they are carried by methyl (—CH<sub>3</sub>), methylene (—CH<sub>2</sub>—), and perhaps aldehydic (—HCO) sidegroups on PAHs (de Muizon *et al.* 1986).

Within the framework of the anharmonicity picture, the prominence of the 2940 cm<sup>-1</sup> band is directly related to the vibrational energy content of the emitter. Thus anharmonicity can account for the presence of a band at these frequencies as well as the observation that it is most prominent in high-excitation objects such as NGC 7027 (Fig. 3) and on the ionization ridge in the Orion Nebula (Fig. 1a). Since the ultraviolet-exciting spectrum can be characterized in several astronomical objects, the dependence on energy content can be used to deduce the size range of the species which dominate the emission. Analysis of the observed 3050–2940 cm<sup>-1</sup> (3.28–3.4 μm) intensity ratios shows that PAHs containing between 20 and 30 carbon atoms dominate the emission in this region (Barker, Allamandola, and Tielens 1987). Spectra taken at several positions near the ionization ridge in the Orion Nebula show that the 2940 and 2850 cm<sup>-1</sup> (3.4 and 3.51 μm) band intensities vary with respect to the major band at 3040 cm<sup>-1</sup> (3.29 μm) in a way which is consistent with the emission originating from upper C-H stretch vibrational levels (Geballe *et al.* 1989). The spatial behavior of the 2890 cm<sup>-1</sup> (3.46 μm) component however seems to track the 3040 cm<sup>-1</sup> major band implying that it arises from an overtone or combination band.

The minor bands in this region probably represent a blend of the ( $v=1$ ) ← ( $v=2$ ) and ( $v=2$ ) ← ( $v=3$ ) aromatic C-H stretching transitions with overtones and combinations involving aromatic C-C stretches and possibly aliphatic C-H stretches as well. Many PAHs which do not have aliphatic side groups show weak absorptions near these frequencies. For example, Figure 5 shows that chrysene, pyrene, and coronene all show substructure on a broad component. Chrysene and coronene show a “peak” at about 2910 and 2845 cm<sup>-1</sup> (3.44 and 3.52 μm), while pyrene has a broad (weak) plateau from 2950 to 2880 cm<sup>-1</sup> (3.39–3.47 μm) (which is similar to the emission plateau observed from the astronomical object BD +30°3639; Geballe *et al.* 1985). In the laboratory spectra these are due to overtone and combination bands of the C-C stretch which have been perturbed sufficiently by solid-state effects to absorb weakly. The perturbations within the PAH clusters that are suspended in salt pellets induce IR activity and broaden the individual bands causing them to overlap. In free vibrationally excited PAHs, perhaps Fermi

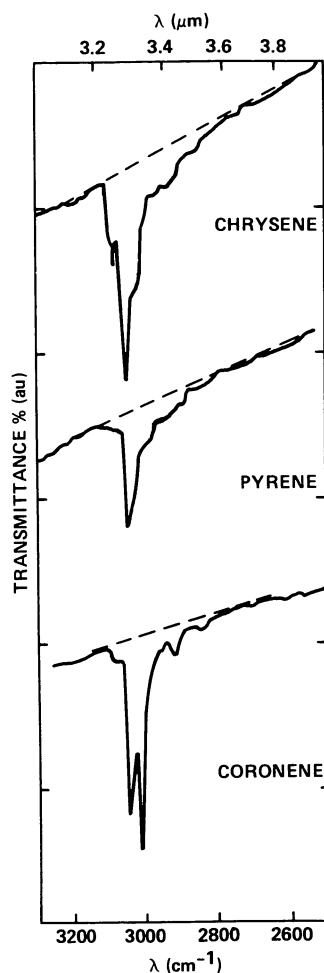


FIG. 5.—Infrared absorption spectra in the  $3000\text{ cm}^{-1}$  ( $3\text{ }\mu\text{m}$ ) region of the PAHs chrysene, pyrene, and coronene suspended in KBr. Spectra courtesy of Drs. Cyvin and Klaeboe, University of Trondheim, Norway.

resonances between the overtones and combinations of C-C stretching vibrations with the highly excited C-H modes can sufficiently enhance the intensities of these presumably weak bands to produce the observed intensities.

3. *The broad component in the  $3200\text{--}2700\text{ cm}^{-1}$  ( $3.1\text{--}3.7\text{ }\mu\text{m}$ ) region.*—Inspection of Figures 1a and 3 show that there is a broad component which stretches from about  $3130$  to  $2750\text{ cm}^{-1}$  ( $3.2\text{--}3.6\text{ }\mu\text{m}$ ) in some interstellar spectra. We have assigned this to a vibrational quasi-continuum produced by the overlapping of the different transitions discussed in the previous section: highly excited aromatic C-H stretching vibrations, overtones, and combinations of C-C stretching vibrations and perhaps C-H stretches on aliphatic side groups. The spatial behavior of the intensity of this broad component appears to follow the distribution of the major and minor bands in this frequency region, rather than the distribution of the lower frequency, broad features discussed in §§ IIc[ii]3 and IIc[iii]3 which are due to much larger PAHs and perhaps PAH clusters and amorphous carbon particles (Bregman *et al.* 1989). Thus this broad component is most likely due to emission from molecule sized free PAHs.

## ii) The $2000\text{--}1000\text{ cm}^{-1}$ ( $5\text{--}10\text{ }\mu\text{m}$ ) Region

1. *The  $1610$ , “ $1350$ ,” and  $1150\text{ cm}^{-1}$  ( $6.2$ , “ $7.7$ ,” and  $8.7\text{ }\mu\text{m}$ ) major bands.*—Leger and Puget (1984) pointed out that the frequency of the  $1610\text{ cm}^{-1}$  ( $6.2\text{ }\mu\text{m}$ ) band is also characteristic of polycyclic aromatic hydrocarbons and attributed it to an aromatic C-C stretching fundamental (Bellamy 1958). As with the  $3040\text{ cm}^{-1}$  band, the width of about  $30\text{ cm}^{-1}$  probably reflects vibrational energy redistribution times within the molecules contributing to this band rather than a blending of narrower lines from different molecules. Some interstellar spectra show a slight asymmetry on the low-frequency side of this feature (e.g., see Figs. 1b and 3b; Cohen *et al.*, 1986, 1989). This is suggestive of a contribution of emission from higher vibrational levels. As the anharmonicity of the C-C stretch is thought to be smaller than the natural bandwidth (a few  $\text{cm}^{-1}$  vs.  $30\text{ cm}^{-1}$ ), blending should skew the band to lower frequencies (Barker, Allamandola, and Tielens 1987).

The peak position and profile of the very broad “ $1310$ ”  $\text{cm}^{-1}$  (“ $7.7$ ”  $\mu\text{m}$ ) band, on the other hand, vary from object to object and its assignment has been correspondingly less straightforward (ATBb; Bregman 1989; Cohen *et al.* 1989). We pointed out that this band could be assigned to the aromatic C-C stretching vibrations for the following reasons (ATBa). The observed variation in peak position is consistent with PAHs since the frequency range across the base of the interstellar feature encompasses the frequencies expected for the strongest IR active C-C stretching modes in a mixture of PAHs (e.g., see Figs. 1d, f, and h). Unlike the  $3040$  and  $1610\text{ cm}^{-1}$  ( $3.29$  and  $6.2\text{ }\mu\text{m}$ ) bands which consistently occur at nearly the same frequency in different aromatic molecules, the precise positions of these other IR active aromatic C-C stretches vary from molecule to molecule. Figure 1 shows that chrysene, pyrene, and coronene have several strong C-C stretching bands in this region. As molecule size, degree of ring condensation, and symmetry increase, the relative intensities of the  $1610$  and  $1460\text{ cm}^{-1}$  ( $6.2$  and  $6.9\text{ }\mu\text{m}$ ) bands seem to reverse. Thus, if the interstellar mixture were complex enough, its IR spectrum in this region would show a broad feature peaking near  $1300\text{ cm}^{-1}$  ( $7.7\text{ }\mu\text{m}$ ), possibly exhibiting some substructure.

In the interstellar medium less stable PAHs will be weeded out, leaving a mixture dominated by the most stable structures (van der Zwet and Allamandola 1985; Crawford, Tielens, and Allamandola 1985). These more stable PAHs are those which are symmetric and generally in the most condensed forms. An example of a mixture comprised largely of the most stable molecular forms is the soot formed in the high-temperature combustion of hydrocarbons. A striking comparison of the Raman spectrum in the  $1670\text{--}1250\text{ cm}^{-1}$  region of auto soot with the interstellar IR emission spectrum from Orion strongly supports a common carrier (ATBa). The Raman spectrum of soot principally probes the aromatic C-C stretching vibrational frequencies in this material because the Raman scattering cross section for these bonds is very large and they are the most dominant type of bond in the mixture. Of course, for free PAHs with an inversion center of symmetry the infrared and Raman active modes will be mutually exclusive. However, the perturbations in the soot particles

break down the symmetry selection rules and the IR and Raman spectra become similar as shown by comparing the IR spectra of high-temperature carbonaceous materials such as shown in Figure 4 (Morterra and Low 1983; Friedel and Carlson 1972; Wdowiak, Flickinger, and Cronin 1988) with the Raman spectrum of soot (ATBa). This comparison shows that the distribution of the C-C stretching frequencies in a mixture of the more stable PAHs coincides quite well with the frequency range of the major interstellar emission bands in the 2000–1000  $\text{cm}^{-1}$  region. Assignment of the “1310”  $\text{cm}^{-1}$  interstellar feature primarily to vibrations in symmetric interstellar PAHs is supported by the comparison of the interstellar emission spectrum from the reflection nebula NGC 2023 (Sellgren *et al.* 1985) with the infrared emission calculated from the measured absorption spectra of symmetric and asymmetric PAHs made by Leger and d’Hendecourt (1987).

The last major band in this region falls near 1150  $\text{cm}^{-1}$  (8.7  $\mu\text{m}$ ) and often appears as a small shoulder to the broad “1310”  $\text{cm}^{-1}$  (“7.7”  $\mu\text{m}$ ) feature but is resolved in certain objects (Figs. 1 and 3). It was assigned to the in-plane aromatic C-H bending vibration.

Summing up, the 1610 and “1310”  $\text{cm}^{-1}$  bands are indicative of aromatic hydrocarbons and have been assigned to the aromatic C-C stretch. The variability of the peak position and profile of the “1310”  $\text{cm}^{-1}$  feature implies further that symmetric PAHs, the most stable members of the PAH family, dominate the interstellar mixture.

2. *The minor bands in the 2000–1000  $\text{cm}^{-1}$  (5–10  $\mu\text{m}$ ) region.*—There are three minor emission bands at about 1920, 1780, and 1460  $\text{cm}^{-1}$  (5.2, 5.6, and 6.8  $\mu\text{m}$ ) which have been associated with the interstellar emission spectrum.

An emission band in the 1900  $\text{cm}^{-1}$  region was anticipated because nearly all laboratory PAH spectra show a weak band between 1960 and 1890  $\text{cm}^{-1}$  (5.1 and 5.3  $\mu\text{m}$ ). Based on this expectation, the spectrum of BD +30°3639 was measured in the 2000–1500  $\text{cm}^{-1}$  (5–6.6  $\mu\text{m}$ ) region and a new emission band at about 1900  $\text{cm}^{-1}$  was indeed found (Allamandola *et al.* 1989). Most spectra of objects which show the major bands start to turn up at about 1850  $\text{cm}^{-1}$ , implying that most objects which emit the features have a band at this position (Cohen *et al.* 1986, 1989). The confirmation of this feature provides strong support for the PAH hypothesis. Although the mode assignment is not well established, consideration of the relative absorption band strengths in previously published spectra and the symmetry assignments suggest that this is a combination (or overtone?) of the C-H bending modes.

The 1780 and 1460  $\text{cm}^{-1}$  (5.6 and 6.9  $\mu\text{m}$ ) band intensities are variable. They were recognized in the spectrum of NGC 7027 (Fig. 3) and attributed to the IR emission band system by Bregman *et al.* (1983). Weak correlation between these and the major bands in several objects confirms that they are part of the emission band family (Cohen *et al.* 1986). There are several possible assignments for the 1780  $\text{cm}^{-1}$  (5.6  $\mu\text{m}$ ) band. It could correspond to one of the weaker PAH features such as shown in Figures 1*d*, *f*, and *h*, either as a weakly allowed C-C stretching fundamental, or, as suggested by Bregman *et al.* (1983), it may be an overtone of the major 885

$\text{cm}^{-1}$  (11.3  $\mu\text{m}$ ) band. Alternatively, since this frequency is highly characteristic of the C=O stretch, it may arise from a carbonyl attached to a PAH or an aliphatic hydrocarbon chain. A carbonyl in the form of an aldehyde can be ruled out since there has been no detection of a prominent feature attributable to an aldehydic C-H stretch near 2860  $\text{cm}^{-1}$  (3.5  $\mu\text{m}$ ) in the objects which show a clear 1760  $\text{cm}^{-1}$  (5.6  $\mu\text{m}$ ) band. It will not be possible to determine which explanation is more likely until additional high-resolution astronomical spectra and laboratory spectra of suitable candidate materials are available.

The 1450  $\text{cm}^{-1}$  (6.9  $\mu\text{m}$ ) band probably corresponds to an aromatic C-C stretching vibration (although it is conceivable that it may be an overtone or combination band involving C-H out-of-plane bending modes). Since only some PAHs absorb at this frequency (Figs. 1*d*, *f*, *h*), emission from a collection of PAHs could produce a relatively weak feature here. Since the strength of this band depends strongly on the symmetry and geometry of the molecule, it may be a probe of the chemistry in the emitting region. An aliphatic C-H deformation seems unlikely because, up to now, bands attributable to the aliphatic C-H stretching modes in the 3000  $\text{cm}^{-1}$  (3  $\mu\text{m}$ ) region do not seem to correlate with the 1450  $\text{cm}^{-1}$  band. Again, more observations are needed to sort this out.

3. *The broad component in the 2000–1000  $\text{cm}^{-1}$  (5–10  $\mu\text{m}$ ) region.*—Inspection of Figures 1*b* and 3*b* clearly shows the presence of a broad, very roughly triangularly shaped hump underlying the 1615 and “1300”  $\text{cm}^{-1}$  (6.2 and “7.7”  $\mu\text{m}$ ) bands. This broad component is also evident in the spectra of other objects (Cohen *et al.* 1986, 1989). As discussed in § c[iii] this feature encompasses the region in which the IR active, C-C stretching modes in PAHs are richest. For example, of the 72 normal modes in pyrene, 42 involve C-C vibrations (59%), while in ovalene, 90 of the 132 (68%) are purely C-C in character. While a certain fraction are infrared inactive, or only weakly allowed, and many involve lower frequency bending modes, it is clear that PAHs (and PAH clusters) possess many bands that can overlap and produce a broad feature in this region. This is the reason that the vibrational spectra of amorphous carbon particles (mixtures of aromatic structural units) have a strong feature in this region (Koike, Hasegawa, and Manabe 1980; Tuinstra and Koenig 1973; Mortera and Low 1983; Wdowiak, Flickinger, and Cronin 1988; Blanco, Bussoletti, and Colangeli 1988).

The importance of this component in the interstellar emission spectrum depends on both the intensity (flux) and energy of the ultraviolet radiation field. In objects where very energetic photons are plentiful, such as in NGC 7027, larger PAHs and materials composed of several smaller PAHs clustered together (loosely or in small amorphous carbon particles) may be excited sufficiently to emit in this band with intensities comparable to the intensities of the discrete features emitted by isolated PAHs. In regions where the ultraviolet radiation field is less intense and less energetic, such as in many reflection nebulae with much cooler exciting stars, small molecules can survive and their emission features tend to dominate the spectrum. The observed variability in intensity of this band with respect to the major band intensities is

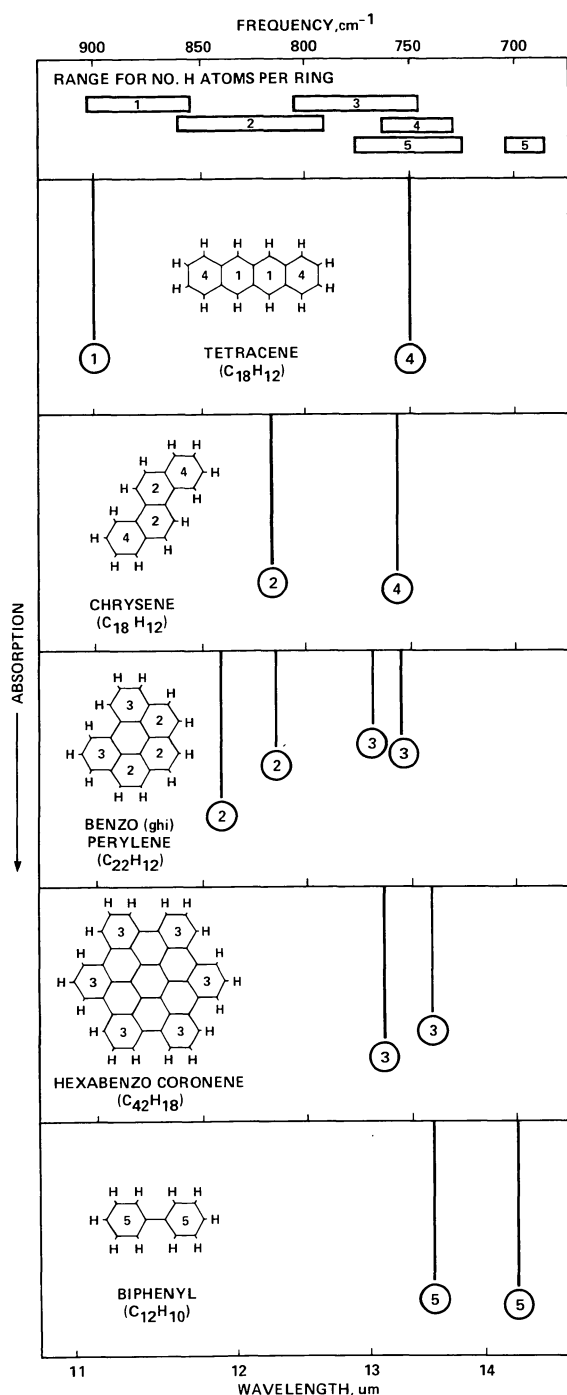


FIG. 6.—Schematic representation of the absorption spectra of PAHs which have different numbers of peripheral H atoms per edge ring in the C-H out-of-plane bending region. The number of H atoms per edge ring are indicated in each ring and the corresponding absorption bands are labeled. The upper frame shows the spectral regions in which different edge structures absorb.

consistent with an origin in C-C vibrations in larger PAHs, PAH clusters, and amorphous carbon particles containing on the order of 500 carbon atoms (see § Va, and Bregman *et al.* 1989).

In conclusion, the 2000–1000  $\text{cm}^{-1}$  (5–10  $\mu\text{m}$ ) region of the interstellar emission spectrum can have two important contributors—free PAHs and small amorphous carbon particles or clusters of PAHs.

### iii) The 1000–500 $\text{cm}^{-1}$ (10–20 $\mu\text{m}$ ) Region

1. *The 890  $\text{cm}^{-1}$  (11.2  $\mu\text{m}$ ) major band.*—For some time, the only feature in this region believed to be associated with the other emission bands was the prominent 890  $\text{cm}^{-1}$  (11.2  $\mu\text{m}$ ) band shown in Figures 1, 2, and 3. This was assigned to the out-of-plane aromatic C-H bending vibration by Duley and Williams in 1981. The 890  $\text{cm}^{-1}$  band is skewed to lower frequencies in most spectra implying that emission from higher vibrational levels contributes to the band (Barker, Allamandola, and Tielens 1987). For highly vibrationally excited molecules the band will be quite asymmetric, broader, and peaked at slightly lower frequencies than that from molecules containing less vibrational energy. The prominence of the band implied that the aromatic carriers be only partially hydrogenated since, as shown in Figure 6, IR activity at 890  $\text{cm}^{-1}$  (11.2  $\mu\text{m}$ ) is characteristic of aromatic systems with edge rings which contain only isolated, nonadjacent peripheral hydrogen atoms (Bellamy 1958). Figures 1d, f, and h, 4, 6 and 7 illustrate that fully hydrogenated PAHs possess several strong bands in the 900–500  $\text{cm}^{-1}$  (11.3–20  $\mu\text{m}$ ) region. Partial hydrogenation is unexpected because hydrogen is more than  $10^7$  times more abundant than the proposed PAHs. This apparent inconsistency was resolved by the results described in the next two subsections.

2. *The minor bands in the 1000–500  $\text{cm}^{-1}$  (10–20  $\mu\text{m}$ ) region.*—Quite recently weak, resolvable substructure has been detected at about 840 and 790  $\text{cm}^{-1}$  (11.9 and 12.7  $\mu\text{m}$ ) by Roche, Aitken, and Smith (1989) and Witteborn *et al.* (1989). These new bands are just where one would expect to find them for PAHs with doubly and triply adjacent H atoms per edge ring, relieving somewhat the constraint of partial dehydrogenation (Fig. 6). As discussed in the next subsection and § IVc, these new bands place important constraints on the molecular geometries of the emitting PAHs. As with some of the minor bands in the 3000–2500  $\text{cm}^{-1}$  (3–4  $\mu\text{m}$ ) region, the intensities of the 890 and 790  $\text{cm}^{-1}$  (11.2 and 12.7  $\mu\text{m}$ ) bands vary across the ionization ridge in the Orion Nebula, suggesting that certain PAHs may be particularly favored under the conditions which prevail in that region (Roche, Aitken, and Smith 1989).

The relative intensities of the bands in this region pose several questions. If one assumes that the integrated absorbance per H atom is comparable for single as well as doubly and triply adjacent H atoms per edge ring, one is still faced with a surprisingly large fraction of partially dehydrogenated PAHs. Detailed analysis of what this means in terms of the interstellar medium must wait until one has reliable band strengths for these different types of peripheral hydrogen atoms in isolated PAHs.

3. *The broad component in the 1000–500 cm<sup>-1</sup> (10–20 μm) region.*—Telluric obscuration at frequencies below about 800 cm<sup>-1</sup> (13 μm) hindered completing measurements in this region until the launch of *IRAS* which detected a low-intensity emission plateau extending from about 950 to 750 cm<sup>-1</sup> (10.5 to 13.5 μm) in the spectra of objects that emit the 890 cm<sup>-1</sup> (11.2 μm) band (Cohen, Tielens, and Allamandola 1985). This observation relieved the difficulty associated with proposing only partial hydrogenation in exceedingly hydrogen-rich environments because it showed that the edge rings of the PAHs responsible for the features can have nonadjacent as well as two or three adjacent peripheral H atoms, but not four or five (Fig. 6). This placed strong, important constraints on the molecular geometries of the aromatic hydrocarbons. These constraints, discussed further in § IVc, are consistent with the conclusion drawn earlier (from the position and profile of the “1310” cm<sup>-1</sup> (“7.7” μm) band) that the most condensed, stable PAHs dominate the interstellar mixture.

This broad component, along with the major and minor bands in this region, are generally much less intense than the “1310” cm<sup>-1</sup> (“7.7” μm) feature whereas the opposite is true in the laboratory spectra (Fig. 1). This later discrepancy has been shown to be the result of a spectral artifact produced by the techniques used to measure most of the PAH spectra published to date. Most laboratory spectra are obtained by mixing PAH crystallites with salt and pressing the mixture into a transparent pellet. *Individual PAH molecules are not isolated in this way.* Molecular interactions between adjacent PAHs produce large band strength enhancements in the 900–500 cm<sup>-1</sup> (11–20 μm) regions (Allamandola and Sandford 1988). This property is not only important because it reconciles an apparently serious intensity inconsistency with the PAH hypothesis but also because it provides a powerful spectroscopic argument in favor of the well-defined bands arising from free, molecule-sized species rather than particles (in which interactions would be expected to enhance emission in this region).

iv) *The 500–10 cm<sup>-1</sup> (20–1000 μm) Region*

Although the laboratory and observational data covering this range are limited, some interesting suggestions can be made. Figure 7 is a schematic representation of a composite absorption spectrum which shows all the bands measured in this region for the four PAHs: naphthalene, chrysene, pyrene, and corone. It illustrates that a mixture of PAHs would produce a broad component in the 625–330 cm<sup>-1</sup> (16–30 μm) range as lower frequency bands are sparse and molecule specific. These bands are at least a factor of 2 weaker than the mid-IR bands in these PAHs (although this may be an artifact produced by the steric constraints placed on such collective large molecule vibrations by the solid matrices in which they are usually studied). These bands are due to out-of-plane bending motions of the carbon skeleton of the PAHs. Since they fall at such low frequencies, emission from larger PAHs (which may not be important at the higher frequencies) could contribute significantly to this region (§ IIIa[iii]3).

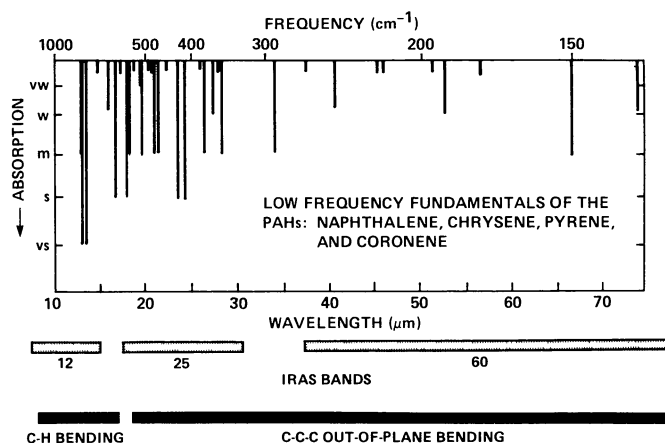


FIG. 7.—A schematic composite absorption spectrum for the out-of-plane vibrations in a mixture of the aromatic molecules: naphthalene, chrysene, pyrene, and coronene in the 1000–130 cm<sup>-1</sup> (10–75 μm) range compared to the *IRAS* bands. The regions in which the CH in- and out-of-plane, and carbon plane bending vibrations fall are also indicated.

Thus, based on the PAH hypothesis, objects showing the major bands and the broad features would also be expected to show broad but low-level emission extending from the mid-IR out to about 330 cm<sup>-1</sup> (30 μm) as well as several discrete lines at much lower frequencies (ATBa). This emission will be difficult to detect since the features may be inherently weak and since emission from large cold dust grains dominates the lower frequencies of this spectral region. However, under the right conditions of excitation and geometry, detection should be possible.

In fact, there are some indications that such emission has already been detected. For example, the low-level plateau measured for NGC 7027 by McCarthy, Forrest, and Houck (1978), reproduced in Figure 8, shows some suggestive similarities to what would be expected based on Figure 7. The plateau extends from about 625 cm<sup>-1</sup> (16 μm) out to 330 cm<sup>-1</sup> (30 μm) and slowly drops thereafter out to 250 cm<sup>-1</sup> (40 μm). Other examples can be found in the *IRAS* LRS Catalog. The high Galactic latitude IR “cirrus” emission reported by Low *et al.* (1984) may originate from low-frequency vibrations in PAHs as well. The correlation between the nonthermal 10 and 25 μm broad-band emission which extends across the Merope nebula (Castelaz, Sellgren, and Werner 1987) may be another manifestation of emission from PAH-related materials. If PAHs and PAH-related materials are indeed responsible, the decrease in the 12 to 25 μm *IRAS* band ratios found as one gets close to the exciting star in reflection nebulae (Luan *et al.* 1988) and H II regions (Puget 1988) indicates that the smaller PAHs are dehydrogenated near the source in a manner similar to that in Orion (Geballe *et al.* 1989). Figure 7 shows that the loss of H will reduce PAH emission in the 1250–670 cm<sup>-1</sup> (8.5–15 μm) C-H in- and out-of-plane bend region, but will not influence the emission intensity in the ~670–10 cm<sup>-1</sup> (15–100 μm) carbon-bending range. Finally, the broad IR excess in this spectral region found in the spectrum of carbon stars may

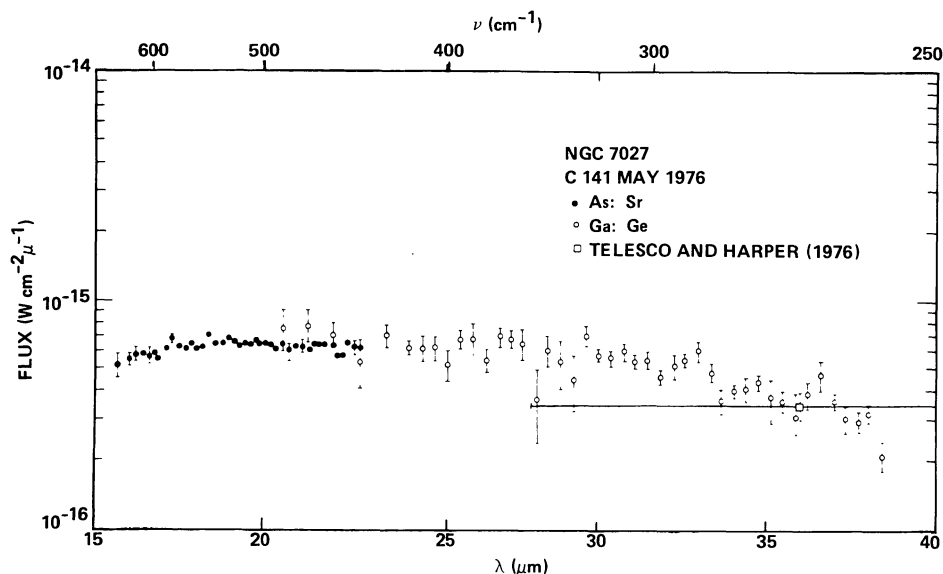


FIG. 8.—The emission from NGC 7027 in the  $665\text{--}250\text{ cm}^{-1}$  ( $15\text{--}40\ \mu\text{m}$ ) range (figure reproduced from McCarthy, Forrest, and Houck 1978).

also arise from these bands (Forrest, Houck, and McCarthy 1981).

v) *The Vibrational Quasi-Continuum from  $5000\text{--}500\text{ cm}^{-1}$  ( $2\text{--}20\ \mu\text{m}$ )*

There is evidence that a weak, basically flat “continuum” spans the entire mid-IR spectral range in many of the objects which show the IR emission features. The flux in this continuum is difficult to determine in most cases because of the poor signal-to-noise ratio inherent in measuring such low-level signals. Nonetheless, the  $3040\text{ cm}^{-1}$  ( $3.29\ \mu\text{m}$ ) line to adjacent continuum ratio has been measured and lies between 5 and 10 in several reflection nebulae (Sellgren, Werner, and Dinerstein 1983; Sellgren *et al.* 1985). The presence of this continuum provides further support of the highly vibrationally excited molecule explanation of the emission bands.

Emission from highly vibrationally excited molecules can produce a vibrational quasi-continuum that spans the entire mid-IR. This is due to the overlapping of many weak bands. When a molecule contains sufficient vibrational energy that the density of vibrational states is quasi-continuous, transitions which are normally forbidden can become weakly allowed. For molecules in the ground state, such combinations are strongly forbidden by symmetry selection rules. In highly vibrationally excited molecules, however, because molecular symmetry is slightly reduced, the selection rules break down and such combinations become weakly allowed. For example, various combinations of several ring puckering and C-C-C bending modes, which fall in the far-IR frequency range ( $600\text{--}10\text{ cm}^{-1}$ ,  $16\text{--}1000\ \mu\text{m}$ ), with C-C stretching modes, which fall in the  $1800\text{--}1000\text{ cm}^{-1}$  ( $5.5\text{--}10\ \mu\text{m}$ ) range, can fill in the region between about  $2700\text{--}1800\text{ cm}^{-1}$  ( $3.7\text{--}5.5\ \mu\text{m}$ ). The  $3100\text{--}2700\text{ cm}^{-1}$  ( $3.2\text{--}3.7\ \mu\text{m}$ ) pedestal can be assigned to overtones and combinations involving pure C-C stretching vibrations. At the higher mid-IR frequencies, combinations of C-H stretching vibrations with the low-lying modes extend

the continuum out to the  $4000\text{--}5000\text{ cm}^{-1}$  ( $2.5\text{--}2.0\ \mu\text{m}$ ) region. Since C-H vibrations can couple only weakly to C-C vibrations, the level of the continuum in this region will be lower. Beyond this, the vibrational quasi-continuum will drop rapidly. At this end however, there is the possibility of overlap with transitions between low-lying electronic states. This is particularly true for such electron-rich systems as PAHs. PAH ions are known to have electronic transitions which extend beyond the  $10,000\text{ cm}^{-1}$  ( $1\ \mu\text{m}$ ) region (Hoiijtink 1959; Hoiijtink and Zandstra 1960).

The requirement for a molecule to produce a vibrational quasi-continuum is a high level of vibrational excitation, not molecular complexity. Extremely simple species can produce vibrational quasi-continua. Figure 9 shows the evolution of the  $4000\text{--}1000\text{ cm}^{-1}$  ( $2.5\text{--}10\ \mu\text{m}$ ) emission spectrum from the highly vibrationally excited radical  $\text{CH}_2\text{I}^*$  reported by Baughcum and Leone (1980). The excited radicals were produced by the photolysis of  $\text{CH}_2\text{I}_2$  with  $37,600\text{ cm}^{-1}$  ( $2660\ \text{\AA}$ ) photons. Depending on the energy carried away by the I photofragment,  $\text{CH}_2\text{I}^*$ , which has only six vibrational modes, contains  $10,000$  or  $17,500\text{ cm}^{-1}$  of vibrational energy. One microsecond after photolysis, the emission spectrum clearly shows nearly flat vibrational emission which extends across the entire mid-IR and may be identified with the quasi-continuum. Superposed on the continuum are broad peaks which correspond to the C-H stretching vibration ( $\sim 3000\text{ cm}^{-1}$ ,  $3.3\ \mu\text{m}$ ), the  $\text{CH}_2$  bending vibrations ( $\sim 1300\text{ cm}^{-1}$ ,  $7.7\ \mu\text{m}$ ), and a combination of the two ( $\sim 3900\text{ cm}^{-1}$ ,  $2.6\ \mu\text{m}$ ). The peaks involving the C-H stretch are strongly broadened and skewed because of the high degree of vibrational excitation and anharmonicity. The peak at about  $1300\text{ cm}^{-1}$  is composed of emission from two species, one centered at  $1330\text{ cm}^{-1}$  ( $\text{CH}_2\text{I}$ ), the other at  $1110\text{ cm}^{-1}$  ( $\text{CH}_2\text{I}_2$ ). Six microseconds later, the ensemble of emitters has relaxed considerably by collisions with other species in the gas. The ratio of the intensity of the band due to the C-H stretch vibration to the intensity of the band due to the  $\text{CH}_2$  bending vibration has dropped consid-

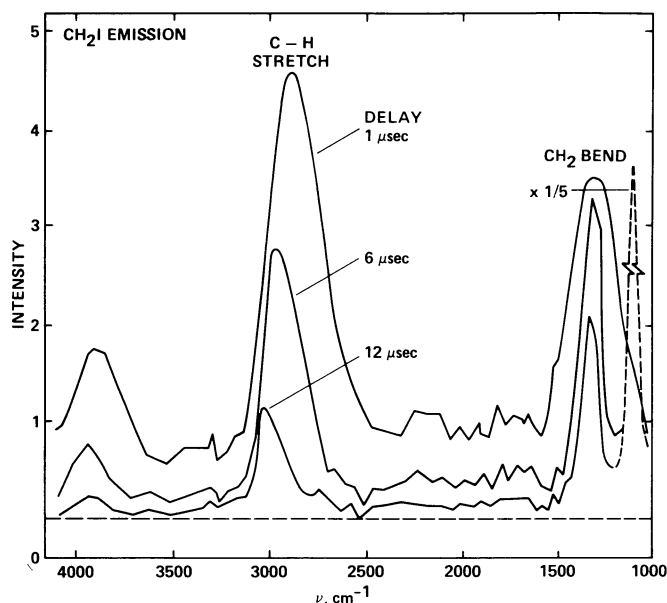


FIG. 9.—The evolution of the  $4000\text{--}1000\text{ cm}^{-1}$  ( $2.5\text{--}10\text{ }\mu\text{m}$ ) emission spectrum from the highly vibrationally excited radical  $\text{CH}_2\text{I}$  as it relaxes. This sequence shows the spectrum, taken using a CVF, at 1, 6, and 12 microseconds after creation of the excited species. This illustrates several general aspects of IR emission from highly vibrationally excited molecules. The vibrational quasicontinuum is essentially flat across the entire spectrum, anharmonicity is important in determining the band shape and position (especially for the CH stretch at  $3000\text{ cm}^{-1}$  [ $3.3\text{ }\mu\text{m}$ ]) and as the molecule relaxes, the relative intensities of the  $3000\text{ cm}^{-1}$  ( $3.3\text{ }\mu\text{m}$ ) to  $1300\text{ cm}^{-1}$  ( $7.7\text{ }\mu\text{m}$ ) bands behave as shown in Fig. 13a. This figure has been reproduced from Baughcum and Leone (1980).

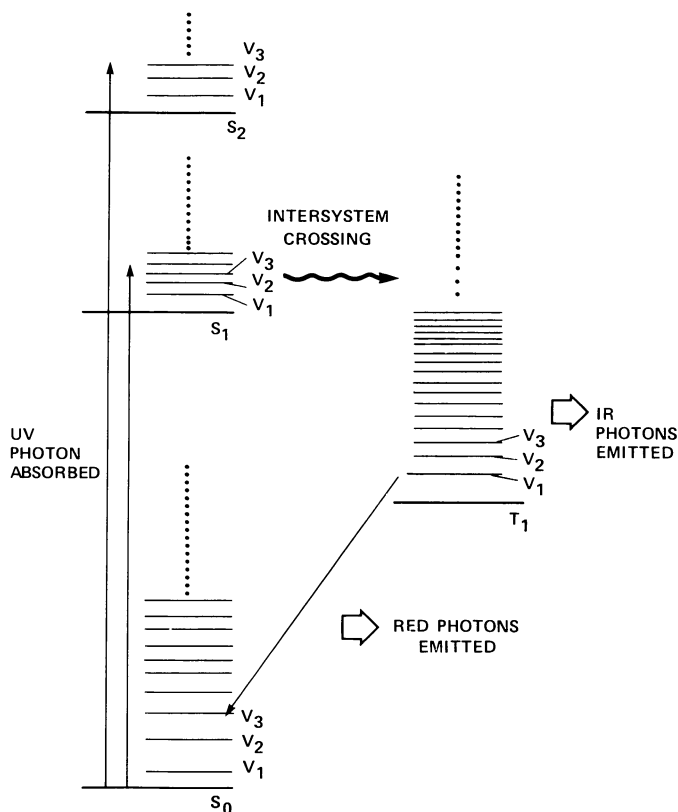


FIG. 10.—Schematic energy level diagram for a neutral PAH, showing the various radiative and nonradiative excitation and relaxation channels possible. Note that in the case of a neutral PAH part of the internal energy will be emitted in the infrared and part in the visible.

erably and the anharmonic skewing and shifting of the  $3050\text{ cm}^{-1}$  band is diminished. The level of the quasi continuum is also reduced but it is still essentially flat. Twelve microseconds later, although the intensity of the  $3030\text{ cm}^{-1}$  band is now less than that of the  $1350\text{ cm}^{-1}$  band, the continuum is still evident. At all stages of relaxation the ratio of the peak intensity of the C-H stretch at  $3050\text{ cm}^{-1}$  to the continuum at about  $2400\text{ cm}^{-1}$  is about 5, a value similar to the ratio observed by Barker, Rossi, and Pladziewicz (1982) with band-pass filters for the IR emission from the vibrationally excited bicyclic aromatic hydrocarbon azulene ( $\text{C}_{10}\text{H}_8$ ). The magnitude of the ratio of quasi-continuum emission to band emission observed by these authors depends on the bandpass filters used.

Anharmonicity dominates emission from the C-H stretching fundamental in this molecule because it is so highly vibrationally excited. With six modes and about  $15,000\text{ cm}^{-1}$  of excess vibrational energy, the average energy per mode in  $\text{CH}_2\text{I}^*$  is  $2500\text{ cm}^{-1}$ . Compare this to the average energy per mode in PAHs such as pyrene ( $\text{C}_{16}\text{H}_{10}$ ) or coronene ( $\text{C}_{24}\text{H}_{12}$ ) which have 72 and 102 modes, respectively. If they absorb the maximum energy which is available per photon in the interstellar medium ( $\approx 106,000\text{ cm}^{-1}$ ) and convert it all to excess vibrational energy, the average energy per mode is  $1470$  and  $1040\text{ cm}^{-1}$ , respectively, about half the energy per mode in  $\text{CH}_2\text{I}^*$ .

### III. INFRARED EMISSION FROM VIBRATIONALLY EXCITED MOLECULES

#### a) Calculated Infrared Fluorescence Intensities

##### i) Infrared Fluorescence Intensities

Many uncertainties are involved in the analysis of the interstellar emission bands, but the emission can be treated theoretically in a relatively simple manner, regardless of the exact identity of the emitting species and the excitation mechanism operative in a particular interstellar environment. Photon absorption is probably the dominant excitation process and we will use it as an example, although the discussion can be readily extended to other excitation mechanisms such as electron-ion recombination and hydrogen addition. In the following discussion, neutral PAHs will be considered specifically, but the principles involved apply equally to any chemical species (cf. Honovich and Dunbar 1982; Dunbar *et al.* 1987).

As an example we will consider optical excitation of the isolated PAH molecule chrysene ( $\text{C}_{18}\text{H}_{12}$ ) for which the photophysics are well known (Birks 1970) and a vibrational assignment is available (Cyvin *et al.* 1982a). Prior to absorption of a photon, the molecule is in the lowest singlet electronic state,  $S_0$ , and contains vibrational energy consistent

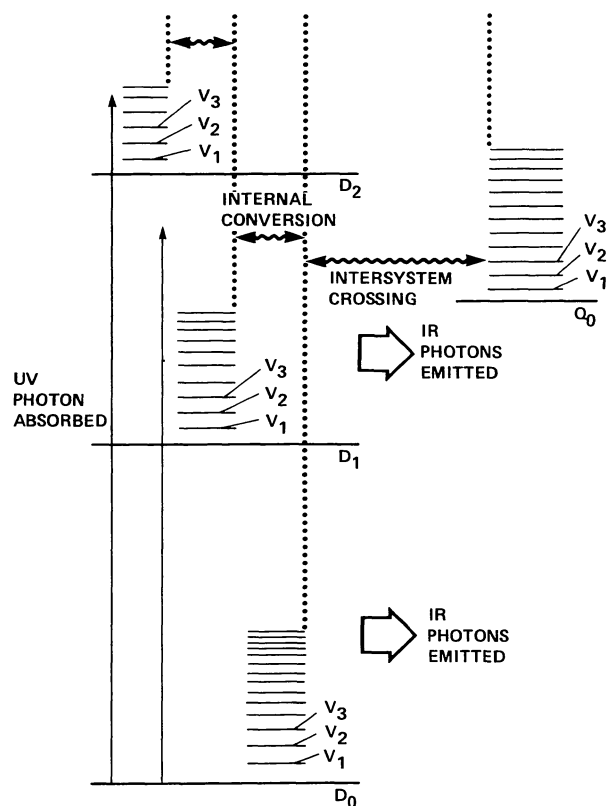


FIG. 11.—Schematic energy level diagram for an ionized PAH, showing the various radiative and nonradiative excitation and relaxation channels possible. Note that in the case of an ionized PAH most of the energy will be emitted in the near- and mid-IR.

with the excitation temperature of the canonical (thermal) ensemble of all chrysene molecules in that region of space... perhaps 10 to 100 K. Photons of many energies are incident on the chrysene and, of those absorbed, some could lead to ionization and others to production of excited states in the neutral molecule. The excited molecule can undergo internal conversion and intersystem crossing to other electronic states (Fig. 10). Chrysene has numerous electronic states, but its strongest absorption band between 2000 Å and 4000 Å is the  $S_3 \leftarrow S_0$  transition near 2675 Å ( $37,400 \text{ cm}^{-1}$ ) (Birks 1970). The  $S_3$  to  $S_1$  internal conversion quantum yield is near unity and very rapid, resulting in complete conversion to vibrationally excited levels of the  $S_1$  electronic state. Subsequently, nearly 90% of the  $S_1$  molecules undergo rapid intersystem crossing to the lowest chrysene triplet state,  $T_1$ , (only 12% of the  $S_1$  molecules fluoresce) leaving about  $17,400 \text{ cm}^{-1}$  of vibrational energy in the triplet molecule a few nanoseconds after absorption of the photon. (Note that in ions internal conversion to the electronic ground state, which is a doublet state, dominates [see, e.g., Leach 1987a], leaving all of the initial excitation energy in the form of vibrational energy, Fig. 11). In the absence of collisions, the only routes for deactivation of the vibrationally excited triplet chrysene are phosphorescence (3 s lifetime) and IR fluorescence (IRF) ( $\sim 0.1$  s lifetime). For the vibrationally excited cation, IRF is the only deactivation route available. Thus, *IRF relaxation is always the dominant process*.

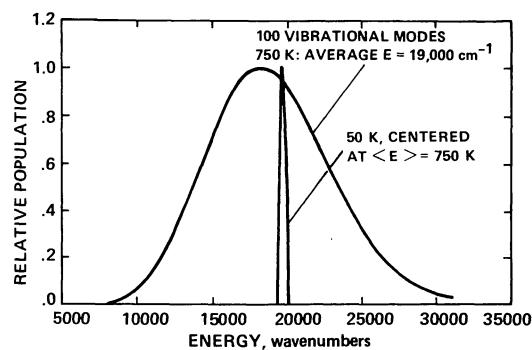


FIG. 12.—Comparison of the distribution function of molecules in thermal equilibrium at 750 K with the distribution function of molecules at 50 K just after absorption of a photon with an energy equivalent to 750 K.

At the low temperatures of the ISM, the initially unexcited molecules contain very little vibrational energy. Thus, all the triplet chrysene molecules formed by photon absorption will have roughly the same energies, resulting in a population distribution that can be approximated by a delta function located at about  $17,400 \text{ cm}^{-1}$ . This narrow distribution function is clearly different from a thermal distribution function having the same average vibrational energy (Fig. 12). Under some conditions, a thermal (canonical) distribution can serve as an approximation to the delta function (microcanonical) distribution, but the approximation fails at low-excitation energies, and its range of validity must be established in numerical tests (§ IIIb).

The infrared emission intensity due to a  $\Delta v = 1$  vibrational transition in a molecule with total vibrational energy  $E$  can be calculated from the fundamental equation:

$$I(E, i, v) = h\nu_i A_i^{v, v-1} N_v(E), \quad (1)$$

where  $\nu_i$  is the frequency,  $A_i^{v, v-1}$  is the Einstein coefficient for the  $(v-1) \leftarrow v$  transition, and  $N_v(E)$  is the population of molecules with energy  $E$  and  $v$  quanta in the  $i$ th vibrational mode (Herzberg 1968; Durana and McDonald 1976; Rossi, Pladziewicz, and Barker 1983). From the harmonic oscillator approximation,  $A_i^{v, v-1} \cong \nu A_i^{1,0}$ , an approximation thought to be accurate to 5%–10% for  $v \leq 2$ . (Note that there may be additional enhancement of emission from the upper vibrational levels because of breakdown of the spin-selection rule in both neutral and ionized species. This is not taken into account here, however, as it is difficult to quantify.) According to the ergodic assumption, the energy is distributed statistically among the accessible vibrational states and the fractional number of molecules with total vibrational energy  $E$  that have  $v$  quanta in the  $i$ th mode is a ratio equal to the number of ways of distributing the energy while the  $i$ th mode has  $v$  quanta, divided by the total number of ways of distributing the energy, subject only to conservation of total energy. Thus  $N_v(E)$  is given by

$$N_v(E) = N(E) \rho_r(E - v h \nu_i) / \rho(E), \quad (2)$$

where  $N(E)$  is the total number of molecules with energy  $E$ ,

$\rho(E)$  is the total density of vibrational states, and  $\rho_r(E - \nu h\nu_i)$  is the density of vibrational states for all modes except the emitting mode. Provided  $\nu h\nu_i \leq E$ , the theoretical expression for the integrated IRF band intensity for a particular  $\Delta\nu = 1$  transition is given by

$$I(E, i, \nu) = N(E) h\nu_i \nu A_i^{1,0} \rho_r(E - \nu h\nu_i) / \rho(E). \quad (3)$$

It should be noted that the most important assumption in equation (3) is the ergodic approximation, which assumes statistical distribution of energy. For energies in excess of a few thousand wavenumbers, the statistical redistribution of energy is completed in picoseconds (Oref and Rabinovitch 1979; Bondybyey 1984). Thus, as long as the densities of states are properly estimated, equation (3) is expected to be reliable, as confirmed in experimental tests (Rossi, Pladziewicz, and Barker 1983; Shi, Bernfield, and Barker 1988).

For best results, exact densities of states should be used in equation (3), but the Whitten-Rabinovitch approximation (1963, 1964) is acceptable for most purposes. This approximation takes the form

$$\rho(E) = (E + aE_0)^{s-1} / \left[ (s-1)! \prod_i^s h\nu_i \right], \quad (4)$$

where  $E$  is the vibrational energy,  $E_0$  is the total zero point energy of the excited species,  $s$  is the number of vibrational modes, and  $\nu_i$  are the vibrational frequencies (usually expressed in wavenumbers). When the parameter "a" is unity, equation (4) gives the semiclassical approximation, which is poor for large molecules.  $E_0$  pertains to all  $s$  oscillators and it is assumed that  $a$  is the same for the  $s$  and  $s-1$  oscillators. The Whitten-Rabinovitch general expression for "a" is given elsewhere (Whitten and Rabinovitch 1963, 1964), but an approximate form suitable for present purposes is

$$a \cong 0.87 + 0.079 \ln(E/E_0) \quad (5)$$

Based on the Whitten-Rabinovitch approximation, a practical general expression for  $I(E, i, \nu)$  can be derived from equations (3) and (4)

$$I(E, i, \nu) \cong N(E) h\nu_i \nu A_i^{1,0} (s-1) \xi \left[ 1 - \left( \nu + \frac{a}{2} \right) \xi \right]^{s-2}, \quad (6)$$

where  $\xi = h\nu_i / (E + aE_0)$ . By using the Whitten-Rabinovitch expression for "a," the calculated intensities agree well within a factor of 2 with those derived using exact methods. For  $E < 20,000 \text{ cm}^{-1}$  exact densities of states should be used for accurate work.

When emission from several  $\Delta\nu = 1$  transitions overlap and when several different modes contribute to emission in the same wavelength region, the total, unresolved emission intensity is obtained by summing over all emitting modes within the spectral bandpass of the filter/detector used and over all  $\Delta\nu = 1$  transitions allowed by conservation of energy. The resulting expression can be written

$$I(E) = \sum_{i=1}^{\text{modes}} \sum_{\nu=1}^{\nu_{\text{max}}} I(E, i, \nu), \quad (7)$$

where the choice of approximation of  $I(E, i, \nu)$  depends on the accuracy desired.

Finally, as an initially excited molecule relaxes by infrared emission, it must emit many infrared photons before it reaches equilibrium with the low temperatures of the ISM. Thus the observed interstellar emission bands are due to emission from molecules in all stages of energy relaxation following excitation to some initial energy. For comparison with the IR emission bands, the calculated energy-dependent intensities were integrated over 2.5 s following photon absorption, to account for the energy-cascade.

In some calculations reported in the present work, the densities of states were calculated using the Beyer-Swinehart exact counting algorithm (Beyer and Swinehart 1973; Stein and Rabinovitch 1973), which is based on vibrational assignments for the specific molecules and assumes harmonic oscillators. The results obtained using equation (6) for intensity ratios were found to be accurate to within  $\pm 30\%$  and most of the predictions are therefore based on equation (6). The wavelengths of the  $\Delta\nu = 1$  transitions originating in higher  $\nu$  levels were estimated using experimental values of anharmonicities. The effect of the anharmonicities on the densities of states calculations is not great, and thus they were neglected.

The  $A_i^{1,0}$  values for the singlet state species can be determined from integrated absorption coefficient measurements, or estimated by analogy with similar molecules. Integrated absorption coefficients for triplet molecules, and other excited states, however, may differ from those of the singlet in ways that are impossible to estimate without elaborate molecular structure calculations or direct experiments (Mitchell, Smith, and Guillory 1981). There are similar uncertainties for ionic species. For example, infrared emission deactivation of benzene cations has been found to be a factor of 4-5 faster than for neutral benzene (Dunbar 1986). In the case of chrysene, the Einstein coefficients for the singlet are not known, but Cyvin *et al.* (1982a) noted the relative intensities of the IR absorption features. By assigning relative integrated absorption coefficients to each of their notations of relative intensity, we can demonstrate how to predict the spectrum of chrysene excited to different vibrational energies. For this purpose, we arbitrarily assumed that the sequence of relative absorption strengths denoted as  $\nu w, w, m, s$ , and  $\nu s$  (very weak, ..., very strong) correspond to relative integrated absorption coefficients  $S_i^{1,0}$  given by 1, 5, 25, 125, and 625, respectively. (Because this assignment is arbitrary, quantitative conclusions derived from the chrysene calculations must be drawn with some caution.)

Using the fact that the Einstein coefficients are proportional to the quantity  $[(h\nu_i)^2 S_i^{1,0}]$ , we calculated IRF spectra (eqs. [3] and [7]; exact densities of states) for chrysene excited to several energies, as shown in Figure 13, where the heights of the peaks are proportional to the total emission from the respective bands and the widths are arbitrary. The approximate emission intensities were placed on an absolute scale by assuming that the 12 C-H stretch modes in chrysene have absorption strengths  $400 \pm 100 \text{ l/mole cm}^2$  (Burberry *et al.* 1979) which is equivalent to a total Einstein coefficient of  $57 \text{ s}^{-1}$ .

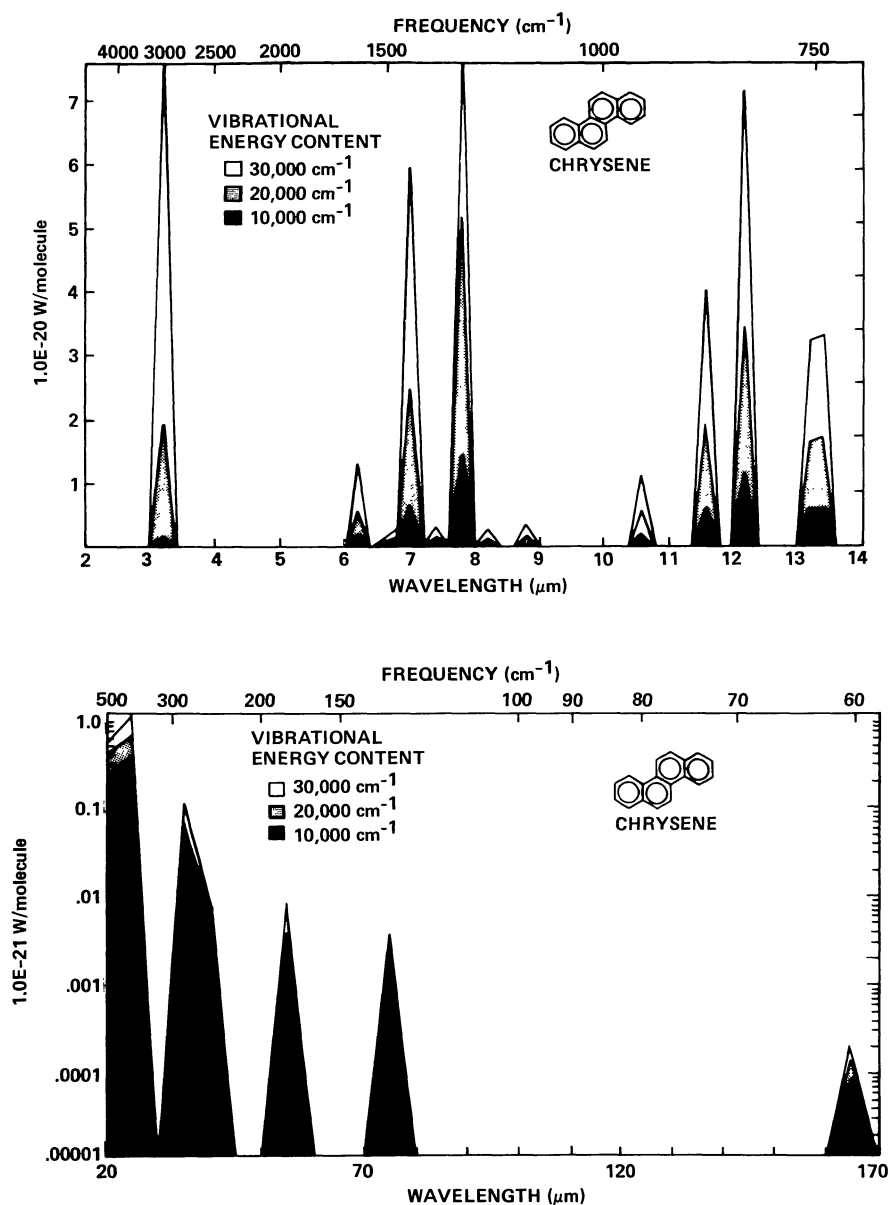


FIG. 13.—(a, b) The calculated IR fluorescence spectrum from chrysenes as a function of vibrational energy content. Note that at low-energy content, emission in the  $3000\text{ cm}^{-1}$  region is negligible with respect to that at longer wavelengths.

Several conclusions may be reached from Figure 13 and from equation (3). First, the IRF spectrum varies dramatically as the vibrational energy is changed and it usually does not match the intensity distribution observed in absorption. Second, no significant IRF emission is observed from the  $3000\text{ cm}^{-1}$  modes unless the molecule contains a significant amount of vibrational energy per vibrational mode. Third, emission from the long-wavelength bands is always observed even at low levels of vibrational energy. Fourth, the intensities of the  $3000\text{ cm}^{-1}$  ( $3\text{ }\mu\text{m}$ ) modes relative to the  $1000\text{ cm}^{-1}$  ( $10\text{ }\mu\text{m}$ ) modes are directly related to the internal energy of the molecule. Thus, if the identity of the emitting species is

known, the relative intensities provide a measure of the vibrational energy content; conversely, if the energy content of the molecules is known, the size of the emitting species can be estimated (§ Va).

#### ii) Rate of Deactivation by Infrared Fluorescence

The rate of deactivation by IRF can be obtained from the data in Figure 13 simply by summing over all emitting modes. It must be emphasized again that only emission from  $\Delta v = 1$  transitions has been considered here. Emission from combination bands and from overtones will also take place to a lesser extent (§ II), but the quantitative importance of such emission

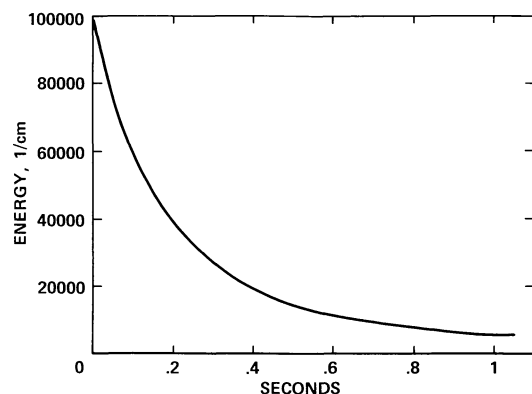


FIG. 14.—The calculated IR emission rate from vibrationally excited free chrysene molecules as a function of vibrational energy content.

cannot be easily estimated without detailed spectroscopic data. Limited experimental data indicate that such emission may be significant in some spectral regions (Barker, Rossi, and Pladziewicz 1982). Thus the sum of IRF emission from the  $\Delta v = 1$  transitions is a lower limit to the total emission rate and should provide order-of-magnitude estimates.

The estimated total IRF emission for chrysene is presented in Figure 14. The total emission rate increases as the total vibrational energy is increased. Moreover, if we note that  $2.5 \times 10^{-18}$  W per molecule corresponds to  $125,000 \text{ cm}^{-1} \text{ s}^{-1}$ , it is clear that for a molecule initially excited to  $40,000 \text{ cm}^{-1}$ , relaxation via the infrared fluorescent cascade is on the order of a few tenths of a second, an order of magnitude faster than the infrared radiative cooling time for a particle. Cool dust particles relax through emission in the low-frequency modes which have smaller Einstein  $A$ -values. Although the total IRF emission rate has been estimated only for chrysene, the general time-dependent decay for other PAHs is probably roughly similar; if they have more vibrational modes, the rate of emission per mode will decrease, but that decrease will be offset by the increased number of modes. The time history of vibrational energy relaxation ( $E$  in  $\text{cm}^{-1}$ ) for chrysene can be described by

$$E(t) = [E(t=0)^{-0.4} + 0.004t]^{-2.5} \quad (8)$$

iii) *Infrared Fluorescence Dependence on Molecular Size and Vibrational Energy Content*

1. *The  $890 \text{ cm}^{-1}/3040 \text{ cm}^{-1}$  ( $11.2 \mu\text{m}/3.3 \mu\text{m}$ ) intensity ratio.*—For each C-H bond in a PAH, one out-of-plane bending mode and one stretching mode will be present; thus, the number of modes emitting near  $885 \text{ cm}^{-1}$  ( $11.3 \mu\text{m}$ ) equals the number of modes emitting near  $3000 \text{ cm}^{-1}$  ( $3.3 \mu\text{m}$ ), regardless of the actual number of C-H bonds present in each molecule. For gas-phase benzene, the integrated absorption coefficients for the two bands are nearly equal (Bishop and Cheung 1982). This is also approximately true for the PAHs naphthalene and anthracene in the gas phase (H. Niki, private communication). Intermolecular interactions between PAHs in salt pellets tend to substantially enhance the absorption strength of the C-H out-of-plane bending

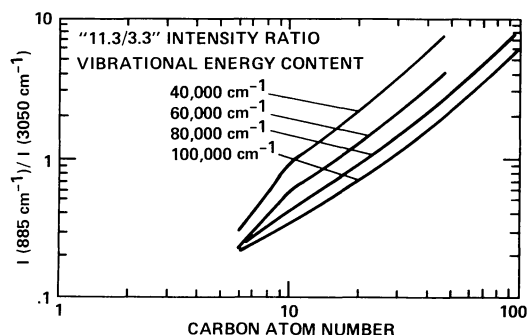


FIG. 15.—The  $885 \text{ cm}^{-1}/3050 \text{ cm}^{-1}$  ( $11.3 \mu\text{m}/3.3 \mu\text{m}$ ) intensity ratio plotted as a function of carbon atom number and vibrational energy content. The relative fluorescence intensities includes integration over the vibrational cascade and assumes the integrated absorbance of the C-H stretch mode is equal to the integrated absorbance for the C-H out-of-plane bend. The carbon atom numbers derived from this plot are upper limits (see § Va).

vibration with respect to the C-H stretch (Allamandola and Sandford 1988). Thus salt pellet spectra intensities should not be used in making these calculations. If the absorption strengths for the C-H stretches and out-of-plane bends for all gas-phase PAHs are the same as for benzene and these simple linear PAHs, the trend of intensity ratios calculated for known PAHs can be applied to the interstellar emission bands to estimate the size of the band carriers. For this purpose, vibrational assignments for benzene ( $\text{C}_6\text{H}_6$ ), azulene ( $\text{C}_{10}\text{H}_8$ ), anthracene ( $\text{C}_{14}\text{H}_{10}$ ), chrysene ( $\text{C}_{18}\text{H}_{12}$ ), and perylene ( $\text{C}_{20}\text{H}_{12}$ ) were used with equations (6) and (7) to predict the relative IRF emission intensities due to one C-H stretch mode and due to one C-H out-of-plane bend mode, assuming they have equal integrated absorption coefficients.

Ratios of averaged IRF intensities of the  $885 \text{ cm}^{-1}$  ( $11.3 \mu\text{m}$ ) band to the  $3050 \text{ cm}^{-1}$  ( $3.3 \mu\text{m}$ ) band, corrected for the energy cascade, were calculated for initial excitation energies ranging up to  $100,000 \text{ cm}^{-1}$ . The calculated ratios of IRF intensities are plotted in Figure 15 as a function of the number of carbon atoms in each molecule. The predictions corresponding to carbon numbers from 6 to 20 are based on the actual vibrational assignments for the five prototype molecules listed above, and the approximate equation (6) was tested for accuracy. For higher carbon numbers, the estimates are based on molecules assumed to consist of 75% carbon and vibrational modes with an average frequency of  $1200 \text{ cm}^{-1}$ . This trend of the relative intensities observed as a function of molecular size and initial excitation energy (Fig. 15) can be used to derive an upper limit to the average sizes for the interstellar PAHs (§ Va).

2. *The  $2940 \text{ cm}^{-1}/3040 \text{ cm}^{-1}$  ( $3.4 \mu\text{m}/3.3 \mu\text{m}$ ) intensity ratio.*—So far, spectral resolution has been neglected and only the total emission from specified bands has been considered. However, the spectroscopic properties of the C-H stretching vibrations have been well characterized for a number of PAH molecules, opening another potential avenue for determining the size of the species present in interstellar space.

In benzene, naphthalene, anthracene, and other PAH molecules that have been studied in detail, the anharmonicities of the C-H stretching vibrations near  $3050 \text{ cm}^{-1}$  are

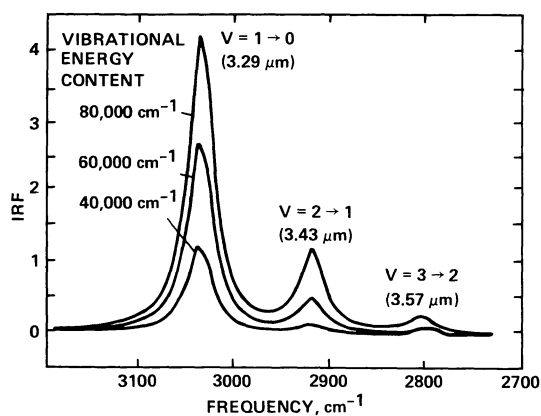


FIG. 16.—The calculated emission spectrum for chrysene in the C-H stretching region as a function of vibrational energy content. The anharmonic frequency is assumed to be  $120\text{ cm}^{-1}$  (Barker, Allamandola, and Tielens 1987).

about  $60\text{ cm}^{-1}$  (Swofford, Long, and Albrecht 1976; Reddy, Heller, and Berry 1982). For other modes the expected anharmonicity is much smaller. The hypothesis that the band emission originates from highly vibrationally excited molecules requires consideration of emission originating from all vibrational levels that are accessible. Emission by  $\Delta v = -1$  transitions originating from the  $v = 2$  state will be shifted by  $\sim 120\text{ cm}^{-1}$  from that originating from the  $v = 1$  state and emission originating from higher  $v$  levels may also be significant. In benzene, the  $v = 2 \rightarrow 1$  and  $v = 3 \rightarrow 2$  transitions are at  $2925$  and  $2814\text{ cm}^{-1}$  ( $3.42$  and  $3.55\text{ }\mu\text{m}$ ), respectively. Since these bands are separated by  $\sim 120\text{ cm}^{-1}$  and the individual band widths are only about  $30\text{ cm}^{-1}$ , the lines are easily resolved. The expected emission spectrum can be generated using equation (3), combined with an assumed Lorentzian line profile ( $30\text{ cm}^{-1}$  width). Rotational structure will contribute very little to the linewidth and is incorporated into the Lorentzian profile.

The calculated emission spectrum for a single C-H stretching vibration for chrysene is shown in Figure 16; all other PAHs will exhibit qualitatively similar spectra, with about  $120\text{ cm}^{-1}$  separation between the peaks for each C-H stretch mode, but the exact location of the pair depends on the particular molecule. The other C-H vibrational stretch modes, which have slightly different frequencies, and the effects of the energy cascade have been neglected in preparing Figure 16.

Figure 16 shows a remarkable resemblance to the spectrum observed from the Orion Bar and NGC 7027 (see Figs. 1 and 3). Note that the vibrationally excited PAH hypothesis requires the presence of  $\Delta v = 1$  emission originating from  $v = 2$  and higher levels when molecules have sufficient excitation energy. Comparison with the observed spectrum shows a distinct satellite peak near the position required. Thus the peaks observed near  $2940\text{ cm}^{-1}$  ( $3.40\text{ }\mu\text{m}$ ) in various objects provide additional strong support for the PAH hypothesis (Barker, Allamandola, and Tielens 1987).

The  $100\text{ cm}^{-1}$  anharmonic shift in the interstellar spectra differs slightly from that of small, neutral PAHs ( $\sim 120\text{ cm}^{-1}$ ). This difference may arise from obscuration caused by

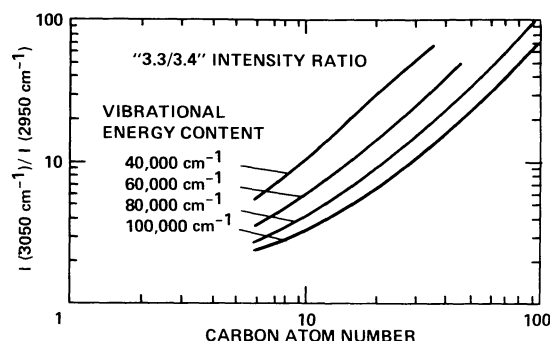


FIG. 17.—The  $3050\text{ cm}^{-1}/2950\text{ cm}^{-1}$  ( $3.3\text{ }\mu\text{m}/3.4\text{ }\mu\text{m}$ ) intensity ratio as a function of carbon atom number and vibrational energy content. Relative fluorescence intensities include integration over the vibrational cascade (Barker, Allamandola, and Tielens 1987).

the overlapping of several bands, larger PAHs producing different frequency bands, or the anharmonicity may depend on the ionization state of the emitting species.

Since the relative importance of the emission from  $v = 2$  depends on the internal energy of the excited molecule, the ratio of intensities from  $v = 1$  and  $v = 2$  emission provides another measure of excitation energy and molecular size (§ IIa). In this case, however, the ratio of the Einstein coefficients is accurately given by the harmonic oscillator approximation:  $A^{1,0}/A^{2,1} \cong 1/2$ . Thus the uncertainties associated with estimating the relative Einstein coefficients for two different vibrational modes are avoided and the predictions are firmer than those provided by the relative intensities of the  $885\text{ cm}^{-1}$  and  $3050\text{ cm}^{-1}$  ( $11.3$  and  $3.3\text{ }\mu\text{m}$ ) lines. Predictions for the intensity of the  $v = 1$  compared to that for the  $v = 2$  line are presented in Figure 17 as functions of molecular size and excitation energy (based on eq. [6]). The effects of the energy cascade were included in this calculation.

#### b) Regions of Applicability of the Thermal Approximation

In descriptions of the nonequilibrium photoexcitation process, a molecule absorbs a single photon of fixed energy, and its internal energy is the sum of the photon energy plus its energy (if any) prior to photon absorption. The statistical ensemble consists of all such molecules that absorb photons of the same energy. If the molecules are in their lowest energy levels prior to photon absorption, all members of the ensemble have exactly the same energy upon excitation and the population distribution function is a delta function or "microcanonical distribution." In microcanonical distributions, all species have identical total energies and the energy within each molecule is distributed statistically among all accessible energy states. Note that "statistical" is *not* equivalent to "thermal"! It means that each quantum state has equal weight in the distribution.

By contrast, in thermal (canonical) systems, each member of the ensemble of molecules may have a different total energy and the probability of the occurrence of that energy is described by the Boltzmann equation and temperature  $T$ . The

possible internal energies range from zero to infinity and the width of the distribution depends on the number of vibrational modes in the molecule, their frequencies, and the temperature. As with the microcanonical distribution, the internal energy in any individual molecule is distributed statistically among the accessible quantum states.

Under conditions discussed below, thermal distributions can be used to *approximate* microcanonical distributions and thereby “simplify” calculations of infrared emission intensity. Unfortunately, the approximation is of limited validity and its range of usefulness must be established in each application by numerical calculations.

For a thermal (canonical) distribution of molecules composed of nondegenerate and separable harmonic oscillators, the population of molecules in level  $v$  of the  $i$ th mode is given by the Boltzmann equation

$$N_{iv}(T) = N \exp(-vhv_i/kT)/Q_i, \quad (9)$$

where  $T$  is the temperature,  $k$  is Boltzmann's constant, and  $Q_i$  is the vibrational partition function for the  $i$ th mode

$$Q_i = [1 - \exp(-hv_i/kT)]^{-1}. \quad (10)$$

For harmonic oscillators, the Einstein coefficient for each transition is related to that for the  $1 \rightarrow 0$  transition:  $A^{v,v-1} = vA^{1,0}$ . The IRF emission rate for the  $i$ th mode is

$$\begin{aligned} I(T) &= hv_i A_i^{1,0} \sum v N_{iv} \\ &= hv_i A_i^{1,0} N \sum v \exp(-vhv_i/kT)/Q_i \\ &= Nh\nu_i A_i^{1,0} \frac{e^{-hv_i/kT}}{1 - e^{-hv_i/kT}}. \end{aligned} \quad (11)$$

Introducing the absorption coefficient,  $\kappa_i$

$$\kappa_i = hv_i B_i N / 4\pi \quad (12)$$

with  $B_i$  the Einstein coefficient, the thermal approximation to the IRF emission reduces to the familiar expression

$$I(T, i, 1) = 4\pi\kappa_i B(\nu_i, T), \quad (13)$$

where  $B(\nu_i, T)$  is the Planck function at temperature  $T$ . This (thermal) approximation has been used to calculate the IR emission from small species (Leger and Puget 1984; Draine and Anderson 1985). Note that anharmonic  $\Delta v = -1$  emission originating from higher  $v$  states (e.g.,  $v = 2-1$ ) is *not* simply given by the absorption coefficient times the Planck function at  $T$  and  $\nu_i$ , but has to be calculated using equations (9) and (10).

If equation (11) is used as an approximation to equation (3), the temperature must be treated as a parameter by selecting the value at which the average energy of the thermal (canonical) distribution equals  $E$ , the energy of the delta function (microcanonical) distribution of equation (3):  $\langle E(T) \rangle = E$ . This must be accomplished by using statistical mechanics and the known vibration frequencies, or by using accurately determined vibrational heat capacities. A useful technique for calculating PAH heat capacities as a function of temperature is described by Stein, Golden, and Benson (1983). Note that the classical thermal vibrational energy content  $\langle E_c \rangle = (3n_A - 6)kT$  (where  $n_A$  is the number of atoms in the molecule) is a poor approximation at the energies of interest here, as illustrated in Figure 18. For the test calculations, the thermal vibrational energy was calculated using the statistical mechanics of separable harmonic oscillators.

As a test, IRF intensities were calculated according to equations (11) and (3) and the results are presented as a ratio in Figure 19. This figure shows that at high-excitation energy per mode and for the low-frequency oscillators, the thermal approximation is acceptable, but for low-energy and high-frequency modes, the approximation fails. This behavior can be understood in terms of the width of the thermal distribution, which produces important contributions to the infrared emission intensity from molecules at both high and low internal energies.

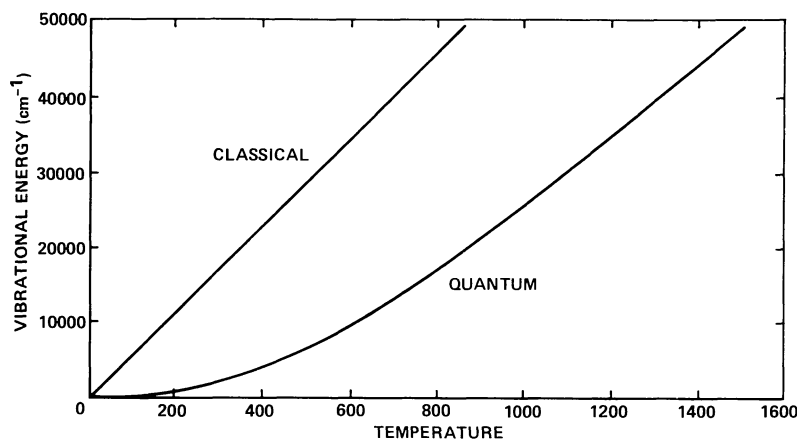


FIG. 18.—Comparison of the temperature dependence of the vibrational energy content,  $C$ , of chrysene calculated using the classical description which is appropriate for bulk material ( $C = 3NkT$ ), vs. the exact solution taking the quantum nature of chrysene into account. The classical approximation severely overestimates the energy content.

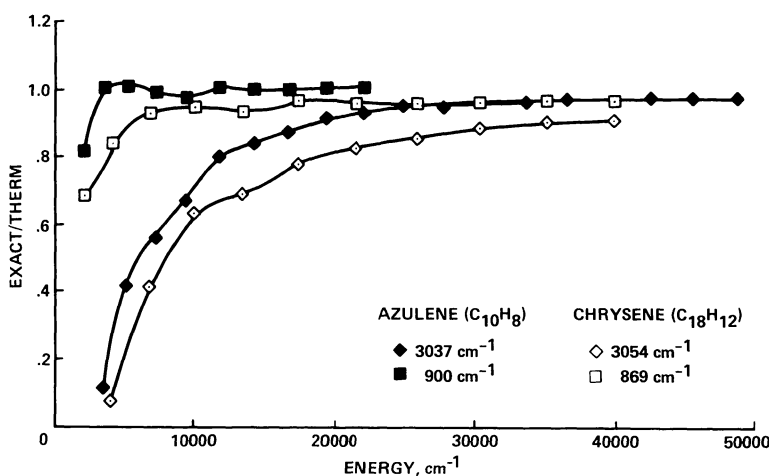


FIG. 19.—Ratio of the IR fluorescence intensity calculated using the exact solution to the emission calculated with the thermal approximation for one high- and one low-frequency mode in the aromatic molecules azulene and chrysene. For high levels of vibrational energy content and low-frequency modes the thermal approximation is acceptable but for larger molecules and high-frequency modes the thermal approximation overestimates the emission intensity.

For most of the cases of interest here, the width of the thermal distribution function is quite substantial, but it becomes relatively narrower under certain limiting conditions. It is under these conditions that the thermal approximation is an adequate approximation. To illustrate the limits of validity of the thermal approximation, we will use the density of states expression for classical harmonic oscillators: equation (4) with  $a = 0$ . The classical expression is not suitable for quantitative calculations, but the functional dependence of the infrared emission intensity on the various parameters is most clearly illustrated for this case.

Let us examine the probability,  $P(E, T)$ , that, in a canonical system with temperature  $T$ , an individual molecule has an internal energy  $E$ . This is given by

$$P(E, T) dE = \rho(E) \exp(-E/kT) dE / Q(T). \quad (14)$$

For classical harmonic oscillators,  $Q_c(T) = (kT)^s / (\prod h\nu_i)$  and, using equation (4) with  $a = 0$ , the probability can be written

$$P_c(E, T) dE = E^{s-1} [(kT)^s (s-1)!]^{-1} \exp(-E/kT) dE. \quad (15)$$

Note that the average thermal energy is  $\langle E_c \rangle = s kT$ , for  $s$  classical oscillators. Figure 20 shows this probability as a function of energy  $E$  for several different values of the number of modes,  $s$ . The density of vibrational states,  $\rho(E)$ , is a rapidly increasing function of  $E$ , while the exponential is a rapidly decreasing function of  $E$ . As a result the probability,  $P(E)$ , will show a maximum. This distribution gets sharper as the system gets larger, that is: the more rapidly  $\rho(E)$  increases with  $E$ . In the limit when the number of degrees of freedom ( $s$ ) goes to infinity,  $P(E)$  approximates a delta function. For a single oscillator (i.e.,  $s = 1$ ) the Boltzman distribution is recovered. To second order the probability  $P(E)$  can be described by a Gaussian around the mean thermal energy,

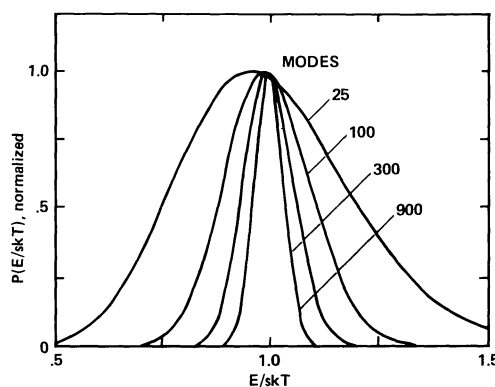


FIG. 20.—The probability that an individual molecule in a canonical ensemble at temperature  $T$  has an internal energy  $E$ . The different curves correspond to molecules with different numbers of vibrational modes.

$\langle E \rangle$ , with a standard deviation,  $\Delta E$ , given by

$$\Delta E \cong \langle E \rangle / \sqrt{2}.$$

In our case,  $s$  lies in the range 50 to 150 and the width of the distribution function is appreciable ( $\Delta E \cong 0.1 \langle E \rangle$ ). Thus, in the canonical (i.e., thermal) approximation, molecules with various amounts of internal energy contribute to the intensity. Effectively, the thermal emission intensity is obtained by averaging the microcanonical intensity (given by eq. [3] or [6]) over this probability distribution function. In the limit of very large  $s$  and very small  $h\nu_i/E$ , the probability function goes to a delta function and the thermal emission intensity is equal to the microcanonical result. However, when these conditions are not fulfilled, as in the IRF of PAH molecules, large errors can result. In particular, even when the average internal energy of the canonical system is chosen to be equal to the actual (microcanonical) energy, the rapid increase of the (microcanonical) emission with the increasing internal energy implies that the average (canonical) intensity calculated in the

thermal approximation is larger than the true intensity (cf. Fig. 19). It is this fundamental property of thermal distributions that invalidates the thermal approximation unless the number of degrees of freedom of the system is sufficiently large.

Moreover, for small  $s$ , the average thermal energy actually does not coincide with  $E$ , but is shifted by an amount that depends on the emission wavelength, as well as the size of the molecule and the internal energy (cf. Fig. 19). For  $s$  classical oscillators (i.e.,  $Q_i = kT/h\nu_i$ ), equation 11 can be written

$$I_c(T, i, \nu) = (h\nu_i)^2 v A_i^{1,0} (kT)^{-1} \exp(-h\nu_i/kT). \quad (16)$$

By equating this "thermal intensity" to that for the microcanonical distribution (eq. [6]), we can obtain the energy  $E$  that gives the same emission intensity as that obtained from the thermal distribution at temperature  $T$ :

$$E = (s-1)kT \left[ 1 - v \frac{h\nu_i}{2kT} \right]^{s-2} \exp(h\nu_i/kT). \quad (17)$$

Writing this expression in terms of the average thermal energy, we have

$$\frac{E}{\langle E_c \rangle} = (1-1/s) \left[ 1 - v \frac{h\nu_i}{2kT} \right]^{s-2} \exp(h\nu_i/kT). \quad (18)$$

Equation (18) clearly shows that  $E \neq \langle E_c \rangle$ , except in the limit of both large  $s$  and infinitesimal  $h\nu_i$ . Although  $E$  can be chosen to be equal to  $\langle E_c \rangle$  at one particular frequency by adjusting  $T$ , large differences can occur at other frequencies. Essentially, for a thermal distribution, the emission at different wavelengths is characterized by emission from molecules that contain different amounts of total energy. Thus, one should be careful in interpreting observed emission ratios, such as the 3.3/11.3  $\mu\text{m}$  intensity ratio, using the thermal approximation. For semiclassical densities of states, we reach the same conclusion, based on closed form integrals in the above equations. For quantum oscillators the integrals cannot be solved in closed forms, but numerical tests such as that presented in Figure 19 support the same general conclusion.

Finally, it should be stressed that use of the thermal approximation in evaluating chemical reaction rates in the presence of a reaction threshold can lead to results that are totally wrong. As an example consider H loss from a small PAH upon UV photon absorption. The bond energy of an H atom attached to an aromatic ring is about 4.8 eV, i.e. 39,000  $\text{cm}^{-1}$ . In the thermal distribution some molecules will have an internal energy above the energy threshold and the reaction can proceed (Fig. 12). Others will have insufficient internal energy and no reaction will occur. In the microcanonical ensemble, in contrast, either all the molecules will possess an internal energy above the reaction threshold or none will. In the latter case the reaction is completely inhibited. In the former case the reaction may proceed and the reaction probability can be calculated using statistical methods (i.e., RRKM theory) by evaluating the probability that enough energy is located in the CH bond for dissociation to occur (cf. § IVa). Clearly, the use of a thermal distribution function in this case

can lead to large errors in the calculation of reaction rates. For this reason, the preferred procedure is to use the microcanonical distribution to predict rate constants that depend on total energy and then evaluate average reaction rate constants with population distributions suitable for particular applications.

#### IV. CHEMISTRY

##### a) Photon-Induced Reactions of Aromatics

As discussed in § IIIa, PAHs will be highly vibrationally excited subsequent to absorption of an ultraviolet photon. If sufficiently excited, the PAHs may undergo unimolecular reactions such as the loss of an H atom or carbon skeleton rearrangement. The purpose of this section is to make order-of-magnitude estimates of some unimolecular rate constants.

Accurate estimates of unimolecular reaction rates can be made only when considerable information is available about the reactant. Such information includes knowledge of all vibrational frequencies, moments of inertia, reaction threshold energies, and transition state parameters for each reaction. Since we are concerned with large ionized PAHs, practically no experimental information is available. Thus, we must base our estimates on the neutral molecule benzene ( $\text{C}_6\text{H}_6$ ), the only aromatic molecule for which (fragmentary) reaction rate information is available on the unimolecular loss of H (Kern *et al.* 1984; Kiefer *et al.* 1984). Dehydrogenation may be particularly important for doubly charged PAHs. Many fragmentation reactions are possible in highly vibrationally excited doubly charged ions. If the level of internal excitation is close to threshold, both dehydrogenation and some fragmentation become important (Ruhl, Price, and Leach 1989; Leach, Eland, and Price 1989).

##### i) CH Bond Rupture

We assume that the reaction threshold energies for C-H bond rupture in aromatic cations are the same as in benzene, since the sigma-bonded C-H linkages are approximately orthogonal to the pi-bonding orbitals from which the cation was ionized. We will also assume that the vibrational frequencies and transition state parameters for the cations are similar to the neutral species. This is a reasonable approximation for the sigma-bonded modes, but the ionized species may have significantly different pi-bonded structures and we conjecture that the cations (and anions as well) are more flexible with respect to isomerization. Since the ionic species are assumed exclusively to undergo internal conversion to the electronic ground state, all of the energy of the ultraviolet photon will appear as vibrational energy. Thus, it is appropriate to consider reactions on the ground-state potential energy surface, rather than those of electronically excited states. This assumption may require revision when better information becomes available. Theoretical molecular calculations may be of great value in refining these assumptions.

The ground electronic state unimolecular reactions of benzene have been the subject of considerable controversy (Kern *et al.* 1984; Kiefer *et al.* 1984). Recent shock-tube investigations have obtained data on the rate of disappearance of benzene, but there is little agreement on the products of the

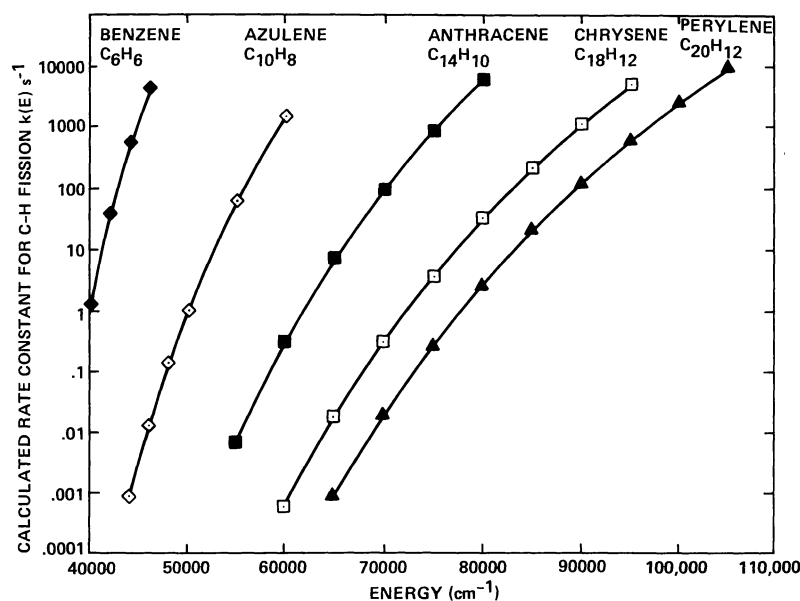


FIG. 21.—The C-H bond rupture rate of specific PAHs calculated as a function of the vibrational energy content using the quantum RRR theory. Note that for C-H bond rupture to be important, the rate has to be larger than the IR emission rate which is about  $10 \text{ s}^{-1}$  for chrysene (Fig. 14). Thus small PAHs may lose a considerable fraction of their hydrogen atoms while large PAHs will be completely hydrogenated. The transition lies in the 20–30 carbon atom range.

reaction, except to rule out simple rupture of a C-C bond. (Rupture of only a C-C bond in an aromatic molecule requires  $> 55,000 \text{ cm}^{-1}$  and will produce a short-lived biradical, which can react only by reformation of the same C-C bond, resulting in no loss by fragmentation). Two reaction channels are accessible at moderate energies and both contribute to the observed loss of benzene: C-H bond rupture at  $39,000 \text{ cm}^{-1}$ , and concerted elimination of three acetylene ( $\text{C}_2\text{H}_2$ ) molecules at  $50,000 \text{ cm}^{-1}$ . The lower energy pathway dominates at all energies because it has the lower threshold energy and the higher frequency factor.

Since little is known about the reactions of PAHs, the use of the RRKM statistical theory of unimolecular reaction rates is not justified. Instead, we will use the simpler quantum RRR (QRRK) statistical theory (Barker 1983; Weston 1986), which requires less detailed knowledge of the molecular species and of the reaction parameters, and is useful for order-of-magnitude estimates. The energy-dependent specific rate constant, according to QRRK theory, is

$$k(E) = A_\infty \Gamma(a - b + s) / [\Gamma(a - b + 1) \Gamma(a + s)] \quad (19)$$

where the gamma functions provide an interpolation formula to give a continuous approximation for  $k(E)$ ,  $s$  is the number of vibrational modes,  $A_\infty$  is the preexponential factor of the high-pressure thermal unimolecular rate constant, and  $a$  and  $b$  are the reduced internal energy and reduced reaction threshold energy, respectively

$$a = E/h\langle\nu\rangle, \quad b = E_\infty/h\langle\nu\rangle, \quad (20)$$

where  $\langle\nu\rangle$  is the geometric mean vibrational frequency of the molecule and  $E_\infty$  is the high-pressure activation energy of the thermal reaction.

In applying the QRRK expression, we assume that  $E_\infty = 39,000 \text{ cm}^{-1}$  and that  $A_\infty = 10^{16.5} \text{ s}^{-1}$  per C-H bond, based on the recent experimental data for benzene (Kiefer *et al.* 1984). Since vibrational assignments are available for benzene, azulene, anthracene, chrysene, and perylene, we used the vibrational assignments to calculate  $\langle\nu\rangle$  for each molecule.

The results are presented in Figure 21. Inspection of the figure shows that for the same internal energy the larger molecules decompose much slower than the smaller molecules. This effect is due to the low excitation per vibrational mode in the larger molecules, relative to the smaller ones. If the molecule is to decompose on a time scale faster than the IRF relaxation rate, the larger molecules must absorb very energetic photons (of course, the relaxation rate also depends on the size of the molecule). For chrysene, the IRF relaxation rate is about  $10 \text{ s}^{-1}$  and decomposition (H atom loss) is faster only for absorbed photon energies greater than about  $80,000 \text{ cm}^{-1}$ . If molecules absorb  $50,000 \text{ cm}^{-1}$  photons most of the time, IRF relaxation dominates and decomposition is a rare event. It is important to note that the smallest molecules are those that will fluoresce most intensely across the entire mid-IR and are also the most likely to suffer H loss. Given that photons with  $\approx 109,650 \text{ cm}^{-1}$  ( $912 \text{ \AA}$ ) are usually the most energetic in the interstellar medium, this analysis implies that PAHs containing more than about 20 C atoms will have their full complement of hydrogens. In some of the IR feature emitting regions more energetic photons are available and correspondingly larger PAHs will undergo H atom loss. The PAH H-loss rates in different environments are discussed in § Vd.

#### ii) Deuterium Enrichment

Hydrogen/deuterium isotope effects in the interstellar medium are of great interest. Because of the low temperatures

and the additional strength of the C-D bond, the rate for D loss from interstellar PAHs will be less than that for H loss and the PAH D/H ratio might be substantially larger than the elemental D/H ratios.

To predict the QRRK specific rate constants for C-D bond rupture, we assumed that  $A_{\infty}(\text{D}) = A_{\infty}(\text{H})/\sqrt{2}$  and that  $E_{\infty}(\text{D}) = E(\text{H}) + 1500(1 - 1/\sqrt{2})$ , where the second term is just the zero-point energy difference between the C-D and the C-H bonds that are broken, giving  $A_{\infty}(\text{D}) = 10^{16.35}$  and  $E_{\infty}(\text{D}) = 39,440 \text{ cm}^{-1}$ . To estimate  $\langle \nu_{\text{D}} \rangle$ , we used the Teller-Redlich product rule (Davidson 1962) and assumed that deuterium substitution did not affect the molecular moments of inertia and the molecular weight, good approximations for the large molecules considered here.

For absorbed photons with  $70,000 \text{ cm}^{-1}$  of energy, the QRRK rate constants for C-D bond rupture in azulene, anthracene, chrysene, and perylene are from 2.5 to 3.5 times slower than those for C-H bond rupture, and larger factors are expected for larger PAHs. Thus, we predict deuterium enrichment in the PAHs, relative to the abundance of free deuterium atoms in the ISM. Some of the astrophysical implications of this result are discussed in § Ve.

#### b) Chemical Attack by O- and H- Atoms

In the interstellar medium, H atoms, O atoms, and other reactive species may attack PAHs and destroy the carbon skeletons. If the resulting lifetime of PAHs is much shorter than the typical cycling time scale between stars and the interstellar medium ( $\approx 2 \times 10^9 \text{ yr}$ ), the observed PAHs have to be made efficiently by a local process, such as shattering of interstellar amorphous carbon grains by grain-grain collisions in interstellar shocks or gas-phase ion-molecule reactions (Tielens and Allamandola 1987b; Bohme 1988). Duley and Williams (1986) have presented estimates for the lifetime of PAHs subject to chemical attack by H, O, and  $\text{He}^+$  species of  $30n^{-1}$ ,  $3 \times 10^5 n^{-1}$ , and  $3 \times 10^{10} n^{-1} \text{ yr}$ , respectively, where  $n$  is the total density. Such an extremely short lifetime, much shorter than the typical lifetime of an emission object ( $\approx 10^5 \text{ yr}$  for an H II region), would imply that free PAHs are unlikely as carriers of the IR emission bands. However, as discussed in this section, our estimates of the chemical lifetime of PAHs are larger by several orders of magnitude.

Given the short IR radiative relaxation time scale of PAHs ( $\approx 0.1 \text{ s}$ ) and the long times between for UV photon absorption and PAH-H atom collisions in the diffuse interstellar medium, reaction of a gas-phase species with an internally excited PAH is generally unimportant. Here we will only consider reactions of gas-phase species with PAHs in their ground state. Duley and Williams (1986) have argued that the attack of gas-phase radicals followed by UV photon absorption would lead to even faster destruction time scales, since the resulting "temperature excursions" would enable activation barriers to be overcome. However, as discussed in § IIIb, the use of the thermal approximation can lead to erroneous conclusions regarding the chemical stability of small systems such as PAHs. The decomposition of a PAH upon UV photon absorption has to be evaluated on the basis of the microcanonical ensemble using statistical methods such as RRKM theory. We show here that UV photon absorption by

TABLE 2  
AROMATIC REACTIONS CONSIDERED IN SECTION IV

Reaction	Reaction Number
$\text{H} + \text{C}_6\text{H}_6 \rightarrow \text{C}_6\text{H}_7^*$ .....	1
$\text{C}_6\text{H}_7^* \rightarrow \text{H} + \text{C}_6\text{H}_6$ .....	2
$\text{H} + \text{C}_6\text{H}_7 \rightarrow \text{H}_2 + \text{C}_6\text{H}_6$ .....	3
$\text{O} + \text{C}_6\text{H}_6 \rightarrow \text{C}_6\text{H}_6\text{O}^*$ .....	4
$\text{C}_6\text{H}_6\text{O}^* \rightarrow \text{C}_6\text{H}_5\text{OH}^*$ .....	5
$\text{C}_6\text{H}_5\text{OH}^* \rightarrow \text{C}_6\text{H}_5\text{O} + \text{H}$ .....	6
$\text{C}_6\text{H}_5\text{OH}^* \rightarrow \text{C}_6\text{H}_5\text{OH} + h\nu$ .....	7
$\text{C}_6\text{H}_5\text{OH}^* \rightarrow \text{CO} + \text{C}_5\text{H}_6$ .....	8

a PAH after attack by a gas phase H or O atom will actually inhibit destruction.

We have estimated the chemical lifetimes of PAHs based on recent chemical kinetics data for reactions with benzene and substituted benzenes, since data are not available for larger PAHs. In most chemical reactions involving an atom and a stable molecule, the attacking atom must surmount an energy barrier, resulting from electron reorganization. Because of the energy barrier, the chemical rate constant depends on temperature:  $k = A \exp(E_a/RT)$ , where the "A-factor" depends on molecular size, geometrical constraints, and (weakly) temperature,  $E_a$  is the activation energy,  $R$  is the gas law constant, and  $T$  is the temperature.

The reaction of hydrogen atoms with benzene has been investigated by Nicovich and Ravishankara (1984), who found the bimolecular rate constant to be  $k_A = 6.7 \times 10^{-11} (\exp - 2.165/T) \text{ cm}^3 \text{ molecule}^{-1} \text{ s}^{-1}$ . In their study, indications of adduct-formation were directly observed, consistent with earlier investigations. The reaction proceeds by addition of the H atom to the benzene ring (Table 2, R1). This is one of the mechanisms for producing vibrationally excited species; the amount of energy involved is on the order of  $40,000 \text{ cm}^{-1}$ . Subsequently, the excited  $\text{C}_6\text{H}_7^*$  can redissociate (R2). The ring structure is not affected by this process. The  $\text{C}_6\text{H}_7^*$  can also emit infrared light and become deactivated. The  $\text{C}_6\text{H}_7$  species is an ordinary carbon-based free radical (Gibian and McCorley, 1973). If the  $\text{C}_6\text{H}_7$  species subsequently absorbs a photon, it is likely to photodissociate by the reverse of reaction (1). If a second H atom attacks  $\text{C}_6\text{H}_7$ , the most likely reaction is to produce  $\text{H}_2$  and benzene (R3) with the PAH acting as a catalyst for H-atom recombination. We expect this disproportionation reaction to have a low activation energy, less than 5 kJ per mole. Thus, reactions of H atoms with benzene do not lead to disruption of the carbon ring.

For larger PAHs, less information is available, but the chemical mechanism is probably the same as with benzene, with a possible reduction in the activation energy for H addition to the ring. In addition, it may be possible for more than one H atom to add to the carbon skeleton, eventually leading to hydrogenation of the aromatic. From the reaction with H atoms on graphite particles at low temperature, Bar-Nun and coworkers (1975, 1980) observed formation of light hydrocarbons, presumably due to the addition of hydrogen to the aromatic rings. This process requires that the hydrogen atoms be added, but not removed. In the interstellar medium, however, photon absorption can lead to photodissociation

and loss of the newly added hydrogens. The newly formed C-H bond is weaker than the C-H bonds on an aromatic ring that already has a full complement of hydrogen. Consequently, subsequent photodissociation will remove the extra hydrogen atom rather than aid its attack on the carbon ring system. In this instance, photon absorption actually helps to protect the aromatic species from further chemical attack, because it reverses the previous chemical reaction. If a second H atom strikes the PAH before UV photon absorption, it will migrate until it finds the initial H atom and produce  $H_2$ .

By extrapolating the experimental value of  $k_A$  for benzene (Nicovich and Ravishankara 1984) to an ISM cloud temperature of 100 K and using  $n_H/n = 0.37$  (Duley and Williams 1986), we find the lifetime with respect to chemical attack by H is  $>10^{12} n^{-1}$  yr. This estimate neglects the effects of quantum mechanical tunneling, which may dominate at low temperature (Bar-Nun 1975; Bar-Nun, Litman, and Rappaport 1980), but which has not been observed in the laboratory. In the limit of very low temperature, all of the reactions may occur by tunneling to produce a limiting value for the rate constant (Kondrat'ev 1964). If the tunneling is through a truncated parabolic barrier (Bell 1935) of height  $V$  and base width  $2a$  by a particle of mass  $m$ , the tunneling rate constant is (Kondrat'ev 1964).

$$k_t = A \exp \left[ -2\pi^2 a h^{-1} (2mV)^{1/2} \right], \quad (21)$$

where  $A$  is the rate constant  $A$ -factor. For reaction (1), the mass is that of H, and we assume  $a = 1 \text{ \AA}$  (for  $a = 0.5 \text{ \AA}$ ,  $k_t$  is larger than the observed  $k_A$  at 298 K). The limiting rate constant is therefore  $k_t = 5 \times 10^{-15} \text{ cm}^3 \text{ molecule}^{-1} \text{ s}^{-1}$ , and the estimated chemical reaction time in the dust cloud is  $>10^7 n^{-1}$  yr. This estimate is five orders of magnitude larger than that of Duley and Williams (1986). Moreover, since the reaction leads to no immediate disruption of the PAH carbon skeleton, the carbon skeleton survives for a much longer period.

For larger PAHs, the energy barrier might be lower, leading to shorter chemical reaction times (note that the reaction still does not affect the carbon skeleton). If, for the larger PAHs, the energy barrier is reduced to only  $4 \text{ kJ mol}^{-1}$ , the chemical reaction time is still  $>10^5 n^{-1}$  yr, which is many orders of magnitude longer than the time constant for photon absorption. If the magnitude of the preexponential factor is proportional to the number of six-membered rings, the lifetime will be shorter for multiring PAHs, but reactions with H atoms still will not lead to destruction of the carbon skeleton, because the reaction is "reversed" by subsequent photodissociation. Indeed, in the diffuse interstellar medium the UV photon absorption rate by PAHs is much larger than the H atom reaction rate. Even inside dense molecular clouds, the internal UV field produced by cosmic-ray excitation of  $H_2$  (Prasad and Tarafdar 1983; Gredel, Lepp, and Dalgarno 1987) will be sufficient to reverse reaction (1).

Another potentially destructive chemical reaction is that with oxygen atoms. As shown in an elegant crossed molecular beam study with benzene (Sibener *et al.* 1980), the mode of attack is oxygen addition to the six-membered ring (R4, Table 2). The reverse of reaction (4) is possible, but apparently,

isomerization to form excited phenol ( $C_6H_5OH$ ) predominates (R5). The excited phenol can lose its energy by loss of the phenolic H atom, or by photon emission (reactions [6] and [7]). In either event, the O atom will be bound to the carbon skeleton. In the molecular beam study (Sibener *et al.* 1980), reaction (6) was observed, but reaction (8) was not, even though this reaction had been inferred from earlier investigations. Similarly, the OH product was not observed. Subsequent reactions and photon absorption might degrade the carbon skeleton. However, the binding energy of the hydrogen atom in the hydroxyl group as well as that of the remaining O atom to the carbon ring are much less than that of the aromatic H atoms or that required to fragment the carbon ring (Benson 1976). Unimolecular decomposition upon UV photon absorption, which again is expected to dominate over reactions with H or other gas-phase species, will lead to the eventual loss of the oxygen substituent. It is noteworthy that the infrared spectrum of the phenolic side groups and derivatives are distinctive, compared to the pure hydrocarbons, and interstellar spectra give no evidence for such functional groups attached to PAHs. Thus, attacks on benzene by O atoms may lead to the addition of oxygen substituents to the carbon skeleton, but little fragmentation.

The attack on larger PAHs by O atoms may produce different reaction products. The speculative reaction mechanism proposed by Duley and Williams (1986) is possible, but it has not been observed in homogeneous gas-phase kinetics studies. In low-temperature experiments by Bar-Nun and coworkers (1974, 1980), graphite powder was exposed to O atoms and H atoms and various carbon-containing gas-phase products were observed. The chemical mechanism that was operative in this heterogeneous system is not known, but they proposed that quantum tunneling allowed the reaction to proceed at the low temperatures. Thus it is conceivable that larger PAHs could be fragmented subsequent to attack by O atoms.

The rate of attack by O atoms in the ISM can be estimated. Recent measurements on benzene by Nicovich, Gump, and Ravishankara (1982) give the rate constant  $k_0 = 4.6 \times 10^{-11} \exp(-2500/T)$ . (This activation energy is very similar to that for oxygen attack on graphite, cf. Draine 1979). Assuming an O abundance of  $6 \times 10^{-4}$  with respect to H and  $T = 100 \text{ K}$ , this leads to a lifetime of  $>10^{16} n^{-1}$  yr, with respect to chemical attack by O atoms, if tunneling is neglected. Tunneling is much less important for the massive O atom than it is for H atoms. Even with a relatively thin potential barrier ( $a = 0.5 \text{ \AA}$ ), the quantum tunneling lifetime is greater than  $>10^{14} n^{-1}$  yr. If the energy barrier to chemical attack is reduced to only  $4 \text{ kJ mol}^{-1}$ , the lifetime is  $>10^8 n^{-1}$  yr, still far too long to be important.

We conclude that chemical attack by O atoms might be destructive, but the reaction rate is far too slow to be important on a time scale less than  $10^6$  yr.

### c) Molecular Structure

As a class, aromatic molecules are much more stable than other types of molecules with the same number of atoms, and among these there is a subclass called superaromatics which are the most stable (Clar 1972). Mass spectroscopic studies of

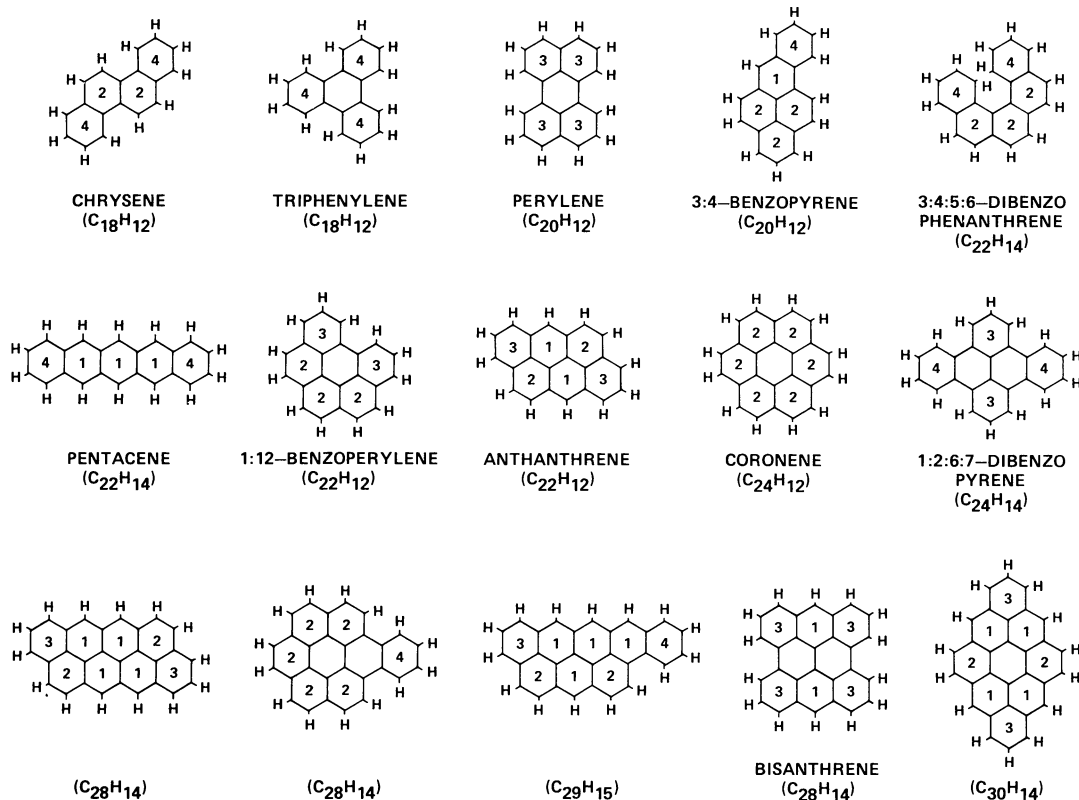


FIG. 22.—Structures of PAHs containing 18–30 carbon atoms. Species in this size range are largely responsible for the interstellar IR emission features. Those containing single as well as doubly and triply adjacent H atoms are the most stable and probably dominate the interstellar PAH population.

ovalene (C<sub>32</sub>H<sub>14</sub>) serve to illustrate this point. Upon bombardment by 75 eV electrons, ovalene may lose up to 5 H atoms, but suffers no loss of skeletal carbon (Burse, Rogerson, and Bursey 1970). Thus, absorption of UV photons (6 eV < E < 13.6 eV) can produce stable ions, induce the loss of an H atom, or rearrange the skeleton to a more stable, condensed form, but will not fragment the carbon skeleton. In general, for a given number of rings, the most stable PAH has the most condensed configuration possible (Stein 1978; Aihara 1987). It is these condensed forms that are most favored under interstellar conditions.

The “plateau” from 950 to 740 cm<sup>-1</sup> (10.5 to 13.5 μm), which is produced by the overlapping of bands due to the out-of-plane bending vibration of H atoms, places an important observational constraint on the molecular structures of the interstellar PAHs (Fig. 6). The range of the plateau indicates that the edge rings of the PAHs responsible for the emission features can have nonadjacent, as well as two or three adjacent peripheral H atoms, but not four or five (see § II[ciii] and Cohen, Tielens, and Allamandola 1985). This is consistent with what is expected based on PAH stability arguments.

Stein and coworkers have shown that, even for large PAHs, the edge structure will determine its stability (Stein and Brown 1985; Stein and Fahr 1985). This is because only certain edge structures allow complete electron delocalization and truly aromatic bonding between all adjacent carbon atoms

in the PAH. PAH structures with single as well as doubly and triply adjacent H atoms are far more stable than PAHs with edge structures which have four and five adjacent H atoms. In Figure 22, structures of some PAHs containing 18–30 carbon atoms are shown. Species in this size range probably dominate the IR emission (§ IIIa and Barker, Allamandola, and Tielens 1987). Among these PAHs, the most stable forms are those with the type of edge structures which contain nonadjacent as well as doubly and triply adjacent peripheral H atoms per edge ring. Using this criterion, one can eliminate many of the PAHs in Figure 22, reducing the number of the smallest, likely, interstellar PAHs to a few. Thus ionized PAHs with these types of structures are probably the most important contributors to the interstellar emission spectrum and among the most abundant small PAHs in the interstellar medium.

#### d) PAH Production and Carbon Particle Formation

##### i) Growth in Circumstellar Shells

Stellar sources that contribute to the carbon in the interstellar medium include carbon-rich red giants, carbon-rich Wolf-Rayet stars, R CrB stars, and supernovae. The relative importance of each in terms of carbon particle formation is not well known, although carbon-rich giants are thought to dominate the production. The presence of the IR emission features in the spectra of carbon-rich planetary nebulae (UV objects

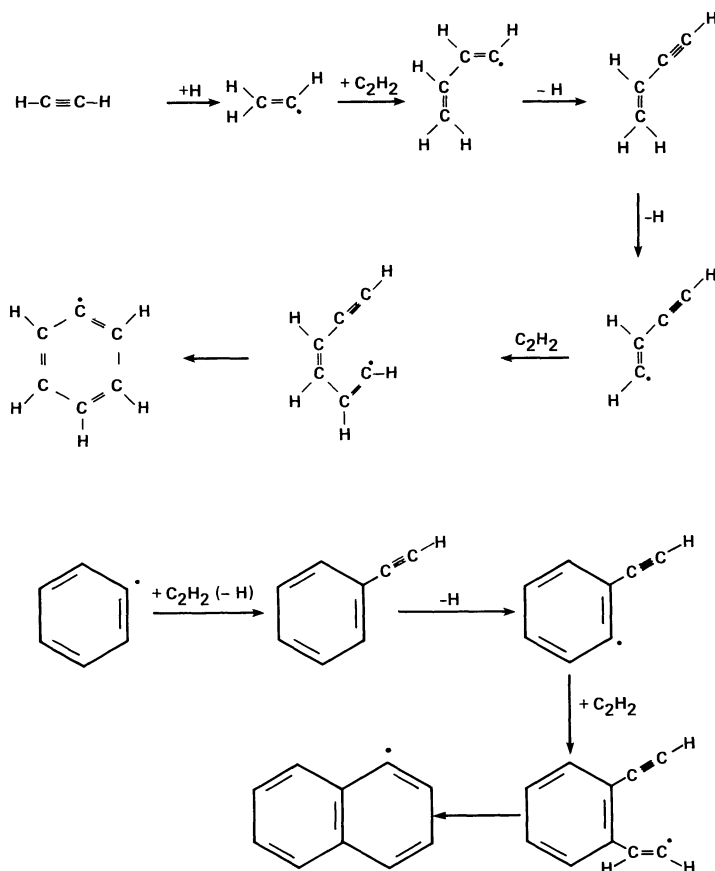


FIG. 23a

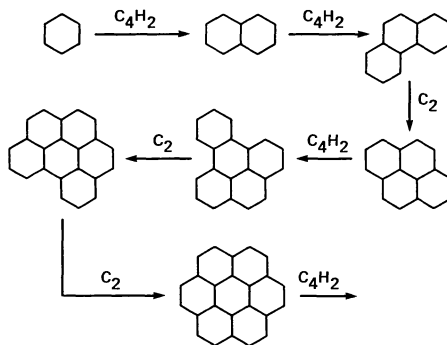


FIG. 23b

FIG. 23.—(a) Possible chemical pathway from  $\text{C}_2\text{H}_2$  to PAHs in carbon-rich circumstellar shells, adapted from Frenklach *et al.* (1984). (b) First six members of the most thermodynamically favorable, high-temperature PAH polymerization route (from Stein 1978). Successive members of this series are formed by adding two or four carbon atoms at a time, the number required to complete an additional fused aromatic ring.

which produced a dust cocoon during their previous carbon-rich giant phase) shows that the carriers are formed in their outflows.

The formation of dust particles in the outflow from carbon-rich giants will be considered in some detail here since these stars are probably the dominant source of interstellar PAHs and carbon dust, and the physical conditions in these outflows are much better determined than those in WC stars or R CB stars. Moreover, their chemical composition resem-

bles that of sooting flames and one can draw on an immense experimental chemical literature on soot formation under similar conditions (e.g., Bittner and Howard 1978; Harris and Winer 1985; Frenklach *et al.* 1986; Frenklach and Warnatz 1987; Bohme 1988, and references therein). The remainder of this discussion is based on this literature and draws heavily from the recent review by Tielens (1988).

Most studies of dust formation in circumstellar environments were based solely on thermochemistry, and considered

that the condensation of solids out of a slowly cooling gas that originally contains no solids took place under equilibrium conditions. Chemical reaction rates, however, are governed to a large extent by kinetic rather than thermodynamic factors. Recently several studies have been published which take both thermodynamics and kinetics into account (Gail, Keller, and Sedlmayr 1984, Gail and Sedlmayr 1984; Keller 1987; Frenklach 1988; Frenklach and Feigelson 1989).

1. *Formation around carbon-rich giants.*—Most of the carbon in the outflow from carbon-rich giants is tied up in CO and C<sub>2</sub>H<sub>2</sub> (Donn 1978) and, consequently, the chemical pathways which convert these molecules into solid dust grains have to be considered. Since CO is so stable, it is not likely to be chemically involved in the reaction scheme leaving acetylene (C<sub>2</sub>H<sub>2</sub>) and its radical derivatives as likely to be the dominant precursor molecules from which soot is formed. The processes which convert C<sub>2</sub>H<sub>2</sub> into carbon grains in the outflow of C-rich red giants are probably very similar to those occurring during the gas-phase pyrolysis of hydrocarbons. Figure 23a shows the first steps in one possible chemical pathway to soot.

Many different branching reaction pathways are possible at all of the intermediate steps. For clarity, these have been ignored since theoretical studies indicate that they are of lesser importance. There are two steps in this reaction scheme: (i) the formation of the first ring out of acetylene and (ii) the growth of additional rings. Formation of the first aromatic ring forms a bottleneck for soot yield. It is started by the formation of the radical C<sub>2</sub>H<sub>3</sub> through H addition to acetylene. This radical can then attack the triple bond in another acetylene molecule and react to form C<sub>4</sub>H<sub>5</sub>. Two more steps of H loss followed by reaction with yet another acetylene yields C<sub>6</sub>H<sub>5</sub>. Cyclization of this radical via interaction of the unpaired electron with the triple bond leads then to the first aromatic ring (Fig. 23a). Once the first ring is formed subsequent chemical growth consists of (more or less) alternating steps of the formation of a radical site through H atom abstraction, acetylene addition, and cyclization. This is illustrated for the formation of the small PAH, naphthalene. Further chemical growth will take place favoring the most stable, fused PAHs pyrene, coronene (Fig. 23b), and ovalene (not shown).

The stable molecular intermediates present in this reaction scheme play an essential role. The reactions leading from one radical to another are reversible at these temperatures and quickly set up an equilibrium distribution. The reactions leading to the stable intermediates, however, are nearly irreversible and thus “pull” the reaction sequence toward molecular complexity and soot formation. The importance of pericondensed aromatic hydrocarbons (such as pyrene and coronene, see Fig. 23b) in this scheme rests mainly in their high thermodynamic stability, resulting from their maximum resonance energy and minimal stress energy (Stein 1978). The gain in the enthalpy of formation can also be maximized by minimizing the entropy change by returning as many H<sub>2</sub> molecules as possible to the gas phase. This favors molecules with short boundary structures and may actually lead to (smaller) aromatic molecules having pentagons or squares in their carbon skeleton (Gail and Sedlmayr 1987). The molecule cyclopentanaphthalene is an example of this latter principle.

The bonding angles introduced by pentagons in the carbon skeleton will lead to warping of the intrinsically planar structure of hexagonal PAHs. If present in an ordered fashion this can even result in a spheroidal molecule such as the recently proposed Buckminsterfullerene and related fullerenes, C<sub>60</sub> (Kroto *et al.* 1985), which is closed upon itself and does not contain any hydrogen. When present in a disordered fashion, pentagons will lead to a curling of the aromatic planes without actual reconnection (Kroto *et al.* 1985; Zhang *et al.* 1985; Kroto 1987). However, cyclopentyl groups are relatively unstable and may be partially lost along the reaction pathway (Frenklach *et al.* 1984). Whether they will persist in the carbon condensation route probably depends on kinetic considerations.

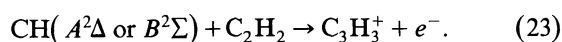
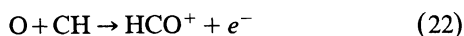
Stein and coworkers have carried out an extensive theoretical study of organic molecule growth from carbon atoms by calculating the stability and reactivity of each type of molecule. They have shown that aromatic hydrocarbons are the most thermodynamically favorable form of hydrocarbon over the temperature range from several hundred to nearly 3000°C (Stein 1978; Stein and Brown 1985, 1986, 1987; Stein and Fahr 1985). This encompasses the temperature (1000 K) in the dust-forming regions of circumstellar envelopes. At temperatures above 3000°C polyacetylenes are favored (Stein and Fahr 1985). One important conclusion from this work is that the PAH with the highest C/H ratio will be the most thermodynamically stable for any given number of H atoms. They have also found that the most stable molecular geometries are those with edge rings which can primarily accommodate non-adjacent, as well as two and three adjacent peripheral H-atoms per ring (§ IVc, above). Recently, Aihara (1988) has described a method which can be used to determine the likelihood of finding specific molecular structures in stellar envelopes and the ISM.

The conditions in the outflow from carbon-rich objects are probably far from thermodynamic equilibrium. This should have a profound influence on the carbon dust condensation process. For example, the vibrational excitation temperature of molecules in the dust condensation zone may be higher than the kinetic gas temperature due to radiative excitation by stellar photons or the trapping of line radiation (Goldreich and Scoville 1976). Since reaction rate constants are often sensitive to vibrational excitation, some reactions may proceed faster than expected from the kinetic gas temperature. The chemical composition may also be far from equilibrium. This is in particular true for the expected H/H<sub>2</sub> ratio. In the photosphere H<sub>2</sub> is formed by three-body reactions and the H/H<sub>2</sub> ratio freezes out when the density drops below about 10<sup>11</sup> cm<sup>-3</sup> (Clegg and Wootten 1980). This results in a disproportionately large abundance of atomic H farther out in the flow. The atomic H abundance is also influenced by the strong shock waves in the extended photosphere. Shock velocities can be as high as 25 km s<sup>-1</sup> and H<sub>2</sub> dissociation will be important. Since the post-shock density may be less than the freezeout density, large deviations from the expected H/H<sub>2</sub> ratio may occur.

The extent of hydrogen coverage of the PAHs as they grow under interstellar conditions depends on carbon atom number, gas kinetic energy, and photon flux. All are difficult to characterize in the PAH forming zone. We infer, from the

arguments presented in § IVa[i], that the smaller species will be less able to accommodate complete hydrogen coverage than the larger species. Once above a certain size (about 30 carbon atoms), the individual PAHs will be fully hydrogenated and further growth by the addition of additional C atoms may well be slowed considerably. This will limit the maximum size of interstellar PAHs produced in these environments. If this is the case, larger interstellar PAHs can only be produced by subsequent very energetic processing of clusters and amorphous carbon particles.

Finally, ionization may also play an important role. Although no ionizing radiation is expected from a cool red giant, chromospheric radiation may produce ions in supergiants. Moreover, chemionization has been shown to be an important ionizing process in sooting flames. Of particular importance are the reactions



These ions are present in the reaction zone in sooting flames and their abundance falls off in the burnt gases. Reactions between these ions and neutral molecules are rapid, as is isomerization into their most stable form (e.g., PAH ions for the larger products). They may actually play an important role in the soot nucleation and condensation process (Barnard and Bradley 1985; Bohme 1988). As with neutral PAHs, pericondensed structures, such as  $\text{C}_{13}\text{H}_9^+$ ,  $\text{C}_{17}\text{H}_{11}^+$  and  $\text{C}_{19}\text{H}_{11}^+$ , are thermodynamically favored and observed to be most abundant in flames. In the circumstellar case, however, oxidation in the stellar photosphere and little atomic oxygen (or CH) is expected to be present in the outflow. Cosmic rays, which have sometimes been considered as an ionizing agent, are unlikely to play a role since they are tied to the galactic field (gyroradius  $\approx 10^{13}$  cm) which will be wrapped around the bubble blown by the stellar wind. Thus ionization processes are likely to be much less important in circumstellar shells around carbon-rich giants than in sooting flames.

2. *Formation around WC 8–10 and R CrB stars.*—The formation of carbon dust around R CrB stars and WC 8–10 stars is expected to follow a completely different chemical pathway than in the outflow from C-rich giants. These objects have lost most of their H-rich envelope, either through nuclear burning or through previous mass loss. The reaction scheme derived from experimental studies of the pyrolysis of hydrocarbons in sooting flames, which may be very relevant in the outflow from C-rich red giants, will play no role in the carbon dust formation in these objects, since no  $\text{C}_2\text{H}_2$ ,  $\text{C}_2\text{H}$ , or H is present. Carbon soot formation is now expected to be initiated through the formation of polyynes (polyacetylene-like C chains without H, i.e.,  $\text{C}_2, \text{C}_3, \text{C}_4$ , etc.). Large molecular structures of this kind (> 20 carbon atoms) are expected to be flexible enough to form aromatic ring structures. One important difference between this soot formation scheme and that discussed above is the presence of a large number of unfilled valences at the periphery of the planar aromatic structure. Therefore, even more than in pyrolysis of hydrocarbons where H can (temporarily) saturate these dangling bonds, minimizing this “surface free energy” is expected to be very important in soot formation in R CrB and WC 8–10 stars.

This may act to enhance the value of pentagons in the aromatic structure (e.g., in order to minimize the number of surface bonds) and enhance the likelihood of fullerene formation.

A second difference between the outflow from these objects and that from C-rich giants is the presence of ionizing radiation. WC 8–10 stars are very hot stars and most of their energy is emitted in the far-ultraviolet. The wind from these stars is highly ionized. The observed column density of neutral C is typically only  $10^{-6}$  of the elemental C. R CrB stars are much cooler, but they do possess an active chromosphere, emitting FUV radiation which may lead to ionization and photodissociation. In this case simple, neutral, carbon-bearing molecules dominate the composition of the envelope. Because ion-molecule reactions are much faster than neutral-radical reactions, ionization may play an important role in soot formation, particularly in WC 8–10 stars. The bottleneck in soot formation is now the formation of the first molecules. In view of the high degree of ionization, the absence of H, and the low pressure, radiative association of C with  $\text{C}^+$  and  $\text{C}_2^+$  are expected to be important reactions in the outflows from WC 8–10 stars. Dissociative recombination of  $\text{C}_3^+$  will lead to  $\text{C}_2$  which can then be used as a building block toward larger acetylenic and aromatic species through ion-molecule reactions. The interstellar infrared emission features have recently been detected in two WC stars (Cohen *et al.* 1989), but not yet in C-rich giants.

#### ii) PAHs, PAH Clusters, and Amorphous Carbon Particles

Once formed, the individual PAHs can become the building blocks, or structural units, of soot (amorphous carbon particles). The relationship between individual PAHs and soot is schematically shown in Figure 24. Soot, a common side product of the combustion and pyrolysis of hydrocarbons, is often morphologically independent of generation method and fuel type. Soot particles are made up of microcrystallites with sizes in the range 10–25 Å. X-ray analyses shows that some of the carbon atoms are arranged in graphite-like planar structures, implying the importance of PAH structural units. Indeed, smaller members of the PAH family are readily extracted from soot particles using organic solvents. Soot-formation occurs in terrestrial sources when the aromatic molecules in the soot-forming region become large enough that condensation processes can occur when they collide (Miller, Mallard, and Smyth 1984). This must also be the nucleation controlling step in amorphous carbon particle production in circumstellar shells. PAH condensation occurs when the magnitude of the attractive forces (binding energies) are greater than the average kinetic energy of the colliding molecules and a bound dimer can be formed that can relax radiatively or collisionally. Miller, Mallard, and Smyth have calculated the attractive force for dimers of the three nonpolar aromatic molecules benzene, coronene, and circumcoronene. Four dimer configurations were considered: face-on, tee, edge-on (planes parallel), and propeller (edge-on, planes perpendicular). When dispersive, quadrupole, orbital overlap, and repulsive forces are taken into account, they predict that the tee form is consistently the most stable, with the angle between the planes of the molecules varying from 90° for the benzene dimer, 42° for the coronene dimer, to 36° for the

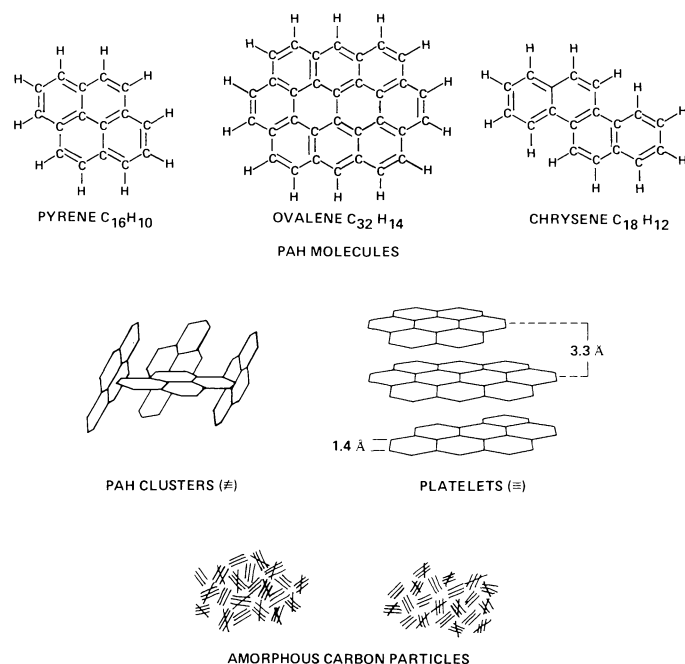


FIG. 24.—The connection between free PAHs and amorphous carbon particles. Complete chemical structures of three individual PAH molecules are shown at the top. Several PAHs grouped together form clusters or platelets (*center*). In this part of the figure, the peripheral H atoms are not shown. Amorphous carbon particles are made up of a randomly oriented mixture of microcrystalline domains (*bottom*) presumed to be clusters and platelets. In an amorphous carbon particle, the individual PAHs can be physically bound by van der Waals forces or chemically bound by various bridging groups (not shown).

dimer of circumcoronene. The dimer binding energies are calculated to be about 0.1, 0.3, and 1.0 eV, respectively. For comparison the hydrogen-bond strength in the H<sub>2</sub>O dimer is about 0.3 eV. Consequently, interstellar amorphous carbon particle growth probably proceeds by the kinetic growth of PAH clusters. The degree of “amorphicity,” or lack of three-dimensional regularity, is therefore built in by the kinetic growth process and the most stable geometries of the various *n*-mers in the cluster-forming zone. Of course, in addition to PAHs, other abundant species can also be incorporated once the size of the cluster is large enough to permit simple accretion. This growth process will slow down, and eventually terminate once the particles and PAHs have been driven into the lower density regions of the circumstellar shell.

Both during coalescence and subsequently, cross-linking between the various aromatic structural units in the particles and clusters can occur during H atom removal by ultraviolet photolysis and cosmic-ray processing. If the geometry is favorable, the radical site produced might form a chemical bond with another PAH, eventually producing a chemically bound collection of PAHs, i.e., an amorphous carbon particle. Some cross-linking can also occur dispersed among the aromatic planes, producing individual, tetrahedrally (*sp*<sup>3</sup>) bonded carbon (“diamond” structure) within the particle.

The distribution of PAHs, PAH clusters, and amorphous carbon particles ejected by carbon-rich objects will be further modified by physical processes in the interstellar medium

(ATBa). Further energetic processes within the amorphous carbon particle may permit rearrangement on a molecular scale (Goebel 1987). As a more ordered structure is both more stable and more graphite-like, repeated energetic events could conceivably tend to convert the amorphous carbon structure to a more graphite-like structure but repeated discrete energetic events could also lead to disorder. Complete graphitization requires several thousand degree temperatures sustained for several hours throughout the particle (Marchand 1987), a situation we view as very unlikely in general, but which may occur occasionally in the interstellar medium. Photolysis and photoisomerization of PAHs not incorporated into particles will tend to convert them to their most stable isomeric form. Photodestruction of the more stable PAHs in the diffuse interstellar medium is unimportant and their lifetimes are expected to be comparable to that of the small carbon particles (§§ IVa, b). The most important PAH destruction mechanism in the interstellar medium is sputtering in fast shocks ( $\geq 200 \text{ km s}^{-1}$ ), as is the case for carbon particles (ATBa). Interstellar shocks may also form a source of molecular sized PAHs. Grain-grain collisions ( $V > 1 \text{ km s}^{-1}$ ) can shatter soot particles, releasing some of their constituent aromatic structural units. This process may also be important in the low-density regions of molecular clouds (Tielens 1989).

In any given object which shows the IR emission bands, there will most likely be some regions in which most of the PAHs are present as free species, and other regions where most of the PAHs will be tied up in grains (either in amorphous carbon particles or frozen on other refractory cores, and in ice mantles). In the very energetic regions such as found in some planetary nebulae, H II regions, and Seyfert galaxy nuclei, some of these grains and PAHs will be “broken up.” It is from these latter regions that we expect the strongest contribution from the emission features as it is there that many of the interstellar PAHs will be in free form, and reduced in size. (Recall that the smallest species will emit most intensely across the mid-IR.) Thus, it is reasonable to expect that the spatial distribution of the underlying broad spectral components, which are likely due to amorphous carbon particle emission in high-excitation regions, will be somewhat different from the distribution of the features due to free molecular species. A suggestion of such spatial differentiation is evident in the maps of NGC 7027 and BD + 30° 3639 in the 1250–770 cm<sup>-1</sup> (8–13 μm) region (Bentley 1982 and Bentley *et al.* 1984). However, broad spectral band-pass filters were used which encompass both the 885 cm<sup>-1</sup> (11.3 μm) free PAH component as well as the plateau. Bregman *et al.* (1989) and Geballe (1989) *et al.* have measured the distribution of the features versus the continuum across the ionization ridge in Orion. These studies clearly show that the spatial distribution of the narrow spectral bands differs from the spatial distribution of the broad features. Further work of this type is needed, as well as laboratory studies of free PAH spectra, if we are to distinguish between the distribution of free PAHs and amorphous carbon particles and so understand the conditions in the various nebulae.

An important, perhaps more powerful probe of the distribution of amorphous carbon particles should be afforded by maps of the extended red emission (ERE), which peaks near 6900 Å and is ~1000 Å wide, discovered by Witt, Schild, and

Kraiman (1984). Witt and Schild (1986, 1988) and Witt (1987) have recently reported that the spectrum, which is very similar to the broad red emission in the Red Rectangle (Schmidt, Cohen, and Margon 1980), is a common characteristic of many reflection nebulae and that it bears a very strong resemblance to UV-visual pumped luminescence from amorphous carbon. They have mapped the distribution of this emission in several reflection nebulae. Similar maps of the IR features due to the molecular-sized PAHs, and continua due to particles in these more benign regions, where local conditions of geometry, photon flux, and optical depth are better characterized, will make it possible to trace the distribution of interstellar carbon from the molecular to the particulate form.

## V. ASTROPHYSICAL APPLICATIONS

### a) Size Estimates

#### i) PAH Molecules

Two independent ways of measuring the size of the PAHs emitting in interstellar space were presented in § III*a*iii. These are based on the comparison of the intensity of the 3040  $\text{cm}^{-1}$  (3.3  $\mu\text{m}$ ) feature with that of the 885 and 2940  $\text{cm}^{-1}$  (11.3 and 3.4  $\mu\text{m}$ ) features, respectively. In Table 3 we present the ratio of the intensities of the 885  $\text{cm}^{-1}$  and 2940  $\text{cm}^{-1}$  features relative to that of the 3040  $\text{cm}^{-1}$  band for the planetary nebula NGC 7027, the ionization bar in the Orion H II region, the reflection nebula NGC 7023, the galactic nucleus M82, and the reflection nebula surrounding HD 44179 (the Red Rectangle), an object now thought to be a proto-planetary nebula. These are well-studied representatives of the classes of objects showing the IR emission features.

The observed 890/3040 and 2940/3040 ratios depend on the energy of the absorbed UV photon in conjunction with the size of the emitting PAH (Figs. 15 and 17). NGC 7023 and the Red Rectangle are illuminated by a B3 V and two A0 V stars, respectively, whose spectra peak in the UV part of the spectrum (1600 and 3000 Å). The other objects are powered by hotter stars and, in principle, very energetic, ionizing

photons ( $h\nu > 13.6$  eV) are available to pump the IR emission. Spatial studies of the Orion Bar show that the IR emission features arise mainly from the interface between the H II region and the molecular cloud (Aitken *et al.* 1979; Sellgren 1981; Gatley and Kaifu 1987; Bregman *et al.* 1989; Roche, Aitken, and Smith 1989). In particular, recent high-resolution spectra at several positions across the Orion Bar show that the 2940/3040 ratio increases dramatically when going into the neutral zone (Geballe *et al.* 1989). Likewise, spatial studies of NGC 7027 suggest that the emission arises predominantly, although not exclusively, from the neutral gas (Aitken and Roche 1982; Bentley 1982; Goebel 1987). Analysis of this source is, however, complicated by the well-known clumpy distribution of the dust and gas (cf. Atherton *et al.* 1979), and a large fraction of the IR emission observed to come from within the boundaries of the ionized zone may actually originate in dense neutral clumps entrained within it. Infrared line studies indicate that the spectrum of M82 is similar to that of an 08.5 star ( $T_{\text{eff}} \approx 35,000$  K; Willner *et al.* 1977; Duffy *et al.* 1987). However, observations of this galaxy probably sample a large collection of H II regions and reflection nebulae similar to the galactic sources discussed above. Thus, it is likely that in all of these objects the 3040, 2940, and 890  $\text{cm}^{-1}$  (3.3, 3.4, and 11.2  $\mu\text{m}$ ) emission features are predominantly pumped by nonionizing UV radiation (e.g.,  $\lambda > 912$  Å,  $\nu < 110,000$   $\text{cm}^{-1}$ ).

Table 3 lists the range of PAH carbon atom number inferred from the observed ratios for 40,000 and 100,000  $\text{cm}^{-1}$  of internal energy (corresponding to the absorption of a 2500 and 1000 Å UV photon, respectively), assuming that no energy is "stored" in electronic excitation energy. This is the situation for ionized PAHs. The number of carbon atoms derived from the 890/3040 ratio ranges from 10 to 120 depending on the assumed internal energy. We note that in the low-excitation source, the Red Rectangle, the derived range of carbon atoms is distinctly smaller (10–50) than in the other sources. Possibly, the relatively benign conditions in this source allow smaller PAHs to survive than in the general interstellar medium (Cohen *et al.* 1986). The size estimates derived from the 2940/3040 (3.4/3.3) ratio are smaller and

TABLE 3

SIZE AND ABUNDANCE OF INTERSTELLAR PAHs

OBJECT (1)	TYPE <sup>a</sup> (2)	890/3040 <sup>b</sup>		2940/3040 <sup>b</sup>		SMALL PAHs <sup>c</sup>		LARGE PAHs <sup>d</sup>	
		Observations (3)	$N_C$ (4)	Observations (5)	$N_C$ (6)	Observations (7)	$f_C$ (8)	Observations (9)	$f_C$ (10)
NGC 7027	PN	5	35–90	6.(–2)	15–40	6.(–2)	0.005–0.05	> 3.(–1)	> 0.03–> 0.3
Orion Bar	H II	10	50–120	6.(–2)	15–40	3.(–2)	0.0025–0.025	5.(–2)	0.04–0.04
NGC 7023	RN	7	45–100	...	...	6.(–2)	0.005–0.05	3.(–2)	0.0025–0.025
M82	GN	7	45–100	...	...	4.(–2)	0.003–0.03	9.(–2)	0.008–0.08
HD 44179	RN?PN?	2	10–50	1.(–1)	10–30	5.(–2)	0.004–0.04	...	...

<sup>a</sup>Type of object: PN = planetary nebula; H II = region; RN = reflection nebula; GN = galactic nucleus.

<sup>b</sup>Observations of the ratio of the integrated intensity in respectively the 885 and 3040  $\text{cm}^{-1}$  (11.3 and 3.3  $\mu\text{m}$ ) and the 2940 and 3040  $\text{cm}^{-1}$  (3.4 and 3.3  $\mu\text{m}$ ) emission features and the derived number of carbon atoms in the emitting PAHs.

<sup>c</sup>The observed ratio of the integrated emission in the IR emission features relative to the far-IR dust continuum observations and the derived lower limit to the fraction of the elemental carbon in the form of small ( $\sim 25$  C atoms) PAHs ( $f_C$ ). The upper limit is 10 times higher.

<sup>d</sup>The observed ratio of the emission in the broad component underlying the 6.2 and 7.7  $\mu\text{m}$  emission features to the far-IR dust continuum (observations) and the derived lower limit to the fraction of the element carbon in the form of large ( $\sim 350$  C atom) PAHs ( $f_C$ ).

REFERENCES TO THE OBSERVATIONS.—Cohen *et al.* 1986; Bregman *et al.* 1989; Sellgren *et al.* 1985; Willner *et al.* 1977; Gillett *et al.* 1975.

the range narrower. This is not too surprising, since the 2940  $\text{cm}^{-1}$  emission will be dominated by the most highly excited and thus smallest PAHs. As described in the next paragraph, there are several uncertainties in the analysis of the 890/3040 (11.2/3.3) ratio that are not present in the 2940/3040 analysis, all of which tend to make the size estimate derived from the 890/3040  $\text{cm}^{-1}$  ratio an upper limit.

The uncertainties in the 890/3040 ratio which make carbon numbers derived from Figure 15 an upper limit follow. First, very small (20–30 C atoms) PAHs will have several adjacent H atoms per ring (Figs. 1 and 22) and will contribute to the 950–750  $\text{cm}^{-1}$  (10.5–13.5  $\mu\text{m}$ ) plateau rather than the 890  $\text{cm}^{-1}$  (11.2  $\mu\text{m}$ ) feature (Cohen, Tielens, and Allamandola 1985). Indeed, a pericondensed (compact) PAH has to contain about 100 C atoms before the number of isolated peripheral H atoms outnumbers the adjacent ones. Since the Einstein  $A$ -values for the out-of-plane modes are unknown, it has been assumed that they will be very similar for these different types of H atoms. If this is so, emission in the 890  $\text{cm}^{-1}$  (11.2  $\mu\text{m}$ ) feature will dominate the 950–750  $\text{cm}^{-1}$  (10.5–13.5  $\mu\text{m}$ ) plateau feature only in such large PAHs. *IRAS* LRS spectra suggest that typically the plateau emission is about half as intense as the 890  $\text{cm}^{-1}$  (11.2  $\mu\text{m}$ ) feature (Cohen, Tielens, and Allamandola 1985). Using this quantity, rather than the 890  $\text{cm}^{-1}$  (11.2  $\mu\text{m}$ ) band intensity, leads to a 30% smaller PAH-size (30–75) than listed in Table 3. Second, large PAHs, while emitting weakly at 3040  $\text{cm}^{-1}$  (3.3  $\mu\text{m}$ ), can contribute substantially at 890  $\text{cm}^{-1}$  (11.2  $\mu\text{m}$ ). Again, this increases the observed 11.2/3.3  $\mu\text{m}$  ratio and thus the derived PAH size. The importance of this effect depends critically on the PAH size distribution and is difficult to estimate at present. One potential measure of the importance of larger PAHs is the intensity in the broad component underneath the 6.2 and 7.2  $\mu\text{m}$  feature, which is so evident in the spectrum of NGC 7027 (cf. Fig. 3). The carrier of this emission contains about 300–400 C atoms (see below and Bregman *et al.* 1989). There does not seem to be a strong correlation between the strength of this broad emission feature and the PAH size estimated from the 890/3040 ratio (Table 3). Thus the influence of the particles or large PAHs responsible for the broad component on the 890/3040 ratio seems to be small. Finally, part of the absorbed UV photon energy may be stored as electronic excitation energy rather than vibrational energy (e.g., interconversion to the triplet state, see § III*ai*) and ultimately lost through phosphorescence (Fig. 10). This is an important process for neutral PAHs where the first excited triplet state lies well below the first excited singlet state. For singly ionized PAHs, however, interconversion, from doublet and quartet states in this case, plays a smaller role, since the first excited quartet state lies well above the first excited doublet state (Fig. 11; Leach 1987*a*). Since most small PAHs ( $\leq 25$  C atoms) will be singly ionized in regions which are bright in the IR emission features, interconversion will not influence the size estimate much. This effect may be more important, however, in the diffuse interstellar medium, where a substantial fraction of the near- and mid-infrared emission (e.g., IR cirrus) may come from neutral PAHs.

Since the 2940/3040 (3.4/3.3) ratio is not sensitive to the molecular geometry (e.g., adjacent peripheral H atoms) and the relative Einstein  $A$ -values are well known, these size

estimates are more reliable than the ones derived from the 890/3040 (11.2/3.3) ratio. In any case, both measures of molecular size indicate that species consisting of considerably fewer than 50 carbon atoms dominate the mid-IR emission.

#### ii) PAH Clusters

The IR spectra of several sources reveal the presence of an independent broad emission component underlying the 6.2 and 7.7  $\mu\text{m}$  (compare Figs. 1, 2, and 3). We attribute this emission to large PAHs or clusters of smaller PAHs, whose vibrational spectrum is dominated by C-C stretching modes (§ II*cii*). In estimating the size of this component we will concentrate on the Orion Bar where the cloud geometry is well known. It is difficult to estimate the excitation temperature of this component since the IR spectrum is dominated by the infrared characteristics of the emitting material. It is likely to be at least 400 K. An estimate of the size of the emitting species can be made by attributing the emission to temperature fluctuations in large PAHs or PAH clusters excited by absorption of a single UV photon, using bulk material properties (LP). Given the structural similarities between such species and an aromatic graphitic carbon network, we approximate the frequency spectrum of vibrational modes with that of graphite. Then, using the measured specific heat for graphite, the peak temperature upon absorption of a UV photon is approximately given by

$$T = 2.1 \times 10^3 [E/N_C]^{0.4}, \quad (32)$$

where  $E$  is the UV photon energy in eV and  $N_C$  is the number of carbon atoms in the emitting species. Taking into account that the average emission temperature is about 2/3 of the peak temperature (de Muizon, D'Hendecourt, and Geballe 1987), we conclude that the number of carbon atoms in the species responsible for the broad pedestal emission is about 300 to 400 for a typical 10 eV photon. This is a very crude estimate, since it is derived using bulk properties of graphite for such species.

#### b) The Abundance of Interstellar PAHs

The fraction of elemental carbon in the form of interstellar PAHs,  $f_C$ , can be determined by comparing the emission in the IR emission features with that in the (far) infrared dust continuum and assuming UV absorption cross sections for the PAHs and the dust (LP; ATBa). In this analysis we assume that IR emission originates in the neutral photodissociation regions (Tielens and Hollenbach 1985*a, b*) surrounding the ionized gas in H II regions and planetary nebulae. Both the PAHs and the dust are excited by photons longward of the H ionization limit ( $\lambda > 912 \text{ \AA}$ ). The fraction of C in the form of PAHs can be written

$$f_C = \frac{A_v}{N_H} \frac{\kappa_{uv}}{\kappa_v} \frac{(1 - \omega_{uv})}{\sigma_{uv} A_C} \frac{f_{ir}}{(1 - f)_{ir}}, \quad (33)$$

where  $A_v/N_H$  is the visual extinction per hydrogen atom,  $\kappa_{uv}/\kappa_v$  is the ratio of the UV and visual dust opacity,  $\omega_{uv}$  is the UV albedo of the dust,  $\sigma_{uv}$  is the average UV absorption cross section of PAHs per carbon atom,  $A_C$  is the elemental

carbon abundance, and  $f_{\text{ir}}$  is the observed ratio of the IR flux in the emission features relative to that in the dust continuum. Inserting typical values for the dust and gas properties ( $A_v/N_H = 5.2 \times 10^{-22}$  magn  $\text{cm}^2$ ;  $\kappa_{\text{uv}}/\kappa_v \cong 3$ ;  $\omega_{\text{uv}} \cong 0.6$ ;  $A_C = 4 \times 10^{-4}$ ; Savage and Mathis 1979; Allen 1973) we find

$$f_C = \frac{1.6 \times 10^{-18}}{\sigma_{\text{uv}}} \frac{f_{\text{ir}}}{(1 - f_{\text{ir}})}. \quad (34)$$

Estimates of the fraction of carbon locked up in the form of PAHs in the emission regions depend thus inversely on the adopted UV absorption properties of the PAHs, which are not well known. In the next section limits on  $\sigma_{\text{uv}}$  and thus on the amount of C in the form of PAHs are derived.

i) *The UV Absorption Properties of PAHs*

PAH molecules absorb strongly in the UV due to  $\pi \rightarrow \pi^*$  and  $\pi \rightarrow \sigma^*$  electronic transitions. For several small PAHs in the linear polyacene series (i.e., benzene, naphthalene, and anthracene) the spectrum has been measured in the gas phase up to  $\cong 20$  eV ( $\lambda > 600$  Å). The FUV and visible spectra of these species are dominated by an extremely strong band in the 2000–2500 Å region, accompanied by a nearly continuous series of weaker bands largely due to  $\pi \rightarrow \pi^*$  electronic transitions which increase in strength from 2000 to 1000 Å (Robin 1974). This series overlaps with strong bands due to  $\pi \rightarrow \sigma^*$  transitions that extend to several hundred angstroms ( $\sim 330$  eV). Vacuum UV and visible spectra ( $\lambda > 1500$  Å) have been measured for many more simple PAHs in solutions, including coronene ( $\text{C}_{24}\text{H}_{12}$ ) and ovalene ( $\text{C}_{32}\text{H}_{14}$ ). Again these spectra show one or sometimes two prominent absorption bands in this wavelength region (Birks 1970). The peak strength (and width) of UV absorption features depend strongly on the solvent. The integrated strength of a feature is generally, however, much less sensitive to the polarity of the solvent and we use this quantity to estimate  $\sigma_{\text{uv}}$ .

The integrated strength of the dominant PAH transition in the 1500–3000 Å region is typically about  $10^{-13}$  cm per C atom, but variations up to a factor of 3 have been measured for some PAHs. This value is comparable to that of the 2200 Å feature produced by small (200 Å) graphite grains (Tielens and de Jong 1979). Note that the graphite 2200 Å feature is actually broader than the UV bands produced by individual PAHs. The sum of the integrated strength of all the weaker features of a PAH longward of 1500 Å is typically about 50%–100% of that of the dominant band. The absorption properties of these larger PAHs are unknown beyond 1500 Å. We will assume that they are similar to those of the smallest members of the linear polyacene series and contribute a total integrated absorption strength equal to that of the dominant peak in the 2000–3000 Å region. The average peak absorption cross section in the 912–3000 Å region of the interstellar PAH family is then about  $4 \times 10^{-18}$   $\text{cm}^2$  per C atom. Since emission in the IR features will be dominated by the emitting PAHs in the interstellar PAH family with the largest UV absorption cross section per carbon atom and the maximum such absorption longward of 1500 Å is about 3 times higher than used to derive this value, we will adopt an absolute upper limit for the UV absorption cross section of interstellar PAHs of  $2 \times 10^{-17}$

$\text{cm}^2$  per C atom. A conservative lower limit for the UV absorption cross section of interstellar PAHs is obtained by setting it equal to the typical value in the 1500–3000 Å range ( $3 \times 10^{-18}$   $\text{cm}^2$  per C atom) and assuming that there is no absorption shortward of 1500 Å.

ii) *The Fraction of C in Small, Interstellar PAHs*

The observed values for the fraction of the flux in the emission features as compared to the IR dust continuum for several typical emission regions are listed in columns (7) and (9) in Table 3. Using the upper limit for the average peak UV absorption cross section derived above, a lower limit to the fraction of carbon in the form of small PAH molecules is given by

$$f_C = 8 \times 10^{-2} \frac{f_{\text{ir}}}{(1 - f_{\text{ir}})}. \quad (35)$$

For the objects in Table 3, these lower limits lie in the range 0.2%–0.5%. However, if we adopt the conservative lower limit to the UV absorption cross section of  $3 \times 10^{-18}$   $\text{cm}^2$  per C atom in the 1500–3000 Å range, the required fraction of elemental C in the form of PAHs is about 10 times higher. The required carbon fraction is thus on the order of 1%–5%. Assuming that the typical IR feature emitting interstellar PAH contains 25 carbon atoms per molecule, the minimum abundance of PAHs per H nuclei is about  $3 \times 10^{-8}$ . This is less than previously estimated (ATBa) due to the assumed higher UV absorption cross section. The actual abundance of the interstellar PAHs which dominate the IR emission is probably about a factor of 3 larger which implies a carbon fraction of 3%–15%.

iii) *The Fraction of C in Large PAHs*

Adopting the same FUV absorption cross section per carbon atom for large PAHs as for the small ones ( $2 \times 10^{-17}$   $\text{cm}^2$  per C atom), the fraction of elemental carbon in the form of large (300–400 C atoms) PAHs or PAH clusters responsible for the broad emission component underlying the 6.2 and 7.7  $\mu\text{m}$  features, was calculated (Table 3). Except for NGC 7027, the lower limits are very similar to those derived for small PAHs, suggesting that the mass distribution function of PAHs is nearly flat. The much larger fraction derived for this component in NGC 7027 reflects directly the pronounced difference in the spectral appearance of this source compared to others (e.g., compare Figs. 1 and 3). Possibly, this is a result of the compact nature of this source and the resulting high temperature, even for classical grains. Alternatively, one must keep in mind that the emission in the other sources listed in Table 3 originates from interstellar rather than “recently” produced circumstellar material. The “older” emitters may have been extensively processed in the interstellar medium by, for example, strong supernova shocks. Shattering due to grain-grain collisions may substantially alter the interstellar amorphous carbon “grain” size distribution and can conceivably be an important source of PAHs (Tielens and Allamandola 1987b). With 0.5% of the elemental C locked up in these large PAHs (Table 3), their abundance by number is  $8 \times 10^{-9}$  of that of H.

The abundance estimates for small and large PAHs agree very well with the values obtained by extrapolating the interstellar carbon grain size distribution into the molecular domain (Tielens 1989). This supports the evolutionary relationship between PAHs and carbon soot particles (§ IV dii).

### c) PAHs and the UV Extinction Curve

From Table 3 we see that the fraction of the energy emitted in the IR emission features relative to the FIR dust continuum is insensitive to the spectral type of the illuminating stars despite their large spread in effective temperature ( $10,000 \leq T_{\text{eff}} \leq 200,000$  K). This implies that the absorption cross section of the carrier of the emission features has a wavelength dependence which is similar to that for the larger dust particles over the relevant wavelength range. Given the low effective temperature of the Red Rectangle, this similarity in absorption characteristics seems to extend well into the visible. Analysis of the  $12 \mu\text{m}$  cirrus has also suggested that the emission carrier has substantial absorption cross section for visible light (Puget 1987). Small ( $< 40$  C atoms), neutral PAHs show only strong absorption bands in the FUV ( $\lambda \leq 3000 \text{ \AA}$ ; Donn 1968), and after averaging over the stellar spectrum substantial variation with stellar effective temperature are expected. For example, the flux-averaged absorption cross section of a small, neutral PAH with one strong absorption band in the  $1000\text{--}1500 \text{ \AA}$  and one in the  $2000\text{--}2500 \text{ \AA}$  range varies by a factor of 5 when the effective temperature is varied from  $30,000$  to  $10,000$  K. In contrast, the flux-averaged absorption cross section of the dust varies by less than 50% over this temperature range. This can be explained because small, ionized PAHs, as well as large ( $> 50$  C atoms) neutral or ionized PAHs, show absorption features in the near-UV and visible region of the spectrum (cf. Crawford, Tielens, and Allamandola 1985; van der Zwet and Allamandola 1985; Fig. 26). Unfortunately their strength relative to the FUV absorption bands is unknown. Since most small PAHs are expected to be singly ionized in the emission zones, this lack of variation in the fraction of energy in the emission features relative to the dust continuum may not pose a serious problem to the PAH hypothesis. UV and visible absorption studies of likely interstellar PAHs are required to test this.

The IR observations indicate that the interstellar PAHs which produce the features absorb on the order of 5% of the UV photons available. It is likely that these will produce some narrow features (due to  $\pi \rightarrow \pi^*$  and  $\pi \rightarrow \sigma^*$  transitions) in the UV portion of the extinction curve. If, as expected, the PAH family has many members, the resulting structure will be small, perhaps on the order of 10% of the average absorption cross section. Relative to the dust extinction, the strength of PAH absorption features in the UV are expected to be on the order of  $5 \times 10^{-3}$ .

UV extinction studies have placed an upper limit on the presence of structure of 7% per magnitude of  $E(B - V)$  color excess, corresponding to about 0.8% per unit magnitude of UV extinction (Seab and Snow 1985). This is (barely) consistent with the structure expected from PAHs calculated above. The *Hubble Space Telescope* will be able to detect structure in the UV absorption curve at a much lower relative level than presently possible. Since electronic transitions are very char-

acteristic for an individual species, eventually it may be possible to identify and determine the abundance of a few specific PAH molecules on the basis of structure in the UV portion of the extinction curve.

### d) Dehydrogenation of Interstellar PAHs

In principle, a PAH molecule may lose an H atom through direct absorption into a dissociative electronic state (Buch 1989), which occurs for C-H bonds shortward of about  $1800 \text{ \AA}$  ( $55,000 \text{ cm}^{-1}$ , Turro 1978). However, for a PAH molecule containing 20 or more C atoms, the density of vibrational states of lower lying electronic states at this high internal energy is so large that internal conversion of this electronic excitation energy into vibrational excitation energy of a lower electronic state is generally very fast. Indeed, the internal conversion rate for the  $S_3 \rightarrow S_1$  state of anthracene [ $E(S_3) \cong 40,000 \text{ cm}^{-1}$ ] is faster than  $10^{13} \text{ s}^{-1}$  and is apparently only limited by nuclear motion (Turro 1978). Thus, direct dissociation of the C-H bonds of interstellar PAHs, while perhaps possible, is probably not the dominant cause of H loss. Subsequent to internal conversion, the resulting highly vibrationally excited PAH can still lose an H atom when the number of vibrational quanta located in one bond is sufficient to cause rupture (i.e., through excitation into the vibrational continuum). The probability of this latter process has been calculated in § IVai) for several small PAHs as a function of vibrational excitation energy. Following Tielens *et al.* (1987) we will assess the hydrogen coverage of interstellar PAHs in this section.

A highly excited PAH molecule has several channels available for decay of its internal vibrational energy, including IR fluorescence and C-H bond rupture. Identifying IR fluorescence, with a typical rate constant of about  $10 \text{ s}^{-1}$ , as the most important one competing with H bond rupture, the probability for H loss upon absorption of a UV photon can be estimated by comparing the respective rate constants. Adopting the calculated H loss rate constant for perylene (Fig. 21) for the smallest ( $\cong 20$  C atoms) interstellar PAHs, we conclude that the H loss and IR fluorescence are equally probable at an internal vibrational energy of about  $85,000 \text{ cm}^{-1}$  ( $\cong 10 \text{ eV}$ ). Since the calculated rate constant for C-H rupture increases rapidly with internal excitation energy, the rate at which such a small PAH loses peripheral H atoms is then given by the absorption rate of UV photons more energetic than  $10 \text{ eV}$ .

The PAH absorption rate of UV photons more energetic than  $10 \text{ eV}$  (Table 4) can now be calculated using the estimated incident FUV field intensity ( $G_0$ ), the effective temperature of the radiation field, and assuming a UV absorption cross section of  $3 \times 10^{-16} \text{ cm}^2$  in this wavelength region. The latter is actually an upper limit to the UV absorption cross section (§ Vb). The calculated H-loss rates are given in Table 4. Since these small PAHs will be mostly singly ionized in the emitting zone, the collision rate constant with H atoms is given by the Langevin rate constant ( $\cong 10^{-9} \text{ cm}^3 \text{ s}^{-1}$ ). The reaction probability of an H atom upon collision with a dehydrogenated PAH is not known, but is probably larger than 0.5. In our calculations we will set it equal to unity. The

TABLE 4  
PHYSICAL CONDITIONS IN THE EMITTING REGIONS

Object	Type <sup>a</sup>	$G_0^b$	$T_{\text{eff}}^c$ [K]	$n_0$ [cm <sup>-3</sup> ]	$n_e$ [cm <sup>-3</sup> ]	$T$ [K]	$R_{\text{uv}}^d$ [s <sup>-1</sup> ]	$R_{\text{H}}^e$ [s <sup>-1</sup> ]	$f_n^f$
NGC 7027	PN	4.7(5)	200,000	7.(4)	7.(1)	500	7.(-3)	7.(-5)	1.6(-2)
Orion Bar	H II	4.4(4)	40,000	1.(5)	3.(1)	500	4.(-4)	1.(-4)	7.1(-2)
NGC 7023	RN	2.6(3)	18,000	4.(3)	1.(0)	250	7.(-6)	5.(-6)	5.9(-2)
M82	GN	3.0(3)	35,350	1.(4)	3.(0)	250	3.(-5)	1.(-5)	1.4(-1)
HD 44179	RN	9.0(4)	10,000	1.(3)	...	...	3.(-5)	1.(-6)	4.0(-2)

<sup>a</sup>PN = planetary nebula; H II = H II region; RN = reflection nebula; GN = galactic nucleus.

<sup>b</sup>Intensity of the incident radiation field between 6 and 13.6 eV in units of the average interstellar UV radiation field,  $8.8 \times 10^6$  photons cm<sup>-2</sup> s<sup>-1</sup> star<sup>-1</sup> (Habing 1968).

<sup>c</sup>Effective temperature of the incident radiation field.

<sup>d</sup>The H-loss rate.

<sup>e</sup>The rehydrogenation rate.

<sup>f</sup>Fraction of 20 C atom PAH which are neutral.

REFERENCES TO THE PHYSICAL CONDITIONS.—Ellis and Werner 1988; Tielens and Hollenbach 1985*b*; Chokshi *et al.* 1988; Wolfire *et al.* 1988; Warren-Smith *et al.* 1981.

calculated rehydrogenation rates ( $R_{\text{H}}$ ) for typical interstellar emission regions are given in Table 4.

Typically, for a 20 C atom PAH the calculated hydrogen loss rate is somewhat larger than the rehydrogenation rate. The photon energy at which the C-H rupture rate constant equals the IR fluorescence rate increases strongly with the size of the PAH (Fig. 21). Limiting the available UV photon energy to less than 13.6 eV, we estimate that PAHs larger than 25 to 30 C atoms will only rarely lose a peripheral H atom. Given the rapid rehydrogenation rate, such large interstellar PAHs are expected to be completely hydrogenated in the emission zones. Conversely, PAHs comprised of less than about 20–25 C atoms will rapidly lose their H atoms. Since the bonds which bind the H atoms to the periphery of the molecule are highly localized, the loss of an H atom will not significantly influence the strengths of the other C-H and C-C bonds in the molecule. Thus a small PAH can be rapidly stripped of most of its H in an intense UV field. Indeed, recent observations of variations in the 2940/3040 (3.4/3.3) ratio across the Orion Bar and at two distances from the illuminating star in the Red Rectangle suggest that the loss of peripheral hydrogen is an important process (Geballe *et al.* 1989).

#### e) Deuterium Enrichments of Interstellar PAHs

In section IV*a*ii the C-D rupture rate constant upon UV photon absorption by small PAHs has been calculated and compared to that of the C-H bond. The results show that hydrogen loss is preferred over deuterium loss and thus that deuterium enrichment can be expected in the interstellar medium. Large deuterium enrichments, up to a factor of 40, have been measured in the acid-soluble and insoluble hydrocarbon phases in carbonaceous meteorites and in interplanetary dust particles (Geiss and Reeves 1981; Kerridge and Chang 1985). These enrichments implicate chemical fractionation due to the zero-point energy difference between deuterated species and their protonated counterparts. The low temperatures ( $T < 150$  K) required for this chemical fractionation process imply nonequilibrium conditions, since neutral-neu-

tral reactions are too slow at these temperatures to produce the measured fractionations. Indeed, explanations for these high deuterium enrichments have been sought in interstellar gas-phase ion-molecule reactions driven by cosmic-ray ionization for which there is observational evidence attesting to its importance (cf. Watson 1976), as well as in reactions catalyzed by grain surfaces, possibly assisted by UV photolysis (Tielens and Allamandola 1987*a*) and the photochemical enrichment of interstellar PAHs (Allamandola, Sandford, and Wopenka 1987). Each of these processes might be able to produce high deuteration enrichments in the interstellar clouds, which could perhaps be incorporated into meteoritic and planetary bodies without major modifications in the solar nebula. Here we will briefly discuss the third mechanism.

Consider a PAH in the center of a molecular cloud illuminated by the ambient interstellar radiation field. Typically, a molecular cloud has a total visual extinction of 10 mag (Solomon *et al.* 1987; Scoville and Sanders 1987). The center of the cloud has thus an  $A_v$  of about 5, corresponding to a  $\tau_{\text{uv}}$  of 10. The hydrogen loss rate of a 20 carbon atom PAH is then about  $10^{-12}$  s<sup>-1</sup> (cf. § V*d*). Thus, over the lifetime of the cloud ( $\approx 3 \times 10^7$  yr) a small PAH will lose a peripheral H atom about  $10^3$  times. The number of peripheral deuterium atoms relative to hydrogen atoms will then reflect the composition of the gas phase enhanced by the difference in rupture rate constants: that is,

$$X_{\text{D}} = 0.7 \frac{k_{\text{D}}^{\text{uv}}}{k_{\text{H}}^{\text{uv}}} \frac{n_{\text{D}}}{n_{\text{H}}} \approx 2 \frac{n_{\text{D}}}{n_{\text{H}}}, \quad (36)$$

where the factor 0.7 takes the difference in thermal velocity into account and the relative UV rupture rates,  $k_i^{\text{uv}}$ , have been taken from § IV*a*ii. Most of the hydrogen is locked up in H<sub>2</sub> in molecular clouds, while a considerable fraction ( $\approx 50\%$ ) of the deuterium is in atomic form. Consequently, the atomic D over atomic H ratio can be greatly enhanced over the cosmic abundance ratio (Tielens 1983; Dalgarno and Lepp 1984). For example, at a density of  $10^3$  cm<sup>-3</sup> and a temperature of 10 K,  $n_{\text{D}}/n_{\text{H}}$  is calculated to be about  $5 \times 10^{-2}$ , so that

deuterium enrichments on the order of  $10^{-1}$  are expected in small PAHs. "Equilibration" with the gas phase at higher densities will lead to even larger deuteration effects and at a density of  $10^4 \text{ cm}^{-3}$  about half the peripheral H atoms on a small PAH may be replaced by D atoms. At this point about 5% of the available elemental D is locked up in PAHs. Although this is substantial, PAHs are not the dominant reservoir of deuterium unless the abundance of small PAHs is 10 times larger than estimated in § Vb. It should be emphasized that, as for icy grain mantles, the expected deuterium enrichment reflects directly the greatly enhanced atomic D/H ratio in the gas phase, which itself results from ion-molecule, gas-phase reactions. Further enrichment may follow from direct gas-phase ion-molecule reactions involving neutral and ionized PAHs (cations and anions) with  $\text{H}_2\text{D}^+$  and HD.

Finally, in a typical emission zone around an early-type star, the UV flux is so high that rapid photodissociation of  $\text{H}_2$  becomes important ( $A_v < 5$  mag; Tielens and Hollenbach 1985a, b) and the atomic H abundance will be many orders of magnitude larger than that of atomic D. Consequently, in these regions deuterium enrichment is then limited to the difference in UV dissociation rates (about a factor of 3) and the expected D/H ratio of PAHs is only about  $3 \times 10^{-5}$ . Larger deuteration effects can be expected farther from the illuminating star or deep inside the molecular cloud where hydrogen is mainly in molecular form. However, the intensity of emission brightness will also be down due to the drop in UV intensity. Possibly, the best place to search for deuteration effects may be around sufficiently cool stars so that the flux of  $\text{H}_2$  photodissociating radiation ( $\lambda < 1100 \text{ \AA}$ ) is considerably down, while the flux of PAH pumping photons ( $\lambda < 2000 \text{ \AA}$ ) and C-H bond rupture photons ( $\lambda < 1500 \text{ \AA}$ ) is still fairly high. The Red Rectangle may be an ideal test case since it is powered by two A0 stars ( $T_{\text{eff}} \cong 1000 \text{ K}$ ; Cohen *et al.* 1975) which fulfill these spectral criteria and since the effects of photochemical evolution of PAHs have already been discovered in this source (Geballe *et al.* 1989).

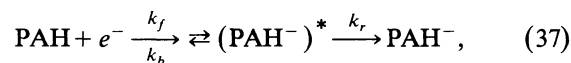
The C-D stretch in the PAHs naphthalene and pyrene ( $\text{C}_{10}\text{D}_8$  and  $\text{C}_{16}\text{D}_{10}$ ) falls in the range  $2300\text{--}2240 \text{ cm}^{-1}$  ( $4.348\text{--}4.464 \text{ \mu m}$ ) and the out-of-plane bending mode in the approximate range  $800\text{--}500 \text{ cm}^{-1}$  ( $12.5\text{--}20 \text{ \mu m}$ ). Spaceborne instrumentation will be required to search for this interstellar emission, since atmospheric transmission is negligible at these wavelengths. The inherent low strength of the C-D in-plane bending modes may make them less favorable for observation, in spite of the fact that they lie in the accessible  $1000\text{--}800 \text{ cm}^{-1}$  ( $10\text{--}12.5 \text{ \mu m}$ ) range. It is important to attempt to measure the strongest of these bands to determine the extent of this interstellar PAH D/H fractionation. A comparison of the interstellar deuterium enrichment in PAHs with that measured in meteorites and interplanetary dust particles will provide important insight into the extent PAHs have evolved in the interstellar medium and in the protosolar nebula.

#### f) Negative PAH Ions

It has been suggested that the thermal sticking coefficient of electrons on neutral PAHs is near unity (Omont 1986). This would imply that most of the negative charges inside dense molecular clouds reside in  $\text{PAH}^-$  ions rather than electrons.

This would have important ramifications for chemistry in interstellar molecular clouds, since the degree of ionization, which regulates the molecular complexity through ion-molecule reactions (Prasad and Huntress 1980; Graedel, Langer, and Frerking 1982) is, in this case, controlled by neutralization reactions between metal or molecular cations and PAH anions. Observations of the  $\text{DCO}^+/\text{HCO}^+$  ratio provide a not very restrictive upper limit of  $6 \times 10^{-7}$  for the fractional abundance of  $\text{PAH}^-$  relative to H in some dark dense clouds (Lepp and Dalgarno 1988, 1989). It should be emphasized that the high electron sticking coefficient is only an assumption. Previously, the electron attachment rate to interstellar radicals has been estimated to be large primarily because of their large electron affinity (Herbst 1981). In this section we will estimate theoretically the electron sticking coefficient as a function of the PAH size and the fractional abundance of PAH anions inside dense molecular clouds.

Electron attachment to neutral PAHs involves the coupling of the kinetic energy of the captured electron to molecular vibrations (nuclear excited Feshbach resonances; Christophorou, McCorkle, and Christodoulides 1984a). The intermediate excited PAH anion can be stabilized by IR photon emission or it can revert again to the neutral state by electron ejection (autoionization). Measured lifetimes of metastable, intermediate anions vary by many orders of magnitudes ( $10^{-15} \leq \tau_a \leq 10^{-2} \text{ s}$ ) depending on the total internal energy of the anion (Christophorou *et al.* 1984a, b). The basic reaction can be schematically represented by



where  $k_f$  is the rate of the forward reaction (capture rate),  $k_b$  ( $= \tau_a^{-1}$ ) is the backward rate (autodetachment rate), and  $k_r$  is the radiative stabilization rate. In this notation, the electron sticking coefficient is given by

$$S(e) = \frac{k_f k_r}{k_r + k_b}. \quad (38)$$

The equilibrium abundance of PAH anions deep inside dense clouds is regulated by the balance between electron capture and recombination with metal or molecular cations.



We find then for the ratio of PAH anions to neutral PAHs

$$\frac{n(\text{PAH}^-)}{n(\text{PAH})} = \frac{k_f S(e)}{k_e}, \quad (40)$$

where we have assumed charge neutrality between electrons and the metal and molecular cations. Strictly speaking this yields only an upper limit to the relative fraction of PAH anions. When the electron sticking coefficient is small this reduces to

$$\frac{n(\text{PAH}^-)}{n(\text{PAH})} = \frac{k_f k_r}{k_b k_e}. \quad (41)$$

In equilibrium the capture and autoionization rate constants are related through the principle of detailed balance,

$$\frac{k_b}{k_f} = \frac{\rho^-}{\rho^0}, \quad (42)$$

where  $\rho^-$  and  $\rho^0$  are the density of states of the negative ion and that of the electron plus neutral molecule, respectively (Klots 1967; Christophorou and Grant 1977). The capture cross section is difficult to estimate quantitatively. At long range the electron-neutral interaction is due to electron-induced dipole interaction. At small distances the electric field produced by the electron is no longer uniform over the molecule, and the Coulomb repulsion between the electrons will decrease the screening of the nuclear charge (e.g., produce an image charge), and the cross section increases. Other correlation effects at short range are associated with spin and spatial symmetry properties of the molecular and electronic wave functions (e.g., Pauli principle). We will assume that the electron capture rate,  $k_f$ , can be approximated by the polarization interaction of an electron with a sphere with mean polarizability,  $\alpha$ , that is

$$k_f = 2\pi \left( \frac{\alpha e^2}{m_e} \right)^{1/2} \quad (43)$$

This includes the effect of the image charge (Draine and Sutton 1987), but may introduce an error of a factor of a few in the resulting capture cross section due to neglect of the other effects. However, in the limit of interest [small  $S(e)$ ], the relative abundance of PAH anions is insensitive to the absolute capture rate. We will further assume that the mean molecular polarizability varies linearly with the number of carbon atoms,  $N_C$ , in the molecule (i.e., the volume) and we adopt

$$\alpha \approx 1.5 \times 10^{-24} N_C. \quad (44)$$

The absolute value for the polarizability has been fitted to experimental measurements of naphthalene, anthracene, tetracene, and pyrene (Silinsh 1980). Omont (1986) assumed an  $N_C^m$  dependence for the polarizability with  $m = 3$  and 1.5 for catacondensed and pericondensed PAHs, respectively (note that the terms pericondensed and catacondensed have been reversed from general usage in his paper). However, it is to be expected that the polarizability is proportional to the number of  $\pi$  electrons in the system. In fact, Omont's assumptions yield a polarizability of  $6 \times 10^{-21} \text{ cm}^3$  for tetracene, much larger than the experimental value of  $3 \times 10^{-23} \text{ cm}^3$ , and we feel that our estimates are probably more appropriate. With this choice the capture rate becomes  $k_f \approx 1.2 \times 10^{-7} (N_C)^{1/2} \text{ cm}^3 \text{ s}^{-1}$ .

We estimate the density of states of an excited, intermediate PAH anion containing  $N$  carbon atoms by assuming that the  $3N-6$  oscillators have equal energy  $h\nu$ , which we have set equal to the typical geometric mean frequency ( $1000 \text{ cm}^{-1}$ ) of a 25 C atom PAH, and using the Whitten-Rabinovitch (1963) expressions for the density of states. The kinetic energy of the

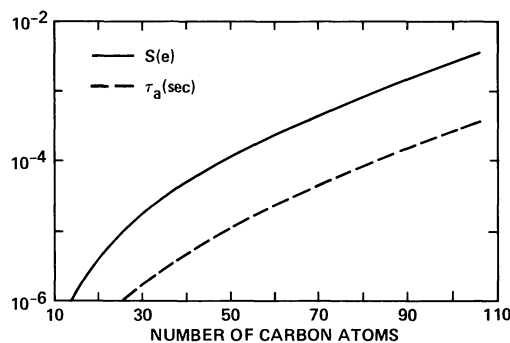


FIG. 25.—The calculated autoionization rate,  $\tau_a$ , and electron sticking coefficient,  $S(e)$ , for PAHs as a function of carbon atom number.

incident electron ( $\approx 10^{-3} \text{ eV}$  at 10 K) has been neglected in comparison to the electron affinity of the neutral PAH. The latter has been set equal to 0.7 eV, appropriate for a pericondensed PAH containing about 25 carbon atoms. For the density of states in the outgoing channel it is assumed that the neutral molecule is left in its ground state after electron ejection, that is

$$\rho_0 \approx \rho_e = \frac{m^2 v}{\pi^2 \hbar^3}, \quad (45)$$

where  $\rho_e$  is the density of states of the free electron. Assuming a radiative stabilization rate of  $k_r = 10 \text{ s}^{-1}$ , the autoionization rate ( $\tau_a$ ), and the electron sticking coefficient [ $S(e)$ ] have been calculated and are shown in Figure 25 as a function of  $N_C$ . The autoionization time scale is much shorter than the radiative stabilization time scale and the electron sticking coefficient is much less than unity. Both  $\tau_a$  and  $S(e)$  increase rapidly with size due to the increase in the internal degrees of freedom which can temporarily store the energy. The weak dependence of the polarizability (initial capture cross section) on size has little influence. Approximating the recombination rate constant for metal atoms ( $M_i = 30 \text{ amu}$ ) with that of a spherical grain with the same radius ( $8 \times 10^{-8} N^{1/2} \text{ cm}^3 \text{ s}^{-1}$ ; Draine and Sutton 1987), the abundance of PAH anions relative to neutral PAHs is equal to  $1.5 \times S(e)$ . As noted before, since the electron sticking coefficient is very small, the relative abundance of PAH<sup>-</sup> does not depend on the uncertain absolute value of the capture rate.

The electron sticking coefficient depends sensitively on the internal energy of the excited intermediate PAH anion and, thus, on the electron affinity of the neutral PAH. Measured and theoretically estimated electron affinities are available for PAHs up to about 24 C atoms (Christodoulides, McCorkle, and Christophorou 1984b, and references therein). For these sizes the electron affinity is typically less than about 0.7 eV but is expected to increase rapidly with size. Theoretical and experimental studies have shown that the molecular electronegativity,  $\chi$ , is essentially constant for aromatic hydrocarbons containing up to about 30 C atoms (Becker and Wentworth 1963; Becker and Chen 1966) where  $\chi$  is given by

$$\chi = \frac{1}{2}(\text{IP} + \text{EA}), \quad (46)$$

where IP is the ionization potential and EA is the electron affinity. Thus, from the ionization potential, the electron affinity can be determined. The molecular electronegativity determined this way, 4.17 eV, is somewhat lower than the work function of solid graphite (4.39 eV).

Although we realize the approximate nature of this relation, it is sufficiently accurate for our purpose. The ionization potential is a strong function of the number of  $\pi$  electrons as well as the molecular symmetry (Gallegos 1968). For pericondensed PAHs, the ionization potential approaches the limiting value very slowly, implying a small electron affinity even for large PAHs. For example, the ionization potentials of ovalene ( $C_{32}H_{14}$ ) and hexabenzocoronene ( $C_{32}H_{18}$ ) are measured to be 7.24 and 7.04 eV, and correspond to estimated electron affinities of 1.10 and 1.29 eV, respectively. For a 32 carbon atom pericondensed PAH with an electron affinity of 1 eV (rather than 0.7 as assumed to produce Fig. 25), the sticking coefficient is calculated to be about  $10^{-2}$ . Thus, only for pericondensed PAHs containing considerably more than 20 C atoms will the electron sticking coefficient approach unity.

The importance of molecular symmetry should, once more, be emphasized. Catacondensed PAHs approach the limiting ionization potential more rapidly than pericondensed PAHs (Galagos 1968). For example, the electron affinity of pentacene ( $C_{22}H_{14}$ ) is calculated to be about 1.3 eV (Dewar, Hashmall, and Trinajstic 1970) which implies an electron sticking coefficient of about 0.2. However, since small pericondensed PAHs are expected to be considerably more stable (and thus more abundant) than catacondensed PAHs, it is likely that the electron sticking coefficient of small interstellar PAHs is very small and that they do not play a major role in the ionization balance of molecular clouds. The larger PAHs responsible for the broad pedestal under the 1610 and "1310"  $\text{cm}^{-1}$  (6.2 and "7.7"  $\mu\text{m}$ ) emission features will, however, have an electron sticking coefficient of the order of unity and thus will be negatively charged. Nonetheless, because of their low abundance by number, their effects on gas-phase chemistry will be small (Lepp and Dalgarno 1988).

### g) Gas Heating

D'Hendecourt and Leger (1987) have recently suggested that the heating of the gas in the diffuse interstellar medium is dominated by photoelectrons ejected from PAHs. PAHs containing about 20 carbon atoms have a first ionization potential of about 7 eV, while the second ionization potential falls above the H ionization limit. The heating efficiency due to the ionization of PAHs is then given by

$$\varepsilon = f_{\text{uv}} f_n (1 - I_p / \bar{E}) f_e, \quad (47)$$

where  $f_{\text{uv}}$  is the fraction of the available photon energy absorbed by PAHs and  $f_n$  is the fraction of neutral PAHs. The factor in parentheses represents the fraction of the photon energy available for gas heating, with  $I_p$  and  $\bar{E}$  the first ionization potential of PAHs and the average photon energy, respectively. The fraction of the excess photon energy that will go into kinetic energy of the ejected photon rather than internal excitation of the PAH is given by  $f_e$ .

The fraction of the stellar energy absorbed by molecular PAHs as opposed to dust is approximately given by the ratio of the flux in the IR emission features at 3.3, 6.2, 7.7, and 11.3  $\mu\text{m}$  to that in the far-IR continuum. Typically, this is measured to be about 5% (Table 3). With a first ionization potential of 7 eV and an average UV photon energy of 10 eV, the fraction of the photon energy available for heating is 0.3. About 50% of that will go into gas heating ( $f_e \cong 0.5$ ; d'Hendecourt and Leger 1987). The neutral fraction is given by

$$f_n = (1 + \gamma)^{-1}, \quad (48)$$

where  $\gamma$  is the ratio of the ionization over the recombination rates. Following d'Hendecourt and Leger (1987) we set  $\gamma$  equal to

$$\gamma = \frac{4 \times 10^{-4} G_0 \sqrt{T}}{n_e}. \quad (49)$$

The coefficient in front is uncertain since it depends on the uncertain UV absorption properties and electron recombination rate coefficient of PAHs. For the conditions in the emission regions (Table 4),  $\gamma$  and  $f_n$  are typically about 15 and 0.05, respectively. The efficiency of the photoelectric heating by PAHs is then about  $4 \times 10^{-4}$  at the surface of the cloud and increases inward inversely proportional to the intensity of the UV radiation field until it reaches the maximum possible heating of  $7.5 \times 10^{-3}$  when all PAHs are neutral.

This provides an upper limit on the contribution of small ( $\cong 20$  C atom) PAHs to the gas heating, since the second ionization potential of larger PAHs drops below the hydrogen ionization limit. Such PAHs will be predominantly doubly ionized in the emission zone. For example, the first and second ionization potential of ovalene are 6.9 and 12.7 eV, respectively (Leach 1987a). As a result, the fraction of the photon energy available for heating is only 0.03 rather than 0.3 estimated above. Moreover, only a limited fraction of the available photon flux will be energetic enough for photoejection, and  $f_{\text{uv}}$  will be less than the fraction observed to be emitted in the emission features.

The charging of the PAHs and the resulting decrease in the gas-heating efficiency is also important for the large ( $\cong 350$  C atoms) PAHs or PAH clusters responsible for the broad feature underlying the 1610 and "1310"  $\text{cm}^{-1}$  (6.2 and 7.7  $\mu\text{m}$ ) emission features. Approximating the large PAHs by thin circular conducting disks with a radius,  $r$ , of about 15  $\text{\AA}$  ( $\cong 350$  C atoms) and a capacity  $C = 8\epsilon_0 r$ , the  $n$ th ionization potential,  $\phi_n$ , is given by

$$\phi_n = w + \left( n - \frac{1}{2} \right) \frac{e^2}{C}, \quad (50)$$

where  $w$  is the work function, which we will set equal to the graphite work function (4.4 eV). This classical expression gives a reasonable approximation to measured ionization potentials of small, condensed PAH molecules (Smith 1961). A 350 C atom PAH can be ionized seven times before the

ionization potential falls above the hydrogen ionization limit. For PAHs the UV photoionization and electron recombination rate are both proportional to the number of carbon atoms and thus their ratio,  $\gamma$ , will be independent of  $N_C$ . Adopting the value given above for small PAHs and solving the charge balance equation analogous to that for classical grains (de Jong 1977), we find that most large PAHs will be charged to the maximum level possible in the emission regions. Again, the contribution to the gas heating will depend on the discrete nature of the ionization process. The fraction of the large PAHs that can be ionized is approximately given by  $\gamma^{-1}$  ( $\approx 0.05$ ). However, the available UV photon energy for heating the gas is at most about 1.5 eV for a 350 C atom PAH. Moreover, for early-type stars only about 15% of the flux longward of 912 Å is emitted shortward of 1000 Å ( $\approx 12$  eV). Since these large PAHs absorb only about 5% of the total FUV flux (Table 3), the efficiency for these large PAHs is about  $3 \times 10^{-5}$ , much less than that estimated for the small PAHs. Of course, in regions of high density or weak UV intensity where all PAHs are neutral, large and small PAHs contribute equally to the heating of the gas since they absorb about equal amounts of the available UV photon flux (Table 3).

For comparison, the photoelectric efficiency due to classical dust grains ( $> 50$  Å) has been estimated to be about  $10^{-3}$  at the surface of the emission zones and to increase to 4% for neutral grains deeper in the cloud (de Jong 1977; Tielens and Hollenbach 1985a). Thus, although classical dust grains absorb a larger share of the available UV photon energy ( $\approx 90\%$ ) in the emission zones, their contribution is only about twice that of 20 C atom PAHs estimated above. This is largely due to the discrete nature of the ionization process (d'Hendecourt and Leger 1987). Even for neutral PAHs and grains the difference in gas heating is not as large as expected on the basis of relative amounts of energy absorbed due to the decrease of the photoelectric yield with size (Watson 1973). Nevertheless, whether or not interstellar PAHs contribute appreciably to the heating of the gas through the ejection of energetic photoelectrons depends critically on the assumed lower limit on the size distribution. In particular, if an appreciable fraction of the available UV photon energy is absorbed by PAHs with less than about 25 C atoms, PAHs may contribute between 20 and 50% of the gas heating. If the smallest PAH is, however, slightly larger than this or catacondensed rather than pericondensed (situations we view as unlikely), their contribution may be negligible.

#### *h) Anionic, Cationic, and Neutral PAHs: Influence on Interstellar Extinction*

Except in dense clouds, a significant fraction of the free PAHs will probably be singly ionized as cations in the interstellar medium because of their low ionization potential ( $\sim 6$  eV) (ATBa). In the IR emitting regions, the degree of ionization is probably greater than 90% (Table 4). In the diffuse medium, because of the reduced radiation field, about half will be present as cations, the rest neutral (van der Zwet and Allamandola 1985; Leger and d'Hendecourt 1985; Crawford,

Tielens, and Allamandola 1985). In regions where photoionization is the dominant ionization route, the singly charged cations should be most important since the second ionization potential is on the order of 15 eV. PAH clusters can be ionized to a much higher degree. In denser regions, where the UV flux is attenuated, the importance of cations will diminish, but collisions between electrons and neutral PAHs will produce negatively charged anions (Omont 1986, § Vf). Under certain conditions, it is also possible that doubly charged anions and cations can be present (Leach 1987b). Thus, depending on the conditions along the line of sight, an observer's field of view may encompass not only a myriad of PAHs, PAH clusters, and amorphous carbon grains of different sizes and geometries, but also a mixture of PAHs in different states of ionization.

The ionization state can have a profound influence on some of the spectroscopic properties of PAHs. Infrared bands correspond to fundamental molecular vibrations. The addition or removal of a  $\pi$  electron will generally only slightly influence the IR band strengths in PAHs and produce frequency shifts which are only a few tens of wavenumbers. Consequently, the IR spectra of the ionic and neutral forms of the same PAH should be quite similar (§ II). Ultraviolet and visible bands, on the other hand, correspond to transitions which involve the promotion of an electron from one electronic state to another. The addition of an electron to, or removal from a molecular system has a profound effect on these states (Herzberg 1966; Leach 1987a).

For neutral PAHs, the wavelength of the lowest energy electronic transition depends on the length of the long axis of the molecule (Platt 1956; Clar 1972; see Birks [1970] for a review of the electronic properties of neutral PAHs). In essence this is because a long chain of aromatic rings has more closely spaced energy levels than a short chain and therefore absorbs at longer wavelengths (analogous to a particle in a box). For coronene ( $C_{24}H_{12}$ ), which has a 3-ring long axis, the absorption starts at about 3600 Å (Birks 1970). The smallest, neutral, hexagonally symmetric condensed PAH that will absorb at the blue end of the visible is circumcoronene ( $C_{54}H_{18}$ ) which has a 5-ring long axis. In order for a neutral species to absorb throughout the visible, larger PAHs are needed if they are hexagonally symmetric. Of course, less symmetric PAHs with fewer carbon atoms can absorb at longer wavelengths. The absorption strength generally increases by several orders of magnitude at the shorter wavelengths (§ Vbi).

Ionized PAHs show markedly different behavior. In addition to absorbing very strongly in the UV, both the mono- and di-negative ions also absorb in an approximately flat continuum from 2500 Å out to 2 microns, with stronger (5–10 x), narrower structure superposed (Fig. 26; Hoijtink 1959). Similar behavior is observed for positive ions (Hoijtink and Zandstra 1960; Shida and Iwata 1973). Thus, in contrast to what is expected for a mixture of neutral PAHs, if a mixture of ionized PAHs were dominant in the interstellar medium, they would tend to produce an increase in the extinction at shorter wavelengths (UV) with a very gradual drop off (if at all) extending across the visible into the near-IR, with well-defined absorption bands.

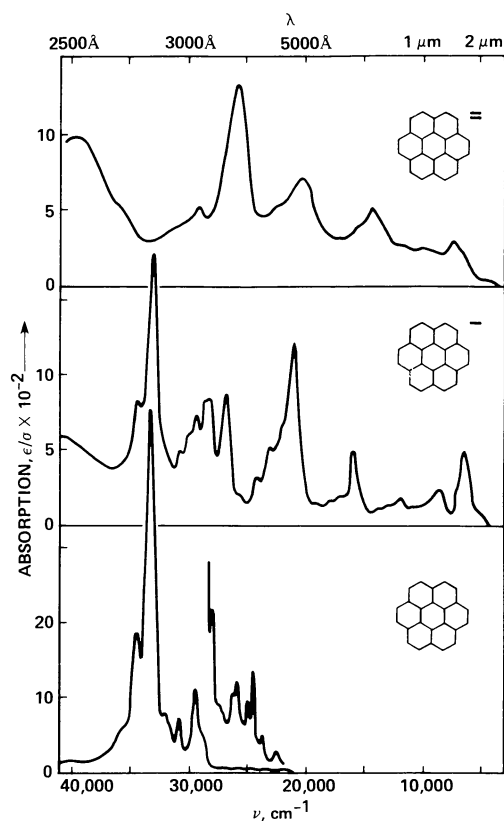


FIG. 26.—The electronic absorption spectra of the neutral coronene molecule and its mono- and di-negative ions. This figure (from Høijtink 1959), illustrates the dramatic differences in the visible and near-IR spectroscopic properties of neutral and ionized PAHs. Because these spectra are of ions suspended in very polar solvents, the bands are shifted from the positions expected for isolated PAHs and must not be used for comparison with interstellar features.

The third important interstellar carbon-based carrier to consider is a collection of amorphous carbon particles. If these were made up of neutral clusters of loosely bound PAHs, it is likely that their UV and visible absorption properties would be similar to those of the individual molecules themselves, i.e., they would show an abrupt rise in the UV. If, however, the PAH structural units were cross-linked by conjugated bonds, this would effectively produce larger and larger PAH units and push the onset of the absorption out across the visible into the near-IR. The extinction of these particles would probably follow the well-known  $1/\lambda$  law.

Thus, since each form of carbon has its own unique signature spanning parts of the UV, visible, and near-IR, observations in individual spectral regions will be contributed to by one or more of these components. All three forms show strong absorption in the ultraviolet and no single component is likely to dominate but weak structure may be discernible (§ Ve). Donn (1968) has shown that a collection of neutral PAHs alone cannot account for the 2200 Å hump. This is not surprising as the molecular sized PAHs comprise only about 1%–3% of the carbon that is available (ATBa).

The visible and near-IR properties of PAHs are of particular interest in view of their possible contribution to the

longstanding problem of the diffuse interstellar bands, DIBs (Herbig 1975; Smith, Snow, and York 1977). The presence (or absence) of PAH related bands in this spectral region depends not only on PAH size, but also upon charge. If PAHs are present along a line of sight through diffuse interstellar matter, a significant fraction would be in the positive (cation) form. If the line of sight encompassed denser interstellar matter, such as along the edge of a molecular cloud, a higher fraction of neutral and possibly negatively charged PAHs (anions) would be included. Under certain interstellar conditions doubly charged PAHs might also be produced and add to the spectral complexity (Leach 1987b). Thus, if a mixture of PAHs is responsible for some of the DIBs (van der Zwet and Allamandola 1985; Leger and d'Hendecourt 1985; Crawford, Tielens, and Allamandola 1985), one would expect that those bands arising from a specific PAH or group of related PAHs would be tightly correlated with each other. While testing for correlations between various DIBs has been a very difficult task, very significant progress has been made recently by Krelowski and Walker (1987), who have carried out an extensive and elegant study of many of the DIBs. The DIBs they studied fall into three families with relative strengths which vary from cloud to cloud. One of the families seems to be associated with dense clouds. Josafatsson and Snow (1987) have also concluded that there is evidence for three groups.

The ultimate test of whether or not PAHs are responsible for some of the DIBs must await the availability of laboratory spectra of isolated PAHs in both the anionic and cationic forms as well as of their doubly charged counterparts. As these data are not currently available, some progress toward this end can be made by searching for vibronic band patterns and band profiles which are characteristic of PAHs within each DIB family. A preliminary comparison of this sort can be made because the spectra of six aromatic cations isolated in an argon matrix have been measured (Andrews, Friedman, and Kelsall 1985; Andrews, Kelsall, and Blankenship 1982). While many of the bands are broadened by the argon matrix and peak positions are somewhat uncertain, ranges of vibronic band spacings can be measured. For the cations of naphthalene ( $C_{10}H_8$ ), phenanthrene ( $C_{14}H_{10}$ ), and tetracene ( $C_{18}H_{12}$ ), the species with the most distinct peak positions, the spacings between the dominant bands fall in the 500–700  $cm^{-1}$  and 1400–1600  $cm^{-1}$  range, with spacings between some of the weaker features in the 100–200  $cm^{-1}$  range. Bear in mind that the PAHs studied do not include any of the more stable pericondensed PAHs. The strongest bands measured fall in the red and near-IR spectral regions. Of the three DIB families discovered by Krelowski and Walker, the elements of the family which is comprised of the sharp bands at 5797, 5850, 6376, 6379, and 6614 Å have spacings of 156, 1411, 7, and 557  $cm^{-1}$ . These fall in the range of the PAH cation vibronic spectra. The spacings suggested by the other families are not similar. This comparison is, of course, very crude but it does suggest that PAH-related species could be responsible for one of the DIB families. When the members of the various DIB families and band profiles become firmly established, and laboratory spectra of isolated, ionized, pericondensed larger PAHs become available, it will be possible to fully test the suggestion that PAH-related species are

responsible for some of the DIBs. The same statement of course, applies to the suggestion that  $C_{60}$  and related species may be responsible for the DIBs (Kroto *et al.* 1985; Kroto 1987).

## VI. CONCLUSIONS

We have described how all of the interstellar infrared emission features may be attributed to various vibrational transitions in polycyclic aromatic hydrocarbon molecules (PAHs) and PAH-related materials such as PAH molecular ions, PAH clusters, and amorphous carbon particles. These assignments are summarized in Table 1. The major infrared bands are the most characteristic of aromatic hydrocarbons. Most of the minor spectroscopic bands are not evident in all interstellar emission spectra and they are probably due to different PAH molecules which are not present in some environments, presumably due to differences in the stabilities between their carriers and the carriers of the major features. The carriers of the major bands are probably the most symmetric, condensed PAHs as these are the most stable. The paucity of laboratory data on PAHs containing between 20 and 50 carbon atoms which are isolated and ionized (and in some cases, completely dehydrogenated) prevents a true comparison of laboratory spectra with interstellar spectra and the identification of specific interstellar molecules.

Spectral analysis of the interstellar emission spectrum, in particular in the  $950\text{--}770\text{ cm}^{-1}$  ( $10.5\text{--}13\text{ }\mu\text{m}$ ) region points to the most likely molecular structures present. These are the pericondensed structures which are symmetric and which maximize the C/H ratio. These are also the most stable PAHs.

The relationship between PAH molecules and amorphous carbon particles (collections of PAH molecules randomly oriented and connected with aliphatic hydrocarbon bridges) is described. The production route of PAHs and PAH-related materials in circumstellar shells of carbon rich stars is also discussed.

The method with which one can calculate the IR fluorescence spectrum from a vibrationally excited, isolated *molecule* is described in detail. Band intensities, relaxation rates, spectral dependence on molecular size, and energy content are discussed. It is shown how one can determine the size (or energy content) of the species which dominate the interstellar emission. This analysis points to PAHs containing between 20 and 40 carbon atoms being the most important emitters of the major bands. On the order of 1%–5% of the available interstellar carbon is tied up in the small (20–40 carbon atom) PAHs, while 3%–10% appears to be tied up in the larger (200–500 carbon atom) PAHs, PAH clusters, and amorphous carbon particles. The clusters and particles are responsible for the broad components underlying the  $1660\text{--}1100\text{ cm}^{-1}$  ( $6\text{--}9\text{ }\mu\text{m}$ ) and  $910\text{--}770\text{ cm}^{-1}$  ( $11\text{--}13\text{ }\mu\text{m}$ ) regions.

The molecular approach to calculate the emission intensities and related phenomena is compared with a thermal approximation. For high levels of vibrational excitation and emission from low-frequency modes, the two methods give similar results. At low levels of vibrational excitation and for the high frequency modes ( $\sim 3000\text{ cm}^{-1}$ ,  $3\text{ }\mu\text{m}$ ), the thermal approach can overestimate the emission intensity. For calcu-

lations of molecular reactions (e.g., H loss, deuterium enrichment, and carbon skeleton rearrangement) the thermal approximation is totally invalid. The H-loss rate of highly vibrationally excited PAHs is calculated using quantum statistics. It is shown that for small PAHs the H-loss rate can be comparable to the IR deactivation rate, leading to dehydrogenation.

The extent of dehydrogenation, and exchange with deuterium, is treated in several different interstellar regions. It is shown that PAHs containing fewer than 20–30 carbon atoms are effectively stripped of H, but that larger PAHs should be completely hydrogenated. The spatial variation of the 2940/3040 (3.4/3.3) ratio in several emission regions probably indicates a spatial variation of PAH composition and hydrogenation close to the excitation source. The smaller PAHs can be dehydrogenated and not contribute to the  $2940\text{ cm}^{-1}$  ( $3.4\text{ }\mu\text{m}$ ) band. Dehydrogenation may also be responsible for the spatial variations in the 12 and  $25\text{ }\mu\text{m}$  IRAS bands seen in reflection nebulae and the Galactic cirrus. Substantial deuterium enrichment occurs during interstellar time scales and predictions are made regarding deuterium enrichment as a function of PAH size. Such size-dependent deuterium fractionation predictions can be tested both observationally and chemically by analysis of meteorites and interplanetary dust particles.

Destructive reactions with oxygen and hydrogen atoms are considered in several regions of the ISM. It is concluded that, in general, these atomic species do not destroy PAHs significantly in the interstellar medium and that H atoms may recombine on PAHs and efficiently produce  $H_2$ .

The presence of negative PAH ions in molecular clouds is reconsidered in light of experimental data. The electron sticking coefficient of small PAHs ( $< 40\text{ C atoms}$ ) is small. Consequently they probably do not play a major role in the ionization balance of molecular clouds. The larger PAHs responsible for the pedestal beneath the 1615 and “1310” ( $6.2$  and “7.7” micron) bands will have an electron sticking coefficient on the order of unity and thus be negatively charged. Because of the low abundance of the smaller PAHs by number, they should not play a major role in the gas-phase chemistry. This effect underscores the importance of finding a reliable means to determine the PAH size distribution.

Finally, the influence of PAH charge and size on the ultraviolet, visible, and infrared spectral regions is described. It is reiterated that charged PAHs can absorb all across the visible and well into the near-IR ( $\lambda \cong 1\text{--}2\text{ }\mu\text{m}$ ). Thus, if interstellar PAHs are ionized, they can be vibrationally excited by the absorption of visible as well as ultraviolet photons. With current instrumentation, the spectral structure expected in the UV portion of the extinction curve lies just below the detection limit.

As so few laboratory data are available regarding PAHs in the forms that exist in the interstellar medium, the need for extensive laboratory work is called for throughout this paper.

It is a pleasure to acknowledge the invaluable assistance of C. Mims of Exxon Research Laboratories (New Jersey) in locating and discussing the IR and Raman spectra of car-

bonized material and of Prof. S. J. Cyvin and colleagues of Trondheim University (Norway) whose generosity with their original IR and Raman spectra of several PAHs has made some of the calculations described here possible. We wish to especially thank S. Sandford (NASA/Ames) for carefully reading this large manuscript and making many suggestions which have improved it significantly and for patiently teaching us about the carbon in interplanetary dust particles and describing how to interpret the deuterium enrichments. W. Schutte also deserves our special thanks for carefully going through the calculation methods described here and eliminating some inconsistencies. We also gratefully acknowledge many stimulating conversations and observing runs with our colleagues at NASA Ames: J. Bregman, M. Cohen, J. Goebel, J. Simpson, M. Werner, F. Witteborn, and

D. Wooden. We are also grateful to Professor S. Leach of the Laboratoire de Photophysique Moléculaire and the Département d'Astrophysique (Paris) for many insightful conversations concerning the physical and spectroscopic properties of PAHs, in particular of doubly charged species, Professor T. Wdowiak (University of Alabama) for several discussions concerning the IR and Raman properties of the many carbonaceous materials he and his colleagues have been studying, and H. Niki for gas-phase FTIR spectra of several PAHs and R. Dunbar for his re- and preprints.

Finally, we wish to acknowledge the important support given this work by NASA grant no. 188-41-57. J. R. Barker also acknowledges partial support from the US Department of Energy, Office of Basic Energy Sciences and from the National Science Foundation.

## REFERENCES

- Abouaf-Marguin, L., Dubost, H., and Legay, F. 1970, *Chem. Phys. Letters*, **7**, 61.
- Aihara, J. 1987, *Bull. Chem. Soc. Japan*, **60**, 3143.
- \_\_\_\_\_. 1988, *Bull. Chem. Soc. Japan*, **61**, 1451.
- Aitken, D. K., and Roche, P. F. 1982, *M.N.R.A.S.*, **200**, 217.
- Aitken, D. K., Roche, P. F., Spenser, P. M., and Jones, B. 1979a, *Astr. Ap.*, **76**, 60.
- \_\_\_\_\_. 1979b, *Ap. J.*, **233**, 925.
- Allamandola, L. J. 1984, in *Galactic and Extragalactic Infrared Spectroscopy*, ed. M. F. Kessler, and J. P. Philips, (Dordrecht: Reidel), p. 5.
- Allamandola, L. J., Greenberg, J. M., and Norman, C. A. 1979, *Astr. Ap.*, **77**, 66.
- Allamandola, L. J., and Norman, C. A. 1978, *Astr. Ap.*, **66**, 129.
- Allamandola, L. J., and Sandford, S. A. 1988, in *Dust in the Universe*, ed. M. Bailey and D. Williams (Cambridge: Cambridge University Press), p. 229.
- Allamandola, L. J., Sandford, S. A., and Wopenka, B. 1987, *Science*, **237**, 56.
- Allamandola, L. J., Tielens, A. G. G. M., and Barker, J. R. 1985, *Ap. J. (Letters)*, **290**, L25 (ATBa).
- Allamandola, L. J., Tielens, A. G. G. M., and Barker, J. R. 1987, *Polycyclic Aromatic Hydrocarbons and Astrophysics*, ed. A. Leger, L. B. d'Hendecourt, and N. Boccarra (Dordrecht: Reidel), p. 255 (ATBb).
- Allamandola, L. J., Bregman, J. D., Sanford, S. A., Tielens, A. G. G. M., Witteborn, F. W., and Wooden, D. H. 1989, *Ap. J. (Letters)*, **345**, L59.
- Allen, C. W. 1973, *Astrophysical Quantities*, London: Athlone.
- Allen, D. A., Baines, D. W. T., Blades, J. C., and Whittet, D. C. B. 1982, *M.N.R.A.S.*, **199**, 1017.
- Allen, D. A., and Wickramasinghe, D. T. 1981, *Nature*, **294**, 239.
- Amirav, A., Even, U., and Jortner, J. 1981, *J. Chem. Phys.*, **74**, 3745.
- Amirav, A., and Jortner, J. 1984, *J. Chem. Phys.*, **81**, 4200.
- Andrews, L., Friedman, R. S., and Kelsall, B. J. 1985, *J. Phys. Chem.*, **89**, 4016.
- Andrews, L., Kelsall, B. J., and Blankenship, T. A. 1982, *J. Phys. Chem.*, **86**, 2916.
- Atherton, P. D., Hicks, T. R., Reay, N. K., Robinson, G. T., Worswick, S. P., and Phillips, T. P. 1979, *Ap. J.*, **232**, 786.
- Bakke, A., Cyvin, B. N., Whitmer, J. C., Cyvin, S. J., Gustavsen, J. E., and Klæboe, P. 1979, *Z. Naturforschung*, **34a**, 579.
- Barker, J. R. 1983, *Chem. Phys.*, **77**, 301.
- Barker, J. R., Allamandola, L. J., and Tielens, A. G. G. M. 1987, *Ap. J. (Letters)*, **315**, L61.
- Barker, J. R., Rossi, M. J., and Pladziewicz, J. R. 1982, *Chem. Phys. Letters*, **90**, 99.
- Barnard, J. A., and Bradley, J. N. 1985, *Flame and Combustion* NY: Chapman and Hall).
- Bar-Nun, A. 1975, *Ap. J.*, **197**, 341.
- Bar-Nun, A., Litman, M., and Rappaport, M. L. 1980, *Astr. Ap.*, **85**, 197.
- Baughcum, S. L., and Leone, S. R. 1980, *J. Chem. Phys.*, **72**, 6531.
- Becker, R. S., and Chen, E. 1966, *J. Chem. Phys.*, **45**, 2403.
- Becker, R. S., and Wentworth, W. E. 1963, *J. Am. Chem. Soc.*, **85**, 2210.
- Bell, R. P. 1935, *Proc. Roy. Soc. A*, **148**, 241.
- Bellamy, L. J. 1958, *The Infrared Spectra of Complex Organic Molecules* (2d ed.; New York: Wiley).
- Benson, S. W. 1976, *Thermochemical Kinetics* (2d ed.; NY: Wiley).
- Bentley, A. F. 1982, *A. J.*, **87**, 1810.
- Bentley, A. F., Hackwell, J. A., Grasdalen, G. L., and Gehr, R. D. 1984, *Ap. J.*, **278**, 665.
- Beyer, T., and Swinehart, D. F. 1973, *Comm. Assoc. Comput. Mach.*, **16**, 379.
- Birks, J. B. 1970, *Photophysics of Aromatic Molecules* (London: Wiley).
- Bishop, D. M., and Cheung, L. M. 1982, *J. Phys. Chem. Ref. Data*, **11**, 119.
- Bittner, J. D., and Howard, J. B. 1978, *Prog. Astron. Aeronaut.*, **62**, 335.
- Blanco, A., Bussoletti, E., and Colangeli, L. 1988, *Ap. J.*, **334**, 875.
- Bohme, D. K. 1988, *Reactive Rate Coefficients in Astrophysics*, ed. T. J. Millar, and D. A. Williams (Dordrecht: Reidel), in press.
- Bondybey, V. 1984, *Ann. Rev. Phys. Chem.*, **35**, 591.
- Borghesi, A., Bussoletti, E., Colangeli, L., Minafra, A., and Rubini, F. 1983, *Infrared Phys.*, **23**, 321.
- Boulanger, F., Beichman, C., Desert, F. X., Helou, G., Perault, M., and Ryter, C. 1988, *Ap. J.*, **332**, 328.
- Bregman, J. D. 1989, in *IAU Symposium 135, Interstellar Dust*, ed. L. J. Allamandola and A. G. G. M., Tielens, (Dordrecht: Reidel), in press.
- Bregman, J. D., Allamandola, L. J., Tielens, A. G. G. M., Geballe, T. R., and Witteborn, F. C. 1989, *Ap. J.*, in press.
- Bregman, J. D., Dinerstein, H. L., Goebel, J. H., Lester, D. F., Witteborn, F. C., and Rank, D. M. 1983, *Ap. J.*, **274**, 666.
- Buch, V. 1989, *Ap. J.*, **343**, 208.
- Burberry, M. S., Morrell, J. A., Albrecht, A. C., and Swofford, R. L. 1979, *J. Chem. Phys.*, **70**, 5522.
- Bursey, M. M., Rogerson, P. F., and Bursey, J. M. 1970, *Org. Mass. Spec.*, **4**, 615.
- Bussoletti, E., Colangeli, L., and Borghesi, A. 1987, in *Polycyclic Aromatic Hydrocarbons and Astrophysics*, ed. A. Leger, L. B. d'Hendecourt, and N. Boccarra, (Dordrecht: Reidel), p. 63.
- Calvert, J. G., and Pitts, J. N. 1966, *Photochemistry* (NY: Wiley).
- Castelaz, M., Sellgren, K., and Werner, M. 1987, *Ap. J.*, **313**, 853.
- Cherchneff, I., and Barker J. R. 1989, *Ap. J. (Letters)*, **341**, L21.
- Chokski, A., Tielens, A. G. G. M., Werner, M. W., and Castelaz, M. W. 1988, *Ap. J.*, **334**, 803.
- Christophorou, L. G., and Grant, M. W. 1977, *Adv. Chem. Phys.*, **36**, 413.
- Christophorou, L. G., McCorkle, D. L., and Christodoulides, L. 1984a, *Electron-Molecule Interactions and their Applications*, Vol. 1, ed. L. J. Christophorou, (NY: Academic), p. 478.
- \_\_\_\_\_. 1984b, Vol. 2, p. 424.
- Clar, E. 1972, *The Aromatic Sextet* (London: Wiley).
- Clegg, R. S., and Wooten, A. 1980, *Ap. J.*, **240**, 828.
- Cohen, M., Tielens, A. G. G. M., and Allamandola, L. J. 1985, *Ap. J. (Letters)*, **299**, L93.
- Cohen, M., Tielens, A. G. G. M., Bregman, J. D., Whiteborn, F. C., Rank, D. M., Allamandola, L. J., Wooden, D., and de Muizon, M. 1989, *Ap. J.*, **341**, 246.
- Cohen, M., Allamandola, L. J., Tielens, A. G. G. M., Bregman, J., Simpson, J. P., Witteborn, F. C., Wooden, D., and Rank, D. 1986, *Ap. J.*, **302**, 737.
- Cohen, M., et al. 1975, *Ap. J.*, **196**, 179.
- Crawford, M. K., Tielens, A. G. G. M., and Allamandola, L. J. 1985, *Ap. J. (Letters)*, **293**, L45.
- Cyvin, B. N., Klæboe, P., Whitmer, J. C., and Cyvin, S. J. 1982a, *Z. Naturforschung*, **37a**, 251.
- Cyvin, S. J., Cyvin, B. N., Brunvoll, J., Whitmer, J. C., Klæboe, P., and Gustavsen, J. E. 1979, *Z. Naturforschung*, **34a**, 876.
- Cyvin, S. J., Cyvin, B. N., Brunvoll J., Whitmer, J. C., and Klæboe, P. 1982b, *Z. Naturforschung*, **37a**, 1359.

- Dalgarno, A., and Lepp, S. 1984, *Ap. J. (Letters)*, **287**, L47.
- Davidson, N. 1962, *Statistical Mechanics* (New York: McGraw-Hill).
- d'Hendecourt, L. B., and Leger, A. 1987, *Astr. Ap.*, **180**, L9.
- de Jong, T. 1977, *Astr. Ap.*, **55**, 137.
- de Muizon, M., D'Hendecourt, L. B., and Geballe, T. R. 1987, in *Polycyclic Aromatic Hydrocarbons and Astrophysics*, ed. A. Leger, L. B. d'Hendecourt, and N. Boccarra (Dordrecht: Reidel), p. 287.
- de Muizon, M., Geballe, T. R., d'Hendecourt, L. B., and Baas, F. 1986, *Ap. J. (Letters)*, **306**, L105.
- Dewar, J. S., Hashmall, J. A., and Trinajstic, N. 1970, *J. Am. Chem. Soc.*, **92**, 5555.
- Donn, B. 1968, *Ap. J. (Letters)*, **152**, L129.
- Donn, B. 1978, in *Protostars and Planets*, ed. T. Gehrels (Tucson: University of Ariz. Press), p. 100.
- Draine, B. T. 1979, *Ap. J.*, **230**, 106.
- Draine, B. T., and Anderson, N. 1985, *Ap. J.*, **292**, 494.
- Draine, B. T., and Sutton, B. 1987, *Ap. J.*, **320**, 803.
- Duffy, P. B., Erickson, E. F., Haas, M. R., and Houck, J. R. 1987, *Ap. J.*, **315**, 68.
- Duley, W. W., and Williams, D. A. 1981, *M.N.R.A.S.*, **196**, 269.
- Duley, W. W., and Williams, D. A. 1986, *M.N.R.A.S.*, **219**, 859, (London: Academic), p. 9.
- . 1988a, *M.N.R.A.S.*, **230**, 1p.
- . 1988b, *M.N.R.A.S.*, **231**, 969 p.
- Dunbar, R. C. 1986, *Chem. Phys. Letters*, **125**, 543.
- Dunbar, R. C., Chen, J. H., So, H. Y., and Asamoto, B. 1987, *J. Chem. Phys.*, **86**, 2081.
- Durana, J. F., and McDonald, J. D. 1976, *J. Chem. Phys.*, **64**, 2518.
- Ellis, H. B., and Werner, M. W. 1988, preprint.
- Forrest, W. J., Houck, J. R., and McCarthy, J. F. 1981, *Ap. J.*, **248**, 195.
- Frenklach, M. 1988, *Carbon in the Galaxy: Studies from Earth and Space*, ed. J. Tarter (NASA Conf. Proc.), in press.
- Frenklach, M., Clary, D. W., Gardiner, W. C., and Stein, S. E. 1984, in *20 Intl. Symposium on Combustion*, p. 887, (The Combustion Institute, Pittsburgh).
- Frenklach, M., Clary, D. W., Yuan, T., Gardiner, W. C., Jr., and Stein, S. E. 1986, *Combust. Sci. Tech.*, **50**, 79.
- Frenklach, M., and Feigelson, E. D. 1989, *Ap. J.*, **341**, 372.
- Frenklach, M., and Warnatz, J. 1987, *Combust. Sci. Tech.*, **51**, 265.
- Friedel, R. A., and Carlson, G. L. 1972, *Fuel*, **51**, 194.
- Gail, H. P., Keller, R., and Sedlmayr, E. 1984, *Astr. Ap.*, **133**, 320.
- Gail, H. P., and Sedlmayr, E. 1984, *Astr. Ap.*, **132**, 163.
- Gail, H. P., and Sedlmayr, E. 1987, in *Physical Processes in Interstellar Clouds*, ed. G. E. Morfill and M. Scholer (Dordrecht: Reidel), p. 275.
- Gallegos, E. J. 1968, *J. Phys. Chem.*, **72**, 3452.
- Gatley, I., and Rajju, N. 1987, in *IAU Symp. 120, Astrochemistry*, ed. M. S. Vardya and S. T. Tarafdar (Dordrecht: Reidel), p. 153.
- Geballe, T. R. 1984, *12 Proc. of Laboratory and Observatory IR. Spectra of Interstellar Dust*, ed. (Occasional Rept. Roy. Obs., Edinburgh) J. Greenberg and R. Wolstoncroft, p. 94.
- Geballe, T. R., Lacy, J. H., Persson, S. E., McGregor, P. J., and Soifer, B. T. 1985, *Ap. J.*, **292**, 500.
- Geballe, T. R., Tielens, A. G. G. M., Allamandola, L. J., Moorhouse, A., and Brand, P. W. J. L. 1989, *Ap. J.*, **341**, 278.
- Geiss, J., and Reeves, H. 1981, *Astr. Ap.*, **93**, 189.
- Gibian, M. J., and McCorley, R. C. 1973, *Chem. Rev.*, **73**, 441.
- Gillett, F. C., Forrest, W. J., and Merrill, K. M. 1973, *Ap. J.*, **183**, 87.
- Gillett, F. C., Kleinman, D. E., Wright, E. L., and Capps, R. W. 1975, *Ap. J. (Letters)*, **198**, L65.
- Goebel, J. 1987, in *Polycyclic Aromatic Hydrocarbons and Astrophysics*, ed. A. Leger, L. B. d'Hendecourt, and N. Boccarra (Dordrecht: Reidel), p. 329.
- Goldreich, P., and Scoville, N. 1976, *Ap. J.*, **205**, 144.
- Graedel, T. E., Langer, L. W., and Frerking, M. A. 1982, *Ap. J. Suppl.*, **48**, 321.
- Gredel, R., Lepp, S., and Dalgarno, A. 1987, *Ap. J. (Letters)*, **323**, L137.
- Habing, H. J. 1968, *Bull. Astr. Inst. Netherlands*, **19**, 421.
- Harris, S. J., and Winer, A. M. 1985, *Ann. Rev. Phys. Chem.*, **36**, 31.
- Herbig, G. H. 1975, *Ap. J.*, **196**, 129.
- Herbst, E. 1981, *Nature*, **289**, 686.
- Herzberg, G. 1966, *Electronic Spectra and Electronic Structure of Polyatomic Molecules* (NY: van Nostrand Reinhold).
- Herzberg, G. H. 1968, *Infrared and Raman Spectra of Polyatomic Molecules* (Princeton: van Nostrand).
- Hojtink, G. J. 1959, *Mole. Phys.*, **2**, 85.
- Hojtink, G. J., and Zandstra, P. J. 1960, *Mol. Phys.*, **3**, 371.
- Honovich, J. P., and Dunbar, R. C. 1982, *J. Am. Chem. Soc.*, **104**, 6220.
- Josafatsson, K., and Snow, T. P. 1987, preprint.
- Keller, R. 1987, in *Polycyclic Aromatic Hydrocarbons and Astrophysics*, ed. A. Leger, L. B. d'Hendecourt, and N. Boccarra (Dordrecht: Reidel), p. 387.
- Kern, R. D., Wu, C. H., Skinner, G. B., Roa, V. S., Kiefer, J. H., Towers, J. A., and Mizerka, L. J. 1984, paper presented at the 20th Symposium Int. Combustion, Ann Arbor, Michigan.
- Kerridge, J. F., and Chang, S. 1985, in *Protostars and Planets II*, ed. D. C. Black and M. Mathews (Tucson: Utah of Arizona Press), p. 738.
- Kiefer, J. H., Mizerka, L. J., Patel, M. R., and Wei, H. C. 1985, *J. Phys. Chem.*, **89**, 2013.
- Klots, C. E. 1967, *J. Chem. Phys.*, **46**, 1197.
- Koike, C., Hasegawa, H., and Manabe, A. 1980, *Ap. Space Sci.*, **67**, 495.
- Kondrat'ev, V. N. 1964, *Chemical Kinetics of Gas Reactions* (London: Pergamon), p. 211.
- Krelowski, J., and Walker, G. A. H. 1987, *Ap. J.*, **312**, 860.
- Kroto, H. W. 1987, *Nature*, **329**, 529.
- Kroto, H. W., Heath, J. R., O'Brien, S. C., Curl, R. F., and Smalley, R. E. 1985, *Nature*, **318**, 162.
- Leach, S. 1987a, in *Polycyclic Aromatic Hydrocarbons and Astrophysics*, ed. A. Leger, L. B. d'Hendecourt, and N. Boccarra (Dordrecht: Reidel), p. 99.
- Leach, S. 1987b, *J. Electron. Spectrosc. Rel. Phen.*, **41**, 427.
- Leach, S., Eland, J. H. D., and Price, S. D. 1989, *J. Phys. Chem.*, in press.
- Legay, F. 1977, in *Chemical and Biochemical Applications of Lasers*, Vol. 2, ed. C. B. Moore (NY: Academic).
- Leger, A., and d'Hendecourt, L. B. 1985, *Astr. Ap.*, **146**, 81.
- . 1987, in *Polycyclic Aromatic Hydrocarbons and Astrophysics*, ed. A. Leger, L. B. d'Hendecourt, and N. Boccarra (Dordrecht: Reidel), p. 223.
- Leger, A., d'Hendecourt, L. B., and Boccarra, N. 1987, *Polycyclic Aromatic Hydrocarbons and Astrophysics* (Dordrecht: Reidel).
- Leger, A., and Puget, J. L. 1984, *Astr. Ap.*, **137**, L5 (LP).
- Lepp, S., and Dalgarno, A. 1988, *Ap. J.*, **324**, 553.
- . 1989, *Ap. J. (Letters)*, in press.
- Low, F. J., et al. 1984, *Ap. J. (Letters)*, **278**, L19.
- Low, M. J. D., and Mortera, C. 1983, *Carbon*, **21**, 275.
- Luan, L., Werner, M. W., Dwek, E., and Sellgren, K. 1988, in *IAU Symposium 135: Interstellar Dust Contributed Papers*, ed. A. G. G. M. Tielens, and L. J. Allamandola (NASA CP-3036), in press.
- Marchand, A. 1987, in *Polycyclic Aromatic Hydrocarbons and Astrophysics*, ed. A. Leger, L. B. d'Hendecourt, and N. Boccarra (Dordrecht: Reidel), p. 31.
- McCarthy, J. F., Forrest, W. J., and Houck, J. R. 1978, *Ap. J.*, **224**, 109.
- Miller, J. H., Mallard, W. G., and Smyth, K. C. 1984, *J. Phys. Chem.*, **88**, 4963.
- Mitchell, M. B., Smith, G. R., and Guillory, W. A. 1981, *J. Chem. Phys.*, **75**, 44.
- Mortera, C., and Low, M. J. D. 1983, *Carbon*, **21**, 283.
- Nicovich, J. M., Gump, C. A., and Ravishankara, A. R. 1982, *J. Phys. Chem.*, **86**, 1684.
- Nicovich, J. M., and Ravishankara, A. R. 1984, *J. Phys. Chem.*, **88**, 2534.
- Oberlin, A. 1984, *Carbon*, **22**, 521.
- Oberlin, A., Boulmier, J. L., and Villey, M. 1980, in *Kerogen*, ed. B. Durand (Paris: Editions Technip), p. 191.
- Omont, A. 1986, *Astr. Ap.*, **164**, 159.
- Oref, I., and Rabinovitch, B. S. 1979, *Accts. Chem. Res.*, **12**, 166.
- Platt, J. R. 1956, *Ap. J.*, **123**, 486.
- Prasad, S. S., and Huntress, W. T. 1980, *Ap. J. Suppl.*, **43**, 1.
- Prasad, S. S., and Tarafdar, S. P. 1983, *Ap. J.*, **267**, 603.
- Puget, J. L. 1988, in *IAU Symposium 135, Interstellar Dust*, ed. L. J. Allamandola and A. G. G. M. Tielens (Dordrecht: Reidel), in press.
- Reddy, K. V., Heller, D. F., and Berry, M. J. 1982, *J. Chem. Phys.*, **76**, 2814.
- Robin, M. B. 1974, *Higher Excited States of Polyatomic Molecules*, Vol. 2, (NY: Academic).
- Roche, P. F., Aitken, D. K., and Smith, C. H. 1989, *M.N.R.A.S.*, **236**, 485.
- Rossi, M. J., Pladzewicz, J. R., and Barker, J. R. 1983, *J. Chem. Phys.*, **78**, 6695.
- Ruhl, E., Price, S. D., and Leach, S. 1989, *J. Phys. Chem.*, **93**, 6312.
- Russell, R. W., Soifer, B. T., and Willner, S. P. 1977, *Ap. J. (Letters)*, **217**, L149.
- Sakata, A., Wada, S., Tanabe, T., and Onaka, T. 1984, *Ap. J. (Letters)*, **287**, L51.
- Savage, B. D., and Mathis, J. 1979, *Ann. Rev. Astr. Ap.*, **17**, 73.
- Schmidt, G. D., Cohen, M., and Margon, B. 1980, *Ap. J. (Letters)*, **239**, L133.
- Scoville, N. Z., and Sanders, D. B. 1987, in *Interstellar Processes*, ed. D. J. Hollenbach and H. A. Thronson (Dordrecht: Reidel), p. 21.
- Seab, C. G., and Snow, T. 1985, *Ap. J.*, **295**, 485.
- Sellgren, K. 1981, *Ap. J.*, **245**, 138.
- . 1984, *Ap. J.*, **277**, 623.

- Sellgren, K., Allamandola, L. J., Bregman, J. D., Werner, M. W., and Wooden, D. H. 1985, *Ap. J.*, **299**, 416.
- Sellgren, K., Werner, M. W., and Dinerstein, H. L. 1983, *Ap. J. (Letters)*, **217**, L149.
- Shi, J., Bernfield, D., and Barker, J. R. 1988, *J. Chem. Phys.*, **88**, 6211.
- Shida, T., and Iwata, S. 1973, *J. Am. Chem. Soc.*, **95**, 3473.
- Sibener, S. J., Buss, R. J., Casavecchia, P., Hirooka, T., and Lee, Y. T. 1980, *J. Chem. Phys.*, **72**, 4341.
- Silinsch, E. A. 1980, *Organic Molecular Crystals* (Berlin: Springer Verlag).
- Smith, F. T. 1961, *J. Chem. Phys.*, **34**, 793.
- Smith, W. H., Snow, T. P., and York, D. G. 1977, *Ap. J.*, **218**, 124.
- Solomon, P. P., Rivolo, A. R., Barrett, J., and Yahil, A. 1987, *Ap. J.*, **319**, 730.
- Stein, S. E. 1978, *J. Phys. Chem.*, **82**, 566.
- Stein, S. E., Golden, D. M., and Benson, S. W. 1977, *J. Phys. Chem.*, **81**, 314.
- Stein, S. E., and Fahr, A. 1985, *J. Phys. Chem.*, **89**, 3714.
- Stein, S. E., and Brown, R. L. 1986, *Carbon*, in press.
- Stein, S. E., and Brown, R. L. 1987, in *Molecular Structure and Energetics*, Vol. 2, ed. J. F. Leibman and A. Greenberg (New York: VCH Publishers, Inc.).
- Stein, S. E., and Rabinovitch, B. S. 1973, *J. Phys. Chem.*, **58**, 2438.
- Swofford, R. L., Long, M. E., and Albrecht, A. C. 1976, *J. Phys. Chem.*, **65**, 179.
- Tielens, A. G. G. M. 1983, *Astr. Ap.*, **119**, 177.
- Tielens, A. G. G. M. 1988, in *Carbon in the Galaxy: Studies from Earth and Space*, ed. J. Tarter (NASA Conf. Proc.), in press.
- Tielens, A. G. G. M. 1989, in *Submillimeter and Millimeter Astronomy*, ed. A. Webster (Dordrecht: Kluwer), in press.
- Tielens, A. G. G. M., and Allamandola, L. J. 1987a, in *Interstellar Processes*, ed. D. J. Hollenbach, and H. A. Thronson (Dordrecht: Reidel), p. 397.
- \_\_\_\_\_. 1987b, in *Physical Processes in Interstellar Clouds*, ed. G. Morfill and M. Scholer (Dordrecht: Reidel), p. 333.
- Tielens, A. G. G. M., Allamandola, L. J., Barker, J. R., and Cohen, M. 1987, Chapter in *Polycyclic Aromatic Hydrocarbons and Astrophysics*, ed. A. Leger, L. B. d'Hendecourt, and N. Boccard (Dordrecht: Reidel), p. 273.
- Tielens, A. G. G. M., Allamandola, L. J., Bregman, J. D., and Witteborn, F. C. 1987, in preparation.
- Tielens, A. G. G. M., and de Jong, E. 1979, *Astr. Ap.*, **75**, 326.
- Tielens, A. G. G. M., and Hollenbach, D. J. 1985a, *Ap. J.*, **291**, 722.
- \_\_\_\_\_. 1985b, *Ap. J.*, **291**, 747.
- Tokunaga, A. T., Nagata, T., Sellgren, K., Smith, R. G., Onaka, T., Nakada, Y., Sakata, A., and Wada, S. 1988, *Ap. J.*, **328**, 709.
- Tuinstra, F., and Koenig, J. L. 1973, *J. Chem. Phys.*, **53**, 1126.
- Turro, N. J. 1978, *Modern Molecular Photochemistry* (Menlo Park: Benjamin Cummings).
- van der Zwet, G. P., and Allamandola, L. J. 1985, *Astr. Ap.*, **146**, 76.
- Warren-Smith, R. F., Scarrott, S. M., and Murrin, P. 1981, *Nature*, **292**, 317.
- Watson, W. D. 1973, in *Interstellar Dust and Related Topics*, ed. J. M. Greenberg and H. C. van de Hulst (Dordrecht: Reidel), p. 335.
- Wdowiak, T. J., Flickinger, G. C., and Cronin, J. R. 1988, *Ap. J. (Letters)*, **328**, L75.
- Weston, R. E. 1986, *Int. J. Chem. Kinetics*, **18**, 1259.
- Whitten, G. Z., and Rabinovitch, B. S. 1963, *J. Chem. Phys.*, **38**, 2466.
- \_\_\_\_\_. 1964, *J. Chem. Phys.*, **41**, 1883.
- Willner, S. P. 1984, in *Galactic and Extragalactic Infrared Spectroscopy*, ed. M. F. Kessler, and J. P. Phillips, (Dordrecht: Reidel), p. 37.
- Willner, S. P., Soifer, B. T., Russell, R. W., Joyce, R. R., and Gillett, F. C. 1977, *Ap. J. (Letters)*, **217**, L121.
- Witt, A. N. 1987, *Bull. AAS*, **18**, 1030.
- Witt, A. N., and Schild, R. E. 1986, *Ap. J. Suppl.*, **62**, 839.
- \_\_\_\_\_. 1988, *Ap. J.*, **325**, 837.
- Witt, A. N., Schild, R. E., and Kraiman, J. B. 1984, *Ap. J.*, **281**, 708.
- Witteborn, F. C., Sandford, S. A., Bregman, J. D., Allamandola, L. J., Cohen, M., Wooden, D., and Graps, A. L. 1989, *Ap. J.*, **341**, 270.
- Wolfire, M., Tielens, A. G. G. M., and Hollenbach, D. J. 1988, *Ap. J.*, submitted.
- Zhang, Q. L., O'Brien, S. C., Heath, J. R., Liu, Y., Curl, R. F., Kroto, H. W., and Smalley, R. E. 1986, *J. Phys. Chem.*, **90**, 525.

LOUIS J. ALLAMANDOLA and A. G. G. M. TIELENS: NASA-Ames Research Center M/S 245-6, Moffett Field, CA 94035

JOHN R. BARKER: Department of Atmospheric, Oceanic and Space Sciences, University of Michigan, Ann Arbor, MI 48109-2143